# Doctoral Thesis

# Removal of hexavalent chromium from tannery wastewater by coprecipitation with ferrihydrite and sulfate green rust: mechanism elucidation and removal optimization

# 水酸化第二鉄および硫酸型グリーンラスト共沈法による製革廃水からの六価クロム除去: 機構解明および除去最適化

**July, 2018**


Waseda University, Japan
Graduate School of Creative Science and Engineering, Department of Earth Sciences, Resources and Environmental Engineering
Research on Environmental Purification and Resources Processing

**Abdullah al MAMUN**
アブドゥラ アル マムン

**List of Contents**

## Abbreviations

| | |
|---|---|
| BSCIC: | Bangladesh Small and Cottage Industry Corporation |
| BOD: | Biochemical Oxygen Demand |
| CETP: | Common Effluent Treatment Plant |
| COD: | Chemical Oxygen Demand |
| DO: | Dissolved Oxygen |
| ECA: | Ecologically Critical Area |
| ESR: | Electron Spin Resonance |
| EXAFS: | Extended X-ray Absorption Fine Structure |
| EDAX: | Energy Dispersive Analysis X-ray |
| FTIR: | Fourier-Transform Infrared Spectroscopy |
| FSG: | Food Safety Guidelines |
| ICP-AES: | Inductively-Coupled Plasma Atomic Emission Spectrometry |
| IC | Ion Chromatography |
| LDH: | Layer Double Hydroxide |
| rpm | Rotation per minute |
| XRD: | X-Ray Diffraction |
| XAFS: | X-ray Adsorption Fine Structure |
| XANES: | X-ray Absorption Near-Edge Structure |
| XPS: | X-ray Photoelectron Spectroscopy |

# [Chapter 1]

# Introduction: background and rationality of the study

## 1.1 Introduction

The tannery is the industrial process that transforms animal raw hides or skins into useable leather products. Although this trade is worth over 100 billion US dollars per year globally [1], the environmental issues related to the tannery process are of great concern. As a matter of fact, 450 kg of chemicals are required to process 1 ton of raw hides but only 72 kg of them are sorbed by the skins [2]. Therefore, the 40 $m^3$ of wastewater that is produced for each ton of processed raw hides contains a significant amount of pollutants.

Leather and leather products industries have been shifting considerably their tanning operations to developing countries, where the production costs are lower and the environmental regulations are less stringent [3]. As a result, a good portion of the 95 sites worldwide identified for tannery-related pollution are located in Bangladesh (Fig. 1.1).

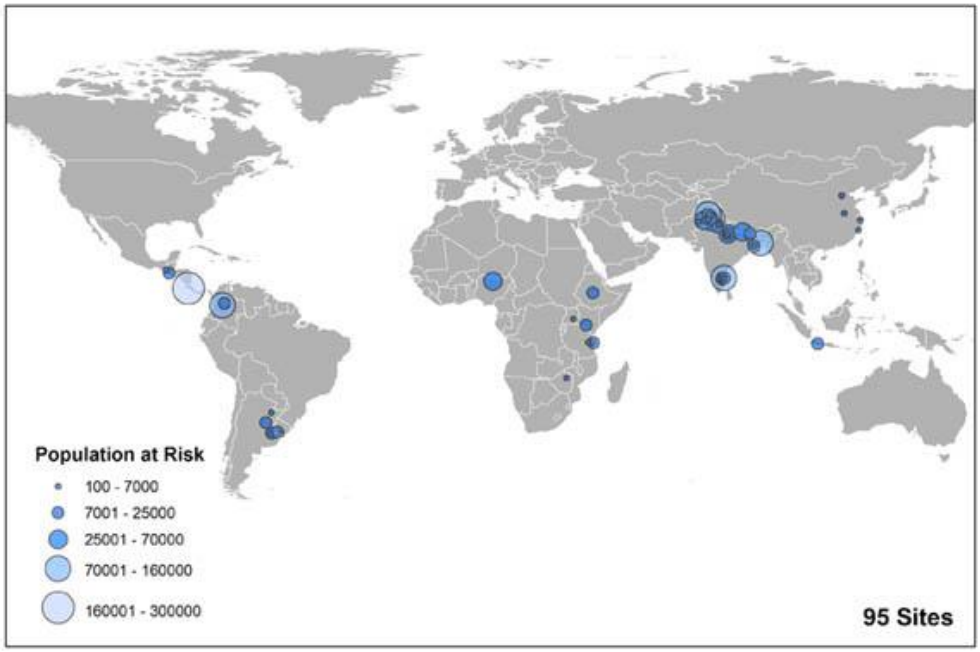


**Fig. 1.1 Tannery pollution all over the world** [4]

The leather manufacturing is one of the most important business in Bangladesh, accounting for approximately 500 million USD per year. However, the manufacturing process and in particular the tanning process determines a significant environmental burden due to the discharge of hexavalent chromium (Cr(VI)) into wastewater. Common

removal methods for Cr(VI) are either not efficient at low concentrations or not sustainable for developing countries like Bangladesh. Therefore the development of new efficient and sustainable technologies is highly anticipated.

### 1.2 Ecological risk by Cr contaminated tannery

There are multifold environmental impacts of tanneries. Depending upon the environmental conditions, the speciation of chromium can vary or persists unchanged for a long time [5]. Factory sites, lagoons, storage areas and temporary waste dumps may severely contaminate the underlying soil if appropriate precautions are not taken. This contamination can interfere with later uses of the land and even potentially contribute to the pollution of groundwater if percolation through the soil occurs [6]. Chromium can even interfere with biological key processes in wastewater treatment plants, thereby affecting their performances. The pollutant may also damage the ecology of the receiving waters in the vicinity of the discharge points [7], thus affecting directly the living conditions of the adjacent microorganisms.

The best example of the devastating effect of inconsiderate Cr tanning operation in Bangladesh is the one in the Buriganga River (adjacent to Hazaribag tannery area, Dhaka). The capital Dhaka was built beside the Buriganga River long ago. However, due to the tannery practice from the 1970s, the river is now almost dead and its water is being used neither in agriculture nor even for industrial cooling.

The Department of Environment of Bangladesh has been measuring physical and chemical parameters in 10 different monitoring points of the Buriganga River. The main measured parameters are reported in Table 1.1. Clearly, the now-closed Hazaribagh tannery was discharging for many years all its polluting load in the river. Although the measured pH was within the standard range, the dissolved oxygen (DO) was very low in dry seasons and remained always below the surface water standard. The monthly variations of pH, DO, BOD (Biochemical Oxygen Demand) and COD (Chemical Oxygen Demand) measured in 2015 are shown in Fig. 1.2. Usually, the dry season lasts 4 months starting from December to March. In the dry season, the DO is almost zero with significantly higher BOD and COD. In contrast, in the rainy season that lasts from May to August the DO increases while the COD and BOD decrease due to dilution. Although Bangladesh does not have any water standard for river waters, the average values of these

parameters exceed greatly the limits of advanced countries, thereby remarking the level of pollution in the Buriganga River.

**Table 1.1 Variations of pH, DO, BOD of water of Buriganga river with seasonal variation during 2010-2014 (supplied by Department of Environment, Bangladesh [8])**

| Year | Season | pH | DO | BOD |
|---|---|---|---|---|
| 2010 | dry | 7.25 | 0.47 | 26.44 |
| | rainy | 7.31 | 3.83 | 8.23 |
| 2011 | dry | 7.27 | 1.35 | 26.06 |
| | rainy | 7.03 | 2.24 | 22.48 |
| 2012 | dry | 7.42 | 0.54 | 18.75 |
| | rainy | 7.19 | 2.55 | 15.90 |
| 2013 | dry | 7.38 | 2.3 | 21.18 |
| | rainy | 6.84 | 2.56 | 9.17 |
| 2014 | dry | 7.24 | 0.61 | 24.97 |
| | rainy | 7.27 | 2.58 | 10.29 |
| Inland surface water standard (irrigation and fisheries) [9] | | **6.5-8.5** | **≥5 mg/L** | **≤6 mg/L** |

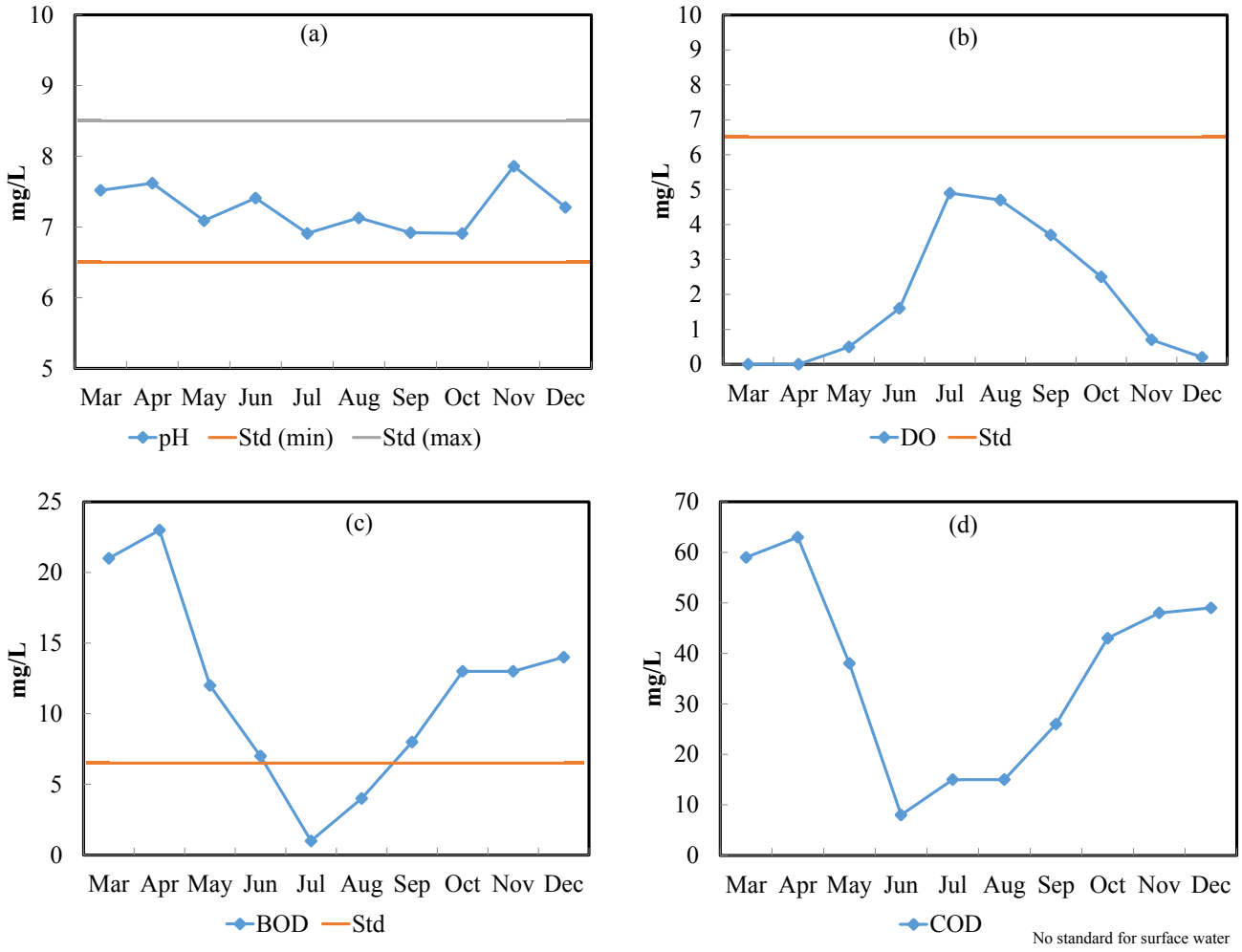


**Fig. 1.2 Mean values for (a) pH, (b) DO, (c) BOD, (d) COD of Buriganga River in 2015 (data provided by Department of Environment, Ministry of Environment and Forests, Bangladesh** [8]**; standards are given wherever available** [9]**)**

Kawsar et al. (2016) [10] examined the uptake of heavy metals by five fish species in the Buriganga River and found an accumulation of Zn, Cr, Mn, Ni, Cu, Zn, Pb. Whereas the maximum concentration of Cr(VI) allowed in aquatic system ranges from 0.05 to 3.95 mg/L depending on the fish species [11], the measured accumulated concentrations were significantly higher. The measured values exceeded the maximum allowed concentrations (MAC) recommended by FAO/WHO, while in case of one species, Rohu (*Labeo rohita),* they were above the Food Safety Guidelines (FSG) standards (Table 1.2) issues by the United States Food and Drug Administration (USFDA) [10]. This high bio-accumulation of Cr might have resulted from the effluent coming from the tannery industries near the Buriganga River.

**Table 1.2 Mean Cr concentration (mg/kg) in five fish species from the Buriganga river, Bangladesh** [10]**.**

| | Fish species | | | | | |
|---|---|---|---|---|---|---|
| | Ticto barb *(Puntius ticto)* | Pool barb *(Puntius sophore)* | Swamp barb *(Puntius chola)* | Rohu *(Labeo rohita)* | Tank goby *(Glossogobius giuris)* | FSG* (mg/kg) |
| Cr (mg/kg) | 5.54±1.52 | 4.33±1.35 | 3.57±1.60 | 18.84±1.72 | 5.13±0.96 | 12 -13 |

***FSG: Food Safety Guidelines**

As a consequence, on September 1st 2009, the government of Bangladesh has declared the Buriganga River as an Ecologically Critical Area (ECA) and moved the tanning operations from Hazaribagh tannery area to the newly Bangladesh Small and Cottage Industry Corporation (BSCIC) tannery estate. However, as it will be explained later in chapter 2, the total concentration of Cr(VI) in the effluent after the wastewater treatment plant at BSCIC is still 10-15 mg/L. Based on the example of the Buriganga river, this concentration is not only a threat to the aquatic life, but for the whole ecosystem. If proper care is not taken, serious ecological alterations have to be expected in the future.

### 1.3 Human health risk by Cr contaminated tannery

Hazard for human health might arise from highly polluted tannery environment. This is due to the presence of chromium. Although Cr(VI) and Cr(III) both threaten the immune system and can determine apoptosis (cell death of human lymphocytes). Cr(VI) is 500 times more toxic than Cr(III) [14,15,16,17]. DNA damages, clastogenicity, mutagenicity and carcinogenicity of soluble and/or insoluble Cr(VI) compounds have been widely demonstrated [18]. These health issues arise mainly from the Cr(VI) ability to easily penetrate the cell membrane [16]. A schematic representation of the mechanisms determining the absorption of Cr(VI) in the human body is shown in Fig. 1.3.

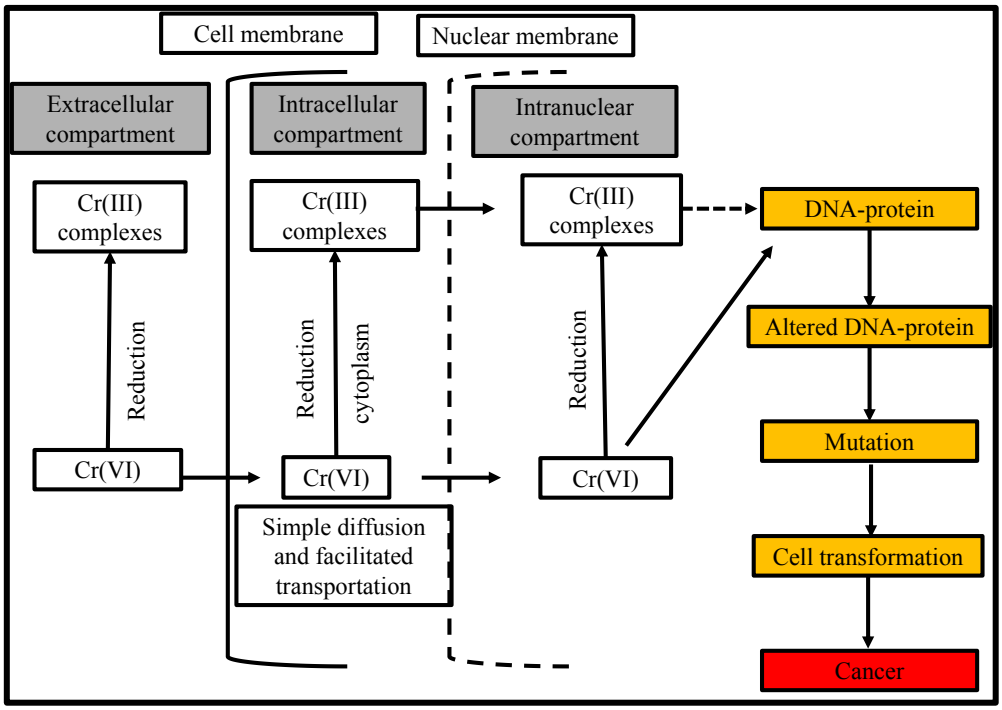


**Fig. 1.3 Cellular model of chromium mutagenicity and carcinogenicity** [18]

Tannery workers are exposed to Cr(VI) by handling chemicals and more in general, by being exposed to the Cr(VI)-bearing waste streams. The exposure can take place through skin-absorption (e.g. tanning and re-tanning) or inhalation of particulate (e.g. skin-cuts burning). In this view, it has been reported that amounts of Cr(VI) as small as 0.000008 mg/m$^3$ may cause respiratory issues [19].

A detailed study reported evidence of chromium accumulation in the serum and blood of tannery workers in Ontario (Canada) [20]. According to the study, the accumulation of chromium in the body is strongly related to amount and length of exposure.

Unfortunately, not much work has been done to investigate and mitigate the effect of Cr(VI) exposure in Bangladesh. The health of tannery workers in Bangladesh is continuously threatened by the direct exposure to Cr(VI) without using proper safety measures. Mazumder et al. (2013) provided a quantitative idea of the threat by measuring the of Cr(VI) in the liver of chickens from the adjacent poultry farm of Hazaribag tannery area, Dhaka, Bangladesh [19]. In the first place, the study suggests that consumption of poultry can determine an additional source of Cr accumulation in the human body [21]. Furthermore, the accumulation of chromium in chicken can provide an idea of risks

related to long-term exposure. The concentration of Cr(VI) was found to be proportional to the chicken's age and reported as high as 13 mg/L in the liver of 2-year-old chickens [19]. In contrast, the average life span of tannery workers is about 55 years which is lower than the average of the total population (72 years). Thus, the threat due to cumulative Cr(VI) absorption is a clear issue that must be countered as soon as possible.

### 1.4 Source of Cr(VI) in tannery process

Although the commonly used chromium tanning agent is Cr(III) sulfate, significant levels of Cr(VI) can be found within the process. This could be possibly due to the several reasons [19]:

- Presence of unreduced Cr(VI) as impurity in Cr(III) tanning salts. The Cr(III) salts used in tanning are prepared through reduction of Cr(VI) as sodium dichromate, as shown in the following equation (1).

$$Na_2Cr_2O_7 + 3SO_2 + H_2O \rightarrow Cr_2(SO_4)_2(OH)_2 + Na_2SO_4 \quad (1)$$

  An incomplete reduction might result in significant amounts of residual Cr(VI) within the Cr(III) product. This risk is particularly high for on-site produced Cr(III) sulfate. However, since professional tanners are recently importing Cr(III) sulfate the quality of the product is higher and the presence of Cr(VI) as impurity has been dramatically reduced.
- Generation during storage under unsuitable storage conditions (high temperature, UV exposure) [19,22].
- Oxidation from the free radicals generated by the unsaturated lipids, vegetable oils and natural fat in the presence of UV exposure [4].
- Direct photo-induced oxidation by natural UV lights in an open air.
- Direct oxidation by air at high pH during the neutralization of Cr(III).
- Direct oxidation in the presence of strong oxidizing agent under acidic conditions.
- Oxidation at high pH aid by mild oxidizing agents (e.g. neutralization of wet blue leather).
- Oxidation by high temperature (e.g. during the thermal treatment at 80°C for 24 hours to enhance the penetration of levelling agents like ammonia and sodium bicarbonate).
- Use of Cr(VI) pigments (e.g. lead chromate) in leather auxiliaries [23].

  Due to the above-mentioned reasons, a significant amount of Cr(VI) is discharged in

wastewater and can be found in the nearby ecosystem (discussed in chapter 2 and 5).

Unfortunately, chromium is a very important element in tanning. A few alternatives such as "green vegetable tanning" with tree barks and pods [24] can sometimes be used to confer specific properties to leather items. However, the long processing times, high costs and poor quality of leather products, along with the low thermal resistance and durability strongly hinder the applicability of vegetable as an alternative to Cr in industrial tannery operation [25,26].

### 1.5 Cr speciation in the aquatic condition in tannery effluent

Chromium in solution exists under two most stable oxidation sates, $Cr^{3+}$ and $Cr^{6+}$. At lower redox potentials Cr(III) is the predominant form that exists as free $Cr^{3+}$ in the range of pH 0-4 or as hydroxy-complex $Cr(OH)_x$ at higher pH (Fig. 1.4) [27]. On the other hand, Cr(VI) is the predominant Cr species in solution at higher redox potentials. At pH 8, which is the pH of the final wastewater produced in the BSCIC tannery industrial estate's CETP plant both $Cr(OH)_3$ and $CrO_4^{2-}$ (chromate ion) could be present in the wastewater.

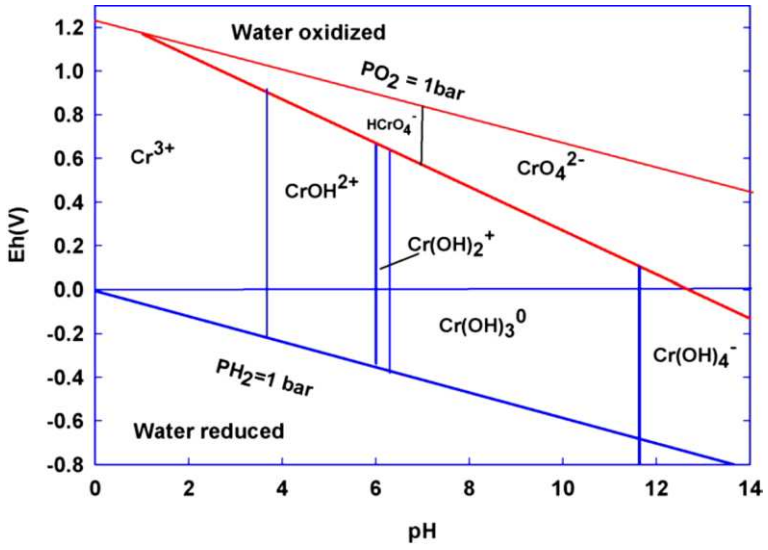


**Fig. 1.4 Eh–pH diagram for chromium** [27]

In the tannery process, chromium is used as $Cr^{3+}$ from a sulfate precursor, under acidic conditions (pH 2-3). Following the tannery operation, chromium enters the wastewater from where it can be easily removed as insoluble hydroxide by neutralization-precipitation with caustic soda (NaOH). The precipitation of Cr(III) occurs according to

equation (2) and takes place along with the precipitation of insoluble heavy metals hydroxides.

$$Cr(H_2O)_6^{3+} + 3OH^- \rightarrow Cr(H_2O)_3(OH)_3 + H_2O \quad (2)$$

The presence of $NH_3$ from the deliming and bating processes can help the precipitation of chromium hydroxide as in equation (3)

$$Cr(H_2O)_6^{3+} + 3NH_3 \rightarrow Cr(H_2O)_3(OH)_3 + 3NH_4^+ \quad (3)$$

However, excessive concentrations of ammonia could replace the water molecules in the chromium hydro-complex and keep Cr(III) soluble as hexa-ammine Cr(III) complex. In addition to chromium, the tanning process releases sulphide and thiosulfate as well as a large amount of COD, as it will be described in the next chapter.

### 1.6 Cr(VI) removal from tannery effluent

The conventional methods for removing Cr(VI) include a chemical reduction to Cr(III) in acid conditions followed by neutralization-precipitation above neutral pH with lime [28]. This precipitation technique was successfully employed to decrease the chromate concentration up to 10 mg/L but failed to meet the prescribed limit by Federal Environmental Protection Agency (FEPA) [29]. In addition, the method determines a large production of sludge.

Adsorption on activated carbon is also widely used [29] as it represents by far the most versatile removal method for Cr(VI) control [30]. However, the methods was proven efficient for chromate concentrations higher than 25 mg/L whereas major drawbacks have been reported for lower concentrations. In addition, the method is relatively expensive and non-suitable to be used in developing countries. This is because the activated carbon loaded with toxic species must be incinerated or disposed of in controlled landfills, whereas such infrastructure is hardly available in Bangladesh.

Innovative and potentially sustainable methods for removal of chromium from industrial effluents utilize lignocellulosic agricultural wastes [31], raw agricultural wastes [32], walnut hulls [33] and agricultural solid waste [34] as modified bio-sorbents. However, these methods are often inefficient to remove low concentrations of Cr(VI). In alkaline conditions. For example, Streptomyces (*Streptomyces rimosus)* biomass pre-treated with NaOH showed the best removal performance towards Cr(VI) at low pH and high initial concentration [35]. Chitosan/fly ash composites chrome shaving dust were

found capable to remove Cr(VI) only up to 33mg/L [36] [37]. Wheat bran from Punjab (Pakistan) [38] and egg-shells and fish scale [39] in Uganda showed interesting ability to remove Cr(VI) at low pH and around neutrality (pH 6-8). Sawdust, rice husk [40] and eucalyptus bark [41] also showed an interesting potential for chromate removal. However, a significant problem with lignocellulosic wastes is that they are not available everywhere and sometimes they are only seasonal. This is also the case of Teak (*Tectona grandis)* leaves [42]. In spite of an interesting removal ability, the leaves are highly localized, deciduous and not available in winter.

$Ba^{2+}$-modified Mongolian natural zeolites also showed a good ability towards the removal of Cr(VI) at high pH [43]. Nevertheless, the main drawback to the use of this kind of material is that its surface area strongly depends on the depth of the natural deposit. Therefore, efficient materials could be found only in deeper deposits, thus affecting the sustainability of the overall process.

Trace amounts of chromate could be removed from tannery wastewater by anion exchange resin with an efficiency higher than 98% within 20 minutes reaction, even in the presence of coexisting competing ions [29]. However, the used ion-exchange resins exhibited the best chromate removal at pH 4, whereas tannery wastewater is slightly alkaline (pH 8.10-8.50) (discussed in chapter 2). In addition, the above mentioned methods might require skilled human resources for resin preparation and maintenance and high costs for developing countries like Bangladesh.

The biological reduction of Cr(VI) through reducing bacteria was also proven possible [44]. However, due to the slow biological kinetics, the process is difficult to be applied in large-scale operations.

### 1.7 Rationale of the study

As later discussed (Chapter 2), the central effluent treatment plant of BSCIC tannery industrial estate has been struggling at removing low-concentrations of Cr(VI). Therefore, the Dhaleswari River area is in Danger and face the same devastating scenario as the Buriganga River.

This research aims to develop an efficient method to remove Cr(VI) from the tannery wastewater produced at the BSCIC tannery estate. The method to be developed must be suitable be integrated in the existing central effluent treatment plant and must be

sustainable for developing countries. The sustainability of the new method requires good removal performances at low-costs and the possibility to be implemented by semi-skilled/unskilled workers. An additional factor of sustainability that will be considered is the ability to remove Cr(VI) with a limited production of by-products like precipitation sludge.

As later explained, we identified suitable removing agents for Cr(VI) in iron oxide species such as ferrihydrite and green rust. The present thesis aims at developing a removal method based on them. Accordingly, the scientific goal of this research addresses the elucidation of the removal mechanism of the new developed method.

The first chapter of the thesis illustrates the major aspects related to Cr(VI) hazard to the environment and human health as well as the pollution arising from leather manufacturing in Bangladesh.

The second chapter presents details of leather manufacturing process at BSCIC tannery industrial estate and provides quantitative information about the pollution caused by Cr(VI). Moreover, it displays the mass balance of chromium within the process and identify the potential sources of pollution and their effect on the nearby living organisms. The chapter lays the foundation for the formulation of the research objectives.

In the third and fourth chapters, the removal of Cr(VI) by two different iron oxide compounds like ferrihydrite (chapter 3) and sulfate green rust (chapter 4), is given in detail. In addition, the chapters provide details on the experimental activity and the results that led to the elucidation of Cr(VI) removal performances and mechanism from simple Cr-bearing solution under controlled Ar atmosphere.

Fifth chapter highlights the industrial application of the outcomes of this research by exploring the ability of green rust to remove Cr(VI) from complex systems reproducing the real wastewater generated at the BSCIC under open-air atmosphere.

In the sixth chapter, the original findings of the thesis are summarized highlighting the removal of low concentrations of Cr(VI) from water by using efficient, low cost and easily accessible iron oxide compounds is practically possible. In addition, emphasizing that by well understood mechanism, it is possible to manipulate the end product and optimize Cr(VI) removal efficiency.

## 1.8 Summary

The leather manufacturing is a very complex process that transforms raw hides into finished leather goods. Tanning processes are mainly performed in developing countries like Bangladesh for low labour costs and loose environmental legislations. Although tanning represents a great business opportunity, it also threatens the environment surrounding the tannery estates. This is because the tannery process requires a great use of chemicals, among which chromium represents one of the main concern due to its well-known toxicity and carcinogenicity. Since more than 60,000 tons of raw hides are processed every year, the immobilization of Cr(VI) from tannery wastewater is essential.

Trying to address the Cr(VI) issue, the government of Bangladesh has shut down the tannery operation at the obsolete Hazaribag estate and moved them to the newly established BSCIC tannery industrial estate, near the Dhaleshwari River. Although the new BSCIC estate is provided with a central effluent treatment, the plant is not able to comply with the existing environmental standard, especially for chromium. Removal methods based on activated carbon and ion exchange resins have been efficiently used in advanced countries to remove Cr(VI) from the water. However, these methods are not suitable for developing countries like Bangladesh due to relatively high costs and maintenance difficulties.

The goal of this research is to develop an innovative method to immobilize chromate from tannery wastewater with high sustainability. The high sustainability requires efficiency, low cost, ease of conduction and maintenance as well as the use of largely available removing agents. Considering the above-mentioned criteria, the present research investigates the use of two iron oxide species, namely ferrihydrite and green rust. The following chapters of this thesis will describe more in details the pollution issue at the BSCIC tannery estate as well as the experimental investigations for efficient removal of Cr(VI) from simulated wastewater.

**References**


[1] UNIDO, Future Trends in the World Leather and Leather Products Industry and Trade, Vienna, Austria, 2010.

[2] H.L. Paul, A.P.M. Antunes, A.D. Covington, P. Evans, P.S. Phillips, SLTC J. 97 (2013) 25–32.

[3] M. Muchie, Technol. Soc. 22 (2000) 537–555.

[4] Green cross switzerland and Blacksmith institute for a pure earth, Pure Earth Green Cross (2016) 1–29.

[5] M. Pantsar-Kallio, S.P. Reinikainen, M. Oksanen, Anal. Chim. Acta 439 (2001) 9–17.

[6] M. Wiemann, H. Schenk, W. Hegemann, Water Res. 32 (1998) 774–780.

[7] M. Mwinyihija, in:, Ecotoxicological Diagnosis Tann. Ind., Springer New York, New York, NY, (2010) 91–123.

[8] Department of Environment, Report on Buriganga River, Dhaka, Bangladesh, 2016.

[9] Department of Environment, The Environment Conservation Rules, Ministry of Environment and Forests, Dhaka, Bangladesh, 1997.

[10] M. Kawser Ahmed, M.A. Baki, G.K. Kundu, M. Saiful Islam, M. Monirul Islam, M. Muzammel Hossain, Springerplus 5 (2016) 1697.

[11] J.O. Nriagu, E. Nieboer, Chromium in the Natural and Human Environments, First, John Wiley & Sons. Inc., New York City, NY, USA, 1988.

[12] B.S.J. Gray, K. Sterling, J. Clin. Invest. 2 (1950) 1604–1613.

[13] D.S. Ross, R.E. Sjogren, R.J. Bartlett, J. Environ. Qual. 10 (1981) 145.

[14] A.I. Hafez, M.S. El-Manharawy, M.A. Khedr, Desalination 144 (2002) 237–242.

[15] Z. Kowalski, J. Hazard. Mater. 37 (1994) 137–141.

[16] R. Shrivastava, R.K. Upreti, P.K. Seth, U.C. Chaturvedi, FEMS Immunology and Medical Microbiology. 34 (2002) 1–7.

[17] C. Vasant, K. Balamurugan, R. Rajaram, T. Ramasami, Biochem. Biophys. Res. Commun. 285 (2001) 1354–1360.

[18] A.G. Levis, V. Bianchi, in:, Biol. Environ. Asp. Chromium, Elsevier, (1982) 171–208.

[19] L.T. Mazumder, S. Hasan, M.L. Rahman, IOSR J. Environ. Sci. Toxicol. Food

Technol. 3 (2013) 44–51.

[20] J.A. Randall, R.S. Gibson, Exp. Biol. Med. 185 (1987) 16–23.

[21] C. Kornhauser, K. Wróbel, K. Wróbel, J.M. Malacara, L.E. Nava, L. Gómez, R. González, Ind. Health 40 (2002) 207–213.

[22] Chandrasekar R, Ganeshjeevan R Muralidharan C and Mandal A B, Central Leather Research Institute, Chennai, India, (2003) 1–7.

[23] B. Basaran, M. Ulas, B.O. Bitlisli, A. Asian, Indian J. Chem. Technol. 15 (2008) 511–514.

[24] M. Mwinyihija, in:, Ecotoxicological Diagnosis Tann. Ind., Springer New York, New York, NY, (2010) 1–15.

[25] B. Chandrasekaran, J. Raghava Rao, K.J. Sreeram, B.U. Nair, T. Ramasami, J. Sci. Ind. Res. (India). 58 (1999) 1–10.

[26] V.J. Sundar, J.R. Rao, C. Muralidharan, J. Clean. Prod. 10 (2002) 69–74.

[27] D. Mohan, C.U. Pittman, J. Hazard. Mater. 137 (2006) 762–811.

[28] A. Esmaeili, A. Esmaeili, A. Mesdaghi nia, R. Vazirinejad, Am. J. Appl. Sci. 2 (2005) 1471–1473.

[29] G. Kabir, S.E. Ogbeide, Int. J. Environ. Res 2 (2008) 377–384.

[30] D. Mohan, C.U. Pittman, J. Hazard. Mater. 137 (2006) 762–811.

[31] K.K. Krishnani, S. Ayyappan, Rev. Environ. Contam. Toxicol. 188 (2006) 59–84.

[32] G. Moussavi, B. Barikbin, Chem. Eng. J. 162 (2010) 893–900.

[33] X.S. Wang, Z.Z. Li, S.R. Tao, J. Environ. Manage. 90 (2009) 721–729.

[34] C. Namasivayam, M. V Sureshkumar, Bioresour. Technol. 99 (2008) 2218–2225.

[35] A. Chergui, M.Z. Bakhti, A. Chahboub, S. Haddoum, A. Selatnia, G.A. Junter, Desalination 206 (2007) 179–184.

[36] A. Rahaman, R. Hosen, M.A. Hena, U.H.B. Naher, M. Moniruzzaman, Int. J. Hum. Cap. Urban Manag. Int. J. Hum. Cap. Urban Manag. 1 (2016) 237–242.

[37] Y. Wen, Z. Tang, Y. Chen, Y. Gu, Chem. Eng. J. 175 (2011) 110–116.

[38] S. Asrar Ahmad, V. Un Nisa, Am. J. Toxicol. Sci. 5 (2013) 41–47.

[39] S. Bamukyaye, W. Wanasolo, Open Access Libr. J. 4 (2017) 1–13.

[40] D. Sivakumar, Glob. J. Environ. Sci. Manag. Glob. J. Environ. Sci. Manag. 1 (2015) 27–40.

[41] A.M. Xavier, A. Logeswari, S. Mano, Res. Inven. Int. J. Eng. Sci. 2 (2013) 2278–

4721.

[42] A.S. Jadhav, S.R. Bamane, C. Avadhutrao, S. Jadhav, International Journal of Applied Research (2016) 724–728.

[43] T. Bolortamir, R. Egashira, J. Chem. Eng. Japan 41 (2008) 1003–1009.

[44] M. Ilias, I.M. Rafiqullah, B.C. Debnath, K.S. Bin Mannan, M.M. Hoq, Indian J. Microbiol. 51 (2011) 76–81.

# [Chapter 2]

# Tannery practice and wastewater treatment process in Bangladesh

## 2.1 Introduction

Tanning is the process of transforming raw hides into leather. To transform the semi-soluble protein "collagen" present in hide/skins into highly durable commercial leather products, a large amount of organic and inorganic substances are required [1,2].

The tannery process is divided into four main stages, namely beam house operation (pre-tanning), tanyard process, retanning and finishing operations [3,4]. Each of them contributes to the generation of contaminated wastewater [1,2]. Most of the polluting load is determined by BOD, COD and TDS generated in soaking, liming, degreasing and pickling, whereas tanning is responsible for chromate discharge [5]. The discharge of this wastewater (Fig. 2.1) to the adjacent water bodies poses a great threat to ecology and human health [6,7].

The type of chemicals used in the tanning process and their quantity is completely based on the desired end-products. In addition to chromium, sulfonated oils and synthetic tannins or syntans (STs) (set of chemicals such as phenol, naphthalene, formaldehyde, melamine and acrylic resins) are used in tanning/retanning to soften the leather [8].

The main objectives of this chapter are to provide an overall idea of the tannery practice in Bangladesh, including the chemical inputs, duration and pollution load of every operation. Furthermore, the chromium mass flow analysis and the conventional wastewater treatment with relative drawbacks will be thoroughly presented. The description of each tannery operation is given through a holistic approach to the ideal condition. The chemical inputs and the relevant images of every step of the process were obtained from Reef leather (Pvt.) limited, Kalurghat industrial area, Chittagong and Samina tannery (Pvt.) limited, BSCIC industrial area, Savar, Dhaka.

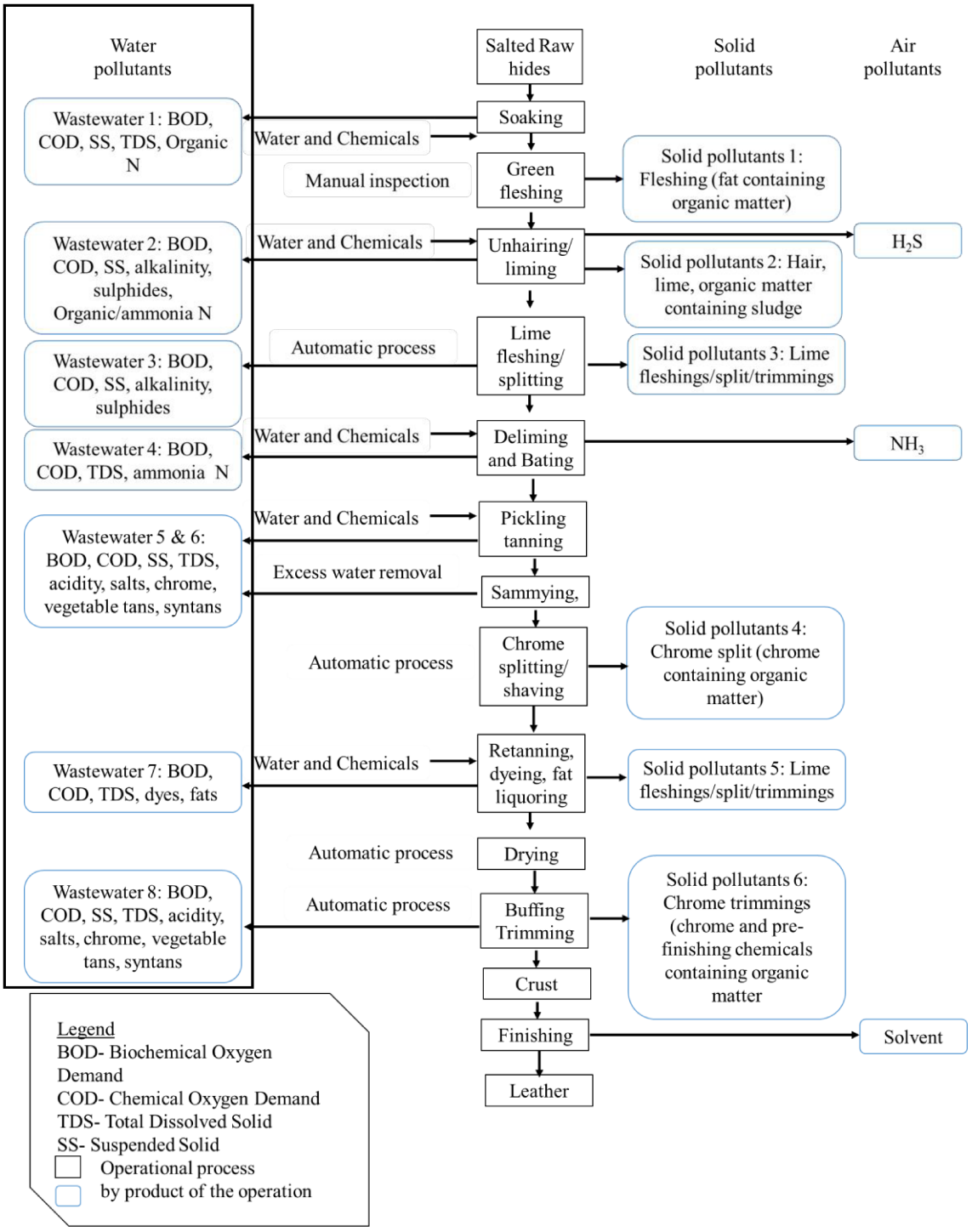


**Fig. 2.1 Flow chart of tannery process** [9]

## 2.2 Description of the tannery process

### 2.2.1 Soaking

Since Bangladesh is a tropical country with relatively high temperatures, the wet salted hides and skin dry-up to a considerable extent during storage and transportation. Therefore, the first operation in leather manufacturing aims to clean the raw hides from the excess of salt, blood and dirt and to soften them as much as possible to the state of green hides through the rehydration of the fibres [10]. This operation is called *soaking*.

The efficiency of soaking depends on the characteristics of the hides, soak water, temperature and duration. Usually, tanners make use of some auxiliary soaking agents to accelerate the operation and to prevent the bacterial contamination. The auxiliary soaking agents can be conveniently divided into three categories: (i) chemical soaking agents (salt, sodium sulphide, sodium sulpha-hydrate etc.), (ii) surface active agents and (iii) wetting and emulsifying agents. In addition, proteolytic enzymes might be used in neutral or slightly alkaline pH.

The ideal conditions for soaking are pH 7-10 and 25-28°C. Under this condition, the above described chemical agents assist soaking and emulsify the fat in hides/skin. Since soaking can be hindered be the presence of curing salts in concentrations higher than 5%, a pre-soaking operation is often carried out. Soaking usually requires 24-48 hours if performed manually and less than 24 hours using mechanical rotating drums (Fig. 2.2 and 2.3). The degree of soaking influences the beam house/pre-tanning and the next tanning operations as the dryness affects the dyes levelling and their penetration. A properly soaked skin contains 60-65% water (Table 2.1).

**Fig. 2.2 Raw salted hides ready to be processed**

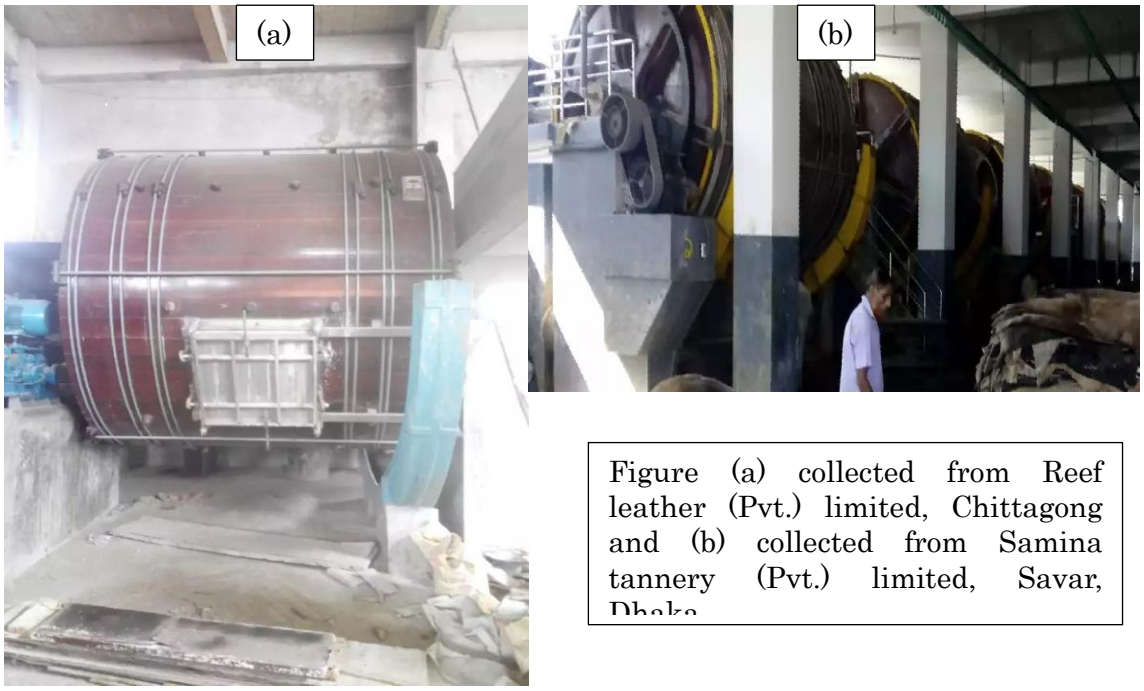


Figure (a) collected from Reef leather (Pvt.) limited, Chittagong and (b) collected from Samina tannery (Pvt.) limited, Savar, Dhaka

**Fig. 2.3 (a) Mechanical rotating drum for soaking and (b) Series of drums oriented for the processing of the raw hides**

**Table 2.1 Chemical inputs for the pre-soaking and main soaking**

| | | |
|---|---|---|
| Pre-soaking | Mixture: | 400% water= 4000 kg |
| | | 0.1% Degreasing and wetting agents= 1 kg |
| | Washing: | 800% water = 8000 kg |
| Main-soaking | Mixture: | 300% water= 3000 kg |
| | | 0.3% Degreasing agents = 3 kg |
| | | 1% soda ash = 10 kg |
| | | 0.2% antibacteria = 2 kg |
| | Washing: | 800%water = 8000 kg |

Inputs for 1000 kg of raw skins/hides.

### 2.1.2 Pre-treatment of the hides: liming-unhairing-fleshing-splitting

After soaking, *liming-unhairing* is performed to remove the epidermis (Table 2.2) and the hair from the skin (the operation is also known as depilation and/or unhairing). First, a lime solution is added to the hides to loosen the hair, and then, the loosened hair is removed in the depilation (unhairing) process. The fat naturally contained in the hides undergoes saponification and can be later removed by washing [10]. The operation is carried out for 24 hours at about 20°C, manually or in drums and produces an increase in weight of the hides of about 8-20% due to absorption of water. During liming, the contact with air should be avoided as much possible to prevent the production of calcium carbonate from the reaction between the calcium hydroxide and the $CO_2$ in the air. If this precaution was not adopted, white patches of calcium carbonate deposits on the skin, thereby leading to rough grains. This issue is known as “lime blasting”.

After loosening the hair and the epidermis, the unhairing operation is performed mechanically through a specific machine that scraps the hair off. This operation is not performed on the hides for chromium-tanning as the unhairing occurs chemically when the strong tanning liquor reduces the hair and the skin to an easily washable pulp.

Following the hair removal, the residual fat and skin are removed from the *fleshing* operation (Fig. 2.4) by passing the hides between two rolls, one with spiral knives, one covered with rubber.

Finally, in the *splitting* operation, the skins are passed through two cylindrical

rolls with knives in between and split horizontally. The top part of the split is valuable and goes to the tanning section. Although the operation is performed mechanically, the thickness of the splits is decided case-by-case by the technician.

**Table 2.2 Chemical inputs for liming**

| | | |
|---|---|---|
| Liming | Mixture: | 400% water = 4000 kg |
| | | 1% liming auxilary = 10 kg |
| | | 4% sodium sulfide = 40 kg |
| | | 4% lime= 40 kg |
| | | 0.2% degreasing agent = 2 kg |
| | Washing: | 800% water = 8000 kg |

Inputs per 1000 kg of skins/hides.

**Fig. 2.4 Automatic fleshing**

### 2.1.3 Deliming

The hides after liming, unhairing, fleshing and splitting are called pelts. Pelts consists of swollen hides due to the absorption of water and contain significant amounts of lime that must be removed before tanning (Table 2.3). For this purpose, a washing operation is carried out for 24 hours in running water, where about 60% of the total residual lime is removed. The final lime content in pelts may vary from 0.5 to 2% as weight. The degree of deliming depends on the flexibility required in the final leather product: the more flexibility is required for the final leather, the greater must be the extent of deliming. Nevertheless, a removal of lime over 60% is not sustainable in industrial applications. Removing the remaining lime requires neutralization with acids and/or acidic ammonium salts. Sometimes, it is advantageous to use a small amount of wetting agents along with delimers to enhance the rate of penetration into the inner layer of the fat pelts [10].

Heavy leather that will be tanned by vegetable tanning agents will be delimed only on the surface by washing for 20 minutes with soft water.

**Table 2.3 Chemical inputs for deliming**

| | | |
|---|---|---|
| Deliming | Mixture: | 200% water= 2600 kg |
| | | 2% ammonium sulfate = 26 kg |

Inputs per 1000 kg of raw hides (approximately 1300 kg of pelts due to water absorption)

### 2.1.4 Bating

Delimed pelts exhibit a very irregular surface with heterogeneous properties. To smoothen the surface and prepare fine pelts for tannery, the pelts undergo *bating* with enzymes (Table 2.4). The enzymes determine the removal of coagulable interfibrillary proteins, thereby increasing softness and stretchiness of the pelts. Important operating parameters in bating are time, temperature and volume of water.

**Table 2.4 Chemical inputs for bating**

| | | |
|---|---|---|
| Bating | Mixture: | 0.5% bating enzyme= 6.5 kg |
| | | 0.3% Degreasing agent = 3.9 kg |
| | Washing: | 1000% water = 13000 kg |

### 2.1.5 Pickling

Due to the natural composition of the hides and to the possible presence of residual lime, Cr(III) sulfate ($Cr_2(SO_4)_3 \bullet 12H_2O$) could be gradually exposed to alkaline conditions when penetrating the pelts and could precipitate as oxide ($Cr(OH)_3$) beyond pH 5. For this reason, the *Pickling* operation is carried out after bating to enhance the penetration of the tanning agents within the pelts. The operation consists of the acidification of the pelts below pH 3 using mineral or organic acids such as sulfuric, hydrochloric and/or formic acid for 14-16 hours. Lowering the pH below the iso-electric point of the proteins contained in the pelts enables also to activate the protein groups, thereby increasing the Cr absorption

### 2.1.6 Degreasing

The presence of excessive amounts of natural fat in the pelts lowers the quality of the final leather. This is because the fat can be oxidized during storage what results in an unpleasant odour of the final product. For this reason, a degreasing operation is performed to remove the residual natural fat contained in the skins before tanning. The most used degreasing agents are fat solvents such as kerosene, methylene chloride and trichloroethylene. Since these degreasing solvents are insoluble in water and could not penetrate the pelts, the use of emulsifiers is essential. Usually, 0.5-1.5% of emulsifiers are mixed with 10-20% solvent. Decreasing is performed in rotating drums by maintaining the rotation speed of 17-18 rpm for 30-45 minutes [10].

### 2.1.7 Cr-tanning

The process of *tanning* consists in the modification of the pelts properties through cross-linking of their collagen sub-units (Table 2.5). This operation is performed using Cr(III) sulfate. [11,12]. Cr(III) first dissolves in water as hexaaquachromium(III) cation $[Cr(H_2O)_6]^{3+}$ at low pH. Then, by increasing the pH, the as-dissolved ion undergoes olation to give polychromium(III) compounds, the active tanning agents [12]. The chemical reactions involved in olation are described in equations (1)-(3). By raising the pH, the Cr(III) hexa hydroxy complex first transforms into its conjugated base (1) and then polymerizes by reacting with hexa hydroxy complex in the acidic form (2).

$$[Cr(H_2O)_6]^{3+} \rightleftharpoons [Cr(H_2O)_5OH]^{2+} + H^+ \quad (1)$$

$$[Cr(H_2O)_6]^{3+} + [Cr(H_2O)_5OH]^{2+} \rightarrow [(Cr(H_2O)_5)_2(\mu\text{-}OH)]^{5+} + H_2O \quad (2)$$

Where $\mu$ denotes the hydroxyl group responsible for bridging the two metals. High pH and heat can favor the formation of polychromium diol, as in equation (3):

$$2[Cr(H_2O)_5OH]^{2+} \rightarrow [(Cr(H_2O)_4)_2(\mu\text{-}OH)_2]^{4+} + 2H_2O \quad (3)$$

The as-generated polychromium(III) penetrates between the protein chains in the skin collagen and establishes a cross-linking of about 15 Å between them [13]. As a consequence, the tanned material becomes lighter, more durable and resistant to heat and water. In addition, the increased distance between the protein chains of collagen determines an easier penetration of the dying agents in the finishing operations. Upon tanning, the pelts' fibres appear dark blue-green and are often called wet blue (Fig. 2.5).

In tanning, the pH must be kept in the low range (pH 2-3.5) to avoid the aquo-complexation of the chromium ions so that the penetration into fibres and collagen residues can take place. A higher pH would not allow a satisfactory penetration of Cr(III) and would cause over tanning of the outer skin layer, thus resulting into the darkness of the grain.

Once the desired level of penetration is achieved, the pH can be gradually raised up to 4.5 through the addition of sodium bicarbonate and the temperature can be increased up to 40°C [14].

**Table 2.5 Chemical inputs for pickling and chrome tanning**

| | | |
|---|---|---|
| pickling and chrome tanning | Mixture | 8% sodium chloride= 104 kg<br>0.2% sodium chlorite = 2.6 kg<br>0.5% Formic acid = 6.5 kg<br>1% sulfuric acid = 13 kg<br>0.4% hypo= 5.2 kg<br>8% chrome(III) sulfate = 104 kg<br>0.5% sodium formate = 6.5 kg<br>0.1% fungicide = 1.3 kg<br>0.5% Magnesium oxide= 6.5 kg<br>100% water= 1300 kg |

Inputs per 1000 kg of raw hides (approximately 1300 kg of pelts)

**Fig. 2.5 Wet-blue piled and waiting for the next operations**

### 2.1.8 Retanning

Performing only one tanning operation is not enough to keep up with the modern demand for high-quality leather products. For this reason, the tanned leathers are always re-tanned a second time. After the first tanning operation, the leather is set out and sammed to reduce the water content to about 45-50% (Fig. 2.6). Following this step, the leather is either split into layers or shaved to reduce the thickness to the required extent (Fig. 2.7). These operations determine a dramatic weight decrease of the feed that goes to retanning. After samming and shaving/splitting, the pelts fed in retanning represent about 20% of initial the initial weight.

**Fig. 2.6 Mechanical samming of pelts**

**Fig. 2.7 Mechanical splitting of pelts**

The presence of acidity prior to dyeing or fat liquoring eventually reduces the leather's strength and can cause the leather rotting. Thus, neutralization is often performed while retanning. The principal retanning agents in Bangladesh are basic chrome with

formaldehyde and neutralizing syntans (Table 2.6).

Retanning with Cr(III) increases the chrome content and enhances softness and firmness of grains. The neutral synthetic retanning agents provide a good aid in equalising the pH throughout the leather thickness so that the subsequent retanning agents (e.g. dye, fats, etc.) can be evenly distributed.

**Table 2.6 Chemical inputs for retanning**

| | | |
|---|---|---|
| Retanning | Mixture: | 0.2% Degreasing agent = 0.4 kg |
| | | 0.3% formic acid = 0.6 kg |
| | | 3% neutralizing syntans = 6 kg |
| | | 6% chrome(III) sulfate = 12 kg |
| | | 2% aldehyde = 4 kg |
| | | 400% water= 800 kg |

Inputs per 1000 kg of raw hides (approximately 200 kg of shaved pelts)

### 2.1.9 Dyeing and fat liquoring

*Dyeing* is performed to improve the aspect of the finished leather. The operation not only increases the product value as a commodity but also contributes to its general quality [10].

**Table 2.7 Chemical inputs for dyeing and fat liquoring**

| | | |
|---|---|---|
| Dyeing and fat liquoring | Mixture: | 1% synthetic fat liquor = 2 kg |
| | | 5% acrylic resin=10 kg |
| | | 10% other synthetic resin= 20 kg |
| | | 5% syntans= 10 kg |
| | | 10% vegetable extract= 20 kg |
| | | 1-6% Dye = 2-12 kg |
| | | 5-10% fat liquor=10-20 kg |
| | | 2-4% formic acid = 4-8 kg |
| | Mixture: | 200% water – 400 kg |

Inputs per 1000 kg of raw hides (approximately 200 kg of shaved pelts)

To prevent the leather from drying out, the tanned products are treated with oils, fats and/or greases in an operation called fat liquoring (Table 2.7). A proper treatment

with oils and fats confers flexibility as well as additional strength to the leather. However, duration of each steps (Table 2.8) as well as processing required for the finish goods are given below for clear understanding of complex tannery process (Fig. 2.8-2.12).

**Table 2.8 Conventional time requirements of every step of tannery practice in Bangladesh**

| Operation | Duration |
|---|---|
| Pre-soaking | 1 hour |
| Main soaking | 14 hours |
| Liming and unhairing | 22-24 hours |
| Deliming | 2-3 hours |
| Bating | 1 hours |
| Pickling and chrome tanning | 14-16 hours |
| Wet blue piling for ageing | Minimum 7 days |
| Retanning | 5-7 hours |
| Dyeing | 9-12 hours |

Data collected from Samina tannery (Pvt.) limited, Savar, Dhaka

**Fig. 2.8 Mechanical setting after retanning and dyeing**

**Fig. 2.9 Manual toggling**

**Fig. 2.10 Hydraulic press machine to emboss the leather**

**Fig. 2.11 Vacuum dryer**

**Fig. 2.12 Tunnel dryer**

## 2.3 Pollution load and material flow analysis (MFA) of Cr

The systematic approach of tannery practice has just begun in Bangladesh. As a result, step wise information is often missing. For this reason, the potential impact of tanning operations is still unknown. Nevertheless, a simplified material flow of chromium based on on-field observations and literature information is reported in Fig. 2.13.

The sectoral pollution load in Table 2.9 shows that soaking produces about 42% of the total wastewater, whereas retanning dyeing and fat liquoring produce below 3% of the total volume. The release of chromium in water is almost entirely due to tanning and re-tanning operations, where about 15 kg of Cr(III) sulfate salts are used per tons of raw hides (Fig. 2.13). About 50-70% of the Cr(III) used in tanning and re-tanning is absorbed by the hides while the remaining part is discharged in water. The Cr-bearing spent liquors from tanning and re-tanning operations are sent to a chromium recovery section, where 90% of Cr(III) is precipitated at pH to 7.5-8 by dosing NaOH. The liquid stream generated in the Cr(III) recovery section is sent to the central effluent treatment plant (CETP). In contrast, the wastewater generated in pre-tanning and post-tanning contains too low concentrations of Cr that are inconvenient to recover and it is sent directly to the CETP.

The concentration of chromium in the final effluent flowing out from the CETP of the BSCIC tannery industrial estate is 10-15 mg/L, accounting for a chromium content of about 2.8% of the total input (Fig. 2.13). The residual Cr in the final wastewater is Cr(VI), which is well-known for remaining soluble even in alkaline media. Given the 20000 $m^3$ of wastewater flowing out of the CETP per day, the adjacent surface water of the Dhaleshwari River is threatened by the continuous discharge of 210 kg of Cr(VI) per day.

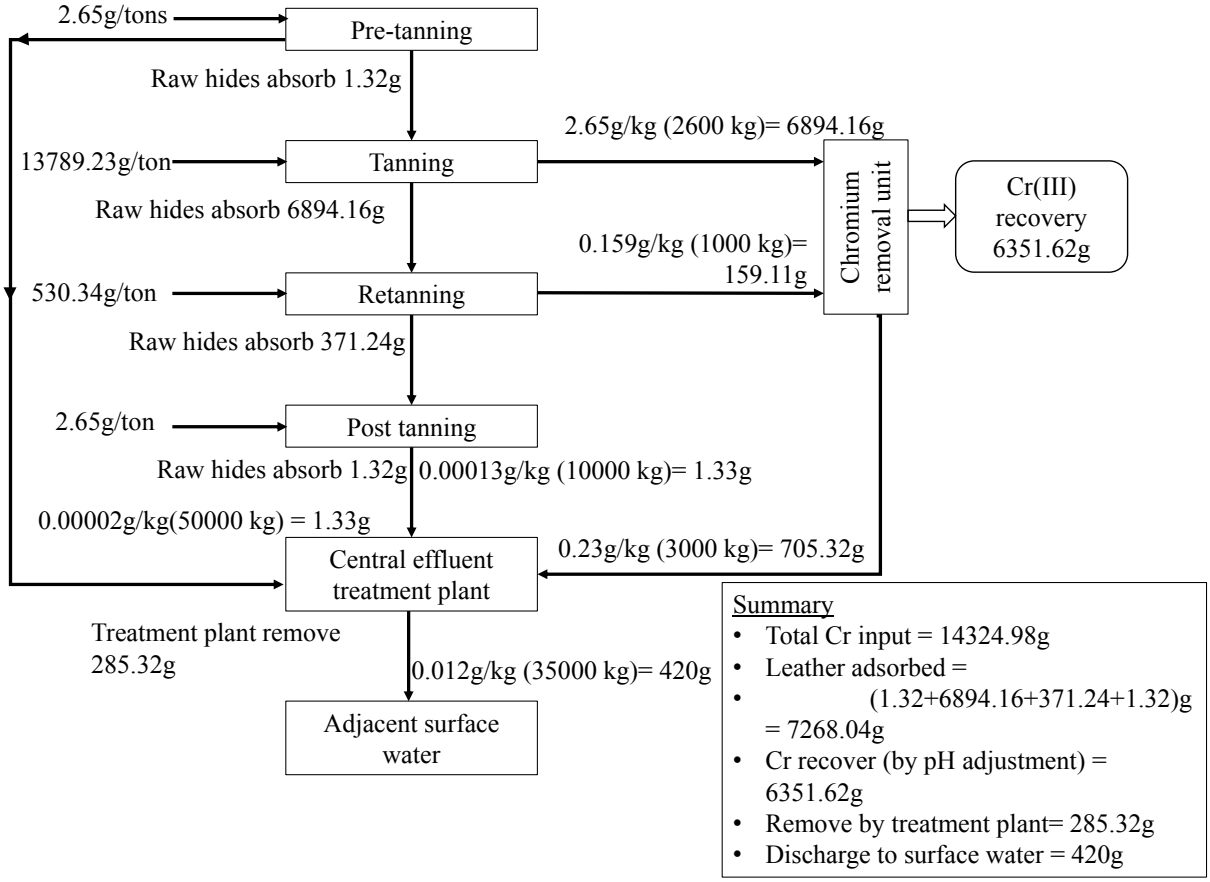


**Fig. 2.13 Flow chart of tannery process at the BSCIC tannery industrial estate and Cr mass balance for 1 ton of raw hides**

**Table 2.9 Chemical load for processing 1 ton raw hides (Data from Samina tannery Pvt. Ltd, Dhaka, Bangladesh)**

| Process name | Chemicals name and input (kg/t) | Wastewater discharged (kg/t) | Sectoral contribution to total (%) |
|---|---|---|---|
| Soaking | Degreasing agents = 3 | 18400 | 42.8 |
| | Soda ash = 10 | | |
| | Antibacterial agent = 2 | | |
| Liming | Sodium sulfide = 40 | 9600 | 22.3 |
| | Lime= 40 | | |
| | Degreasing agent = 2 | | |
| Deliming | Ammonium sulfate = 26 | 2080 | 4.8 |
| Bating | Bating enzyme= 6.5 | 10400 | 24.1 |
| Tanning | Sodium chlorite = 5.2 | 1300 | 3 |
| | Cr(III) sulfate=104 | | |
| | Formic acid = 13 | | |
| | Hypo= 10.4 | | |
| | Sodium formate = 13 | | |
| | Fungicide = 2.6 | | |
| | Magnesium oxide= 13 | | |
| Retanning | Formic acid = 0.6 | 800 | 1.9 |
| | Cr(III) sulfate= 12 | | |
| | Neutralizing syntans = 6 | | |
| | Aldehyde = 4 | | |
| Dyeing and fat liquoring | Synthetic fat liquor = 2 | 400 | 0.9 |
| | Acrylic resin=10 | | |
| | Other synthetic resin= 20 | | |
| | Syntans= 10 | | |
| | Vegetable extract= 20 | | |
| | Fat liquor=10-20 | | |
| | Formic acid = 4-8 | | |

## 2.4 Wastewater in conventional tannery of Bangladesh

At present, there are 220 tanneries in Bangladesh that are continuously discharging hazardous wastewater into the environment. In general, processing 1 ton of raw hides results in the generation of 30-40 $m^3$ of effluents containing chlorides, tannins, chromium, sulphate, sulphides, synthetic organic chemicals such as pesticides, dyes, finishing agents and chemical solvents [19]. Tannery wastewater is also highly rich in COD and contain organic nitrogen and phosphorous [15] that can facilitate the eutrophication in water catchment areas [2]. Moreover, the dark brown colour of wastewater can hinder the natural photosynthetic processes [20].

The beam house (pre-tanning) operation are responsible mainly for the discharge of COD and sulphide (Table 2.10) at high pH. Tanning operation produces chloride, ammonium, sulfate and chromium release [4], often at low pH [8,21]. Retanning operations release in water synthetic tannin (syntans), oils and resins [22] while dyeing and fat liquoring contribute to the overall polluting load with volatile organic compounds (VOC) due to the use of solvents [23].

Bosnic et al. (2000) reported that post-tanning processes are the main sources of metallic pollution in the tannery wastewater. This is because different types of azo dyes, insecticides, biocides, heavy metal's derived pigments are often utilized to improve the aspect of leather products [24]. The concentrations of trace metallic constituents in the tannery wastewater are listed in Table 2.11. Samples collected from the equalizer tank showed the highest concentration of metals whereas the ones from the adjacent discharged drain exhibited the lowest concentrations. This might be due to the dilution of the samples with drain water, sedimentation, coagulation, and precipitation of metals from the effluent samples [25].

**Table 2.10 Physical-chemical characteristics of tannery effluents at different manufacturing stages in Bangladesh** [26]

| Parameter | Soaking | Liming and unhairing | Deliming and bating | Pickling and tanning | Retanning and dyeing | Fat liquoring | Post-tanning and finishing operational effluents |
|---|---|---|---|---|---|---|---|
| Colour | Dark brownish | White | Creamy white | Dark blue | Black | Light black | Black |
| Temp (°C) | 27 ± 1 | 25 ± 0.5 | 35 ± 1 | 25 ± 1 | 40 ± 3 | 50 ± 4 | 30 ± 1 |
| pH | 8.2 ± 0.5 | 12.5 ± 0.5 | 6.5 ± 0.6 | 3.8 ± 0.2 | 4.0 ± 0.5 | 4.01 ± 0.5 | 4.2 ± 0.5 |
| EC (mS/cm) | 19 ± 1 | 13 ± 2 | 12 ± 1 | 295 ± 15 | 142 ± 10 | 94 ± 10 | 8.2 ± 1.2 |
| TSS(mg/L) | 6080 ± 10 | 11000 ± 5 | 11000 ± 10 | 1000 ± 20 | 850 ± 20 | 820 ± 90 | 1240 ± 40 |
| TDS(mg/L) | 14500 ± 10 | 12500 ± 6 | 12000 ± 25 | 156700 ± 50 | 50950 ± 10 | 4100 ± 100 | 8100 ± 50 |
| TS(mg/L) | 20580 ± 11 | 23300 ± 6 | 22800 ± 25 | 157700 ± 50 | 51800 ± 50 | 4920 ± 100 | 9340 ± 70 |
| COD(mg/L) | 10560 ± 6 | 4800 ± 5 | 4200 ± 10.5 | 49000 ± 40 | 71040 ± 40 | 17000 ± 70 | 7200 ± 20 |
| $BOD_5$(mg/L) | 1200 ± 6 | 700 ± 8 | 700 ± 10 | 2000 ± 10 | 2400 ± 70 | 1900 ± 100 | 1000 ± 50 |

Data collected from three selected tannery at Hazaribagh, Dhaka

**Table 2.11 Concentration of trace metallic constituents in equalization tank and discharged drain of tannery wastewater in Bangladesh** [25]

| | Cr | Cd | Pb | Cu | Zn | Fe | Mn |
|---|---|---|---|---|---|---|---|
| Equalization tank (mg/L) | 6769.5 ± 1.6 | 2.2 ± 2.0 | 32.0 ± 6.9 | 2.6 ± 4.4 | 8.7 ± 2.1 | 108.6 ± 3.0 | 17.2 ± 5.6 |
| Discharged drain (mg/L) | 14.3 ± 1.2 | 1.5 ± 4.1 | 18.8 ± 4.1 | 1.5 ± 5.8 | 0.7 ± 3.5 | 1.4 ± 5.4 | 3.5 ± 3.0 |

## 2.5 Wastewater treatment process at the BSCIC tannery industrial estate

The nature of tannery effluent is complex and depends on the end leather product that is produced [15]. For this reason, no specific treatment process can be prescribed as the best treatment option and the most appropriate approach must be developed case by case [16].

The conventional tanneries in Bangladesh mix the beam house wastewater with tan yard wastewater, thus producing lethally poisonous hydrogen sulphide gas, which is still by far the most frequent cause of death in tannery accidents. Considering this trend of tannery effluent treatment/management, Paul et al. (2013) [17] proposed a simplified and generalized tannery effluent treatment process for Bangladesh. Although their process was cost-effective and easy to implement, it could not ensure the environmental compliance. Furthermore, in the recent times, the Government of Bangladesh expressed the preference for ad-hoc designed processes, where each operation would be optimized for the specific wastewater and chromium could be recovered from the sludge.

In 2010, UNIDO (United Nations Industrial Development Organization) suggested that the effluent treatment plant [9] should have a section for chromium recovery. Following this suggestion, the Government of Bangladesh has set up a common effluent treatment plant (CETP) at BSCIC tannery industrial estate (Fig. 2.14). The CETP is designed to treat 20,000 $m^3$ of tannery effluent and 5,000 $m^3$ of sewerage per day. The treatment process is comprised of 3 chromium recovery units and it is linked with 3 effluent pumping station (EPS). In EPS, wastewater is firstly screened and pumped to the CETP where ferrous sulphate, poly aluminium chloride and poly acrylamide are used as coagulants and flocculants. Following these operations, sedimentation, clarification and denitrification are carried out in oxidation ditches A and B (Fig. 2.14).

**Table 2.12 Quality of the effluent discharged at the BSCIC tannery industrial estate**

| Parameter | CETP inlet (after Cr recovery) | CETP outlet | Standard effluent discharge limit in Bangladesh [27] |
|---|---|---|---|
| pH | 6.2 | 8.2 | 6-9 |
| DO (mg/L) | 0 | 0.2 | >5 (Surface water) |
| BOD (mg/) | 495 | 100-350 | 100 |
| COD (mg/L) | 1400 | 250-1000 | - |
| Total Cr (mg/L) | 203 | 10-15 | 2 |

The effluent discharged at the BSCIC tannery estate, (Table 2.12) contains high BOD, COD and very low DO. The DO of the discharged effluent is extremely low compared to the standard of inland surface water for irrigation and fisheries in absence of tannery effluent/river water standard in Bangladesh.

Since the foreign contractor at the CETP does not handover any technical information related to the treatment process to the BSCIC authority, further details cannot be provided in this thesis. Nevertheless, although the CETP is equipped with Cr recovery sections, the regular monitoring highlighted excessive concentration of Cr after the CETP. This evidence proves the inefficiency of the wastewater treatment process and suggests that an improvement is highly required to reduce the chromium pollution.

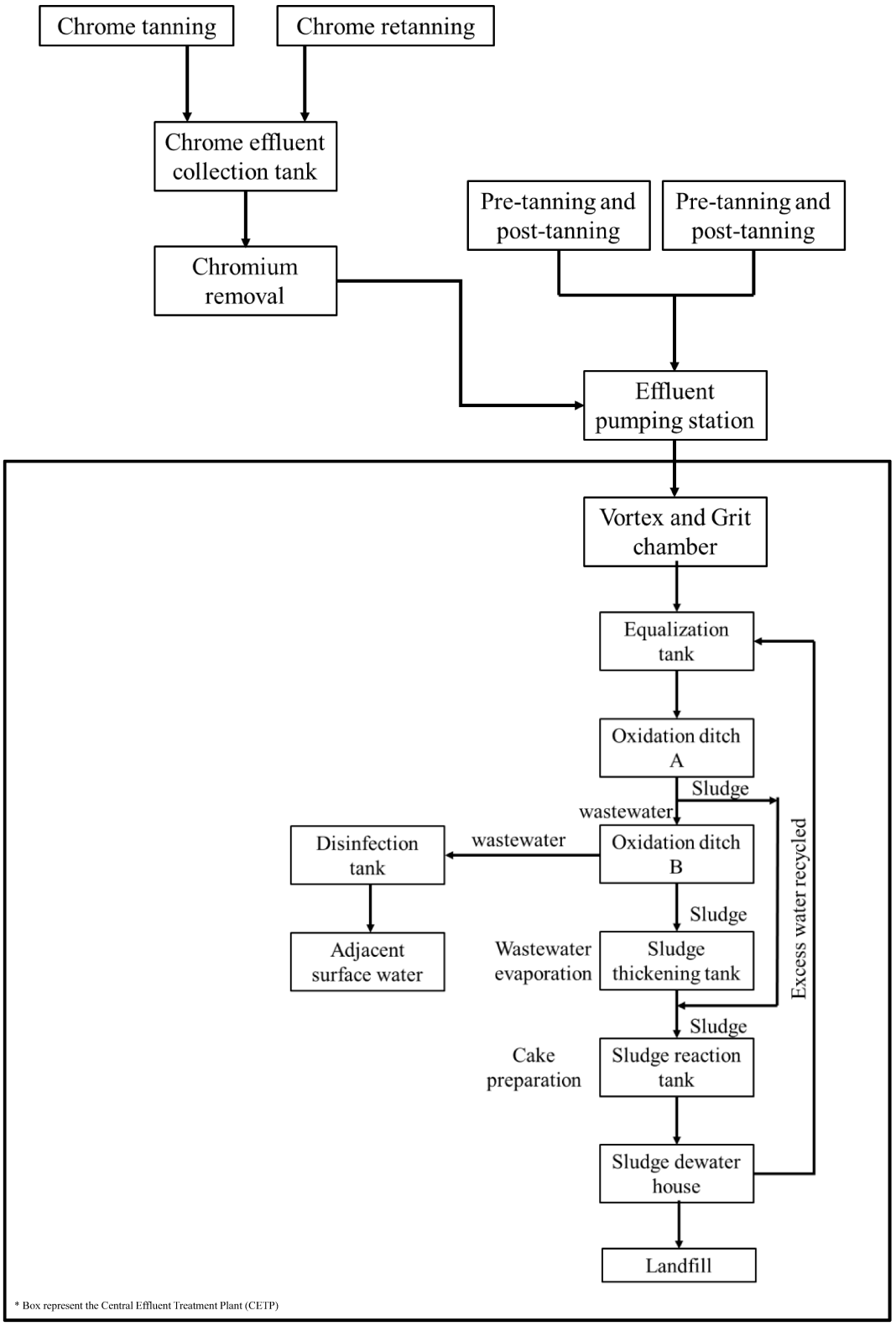


**Fig 2.14 Wastewater treatment flowchart at BSCIC tannery industrial estate**

## 2.6 Summary

The tannery process consists of a complex sequence of operations. The main operations in the process are soaking (preliminary washing to rehydrate the skins and remove dirt and excess of salt), liming (removal of hair and fat), deliming (removal of excess of lime used on liming), bating (softening through enzyme baths), tanning-retanning (absorption of chromium into the skins), dyeing and fat liquoring (coloring and fixing the texture), each of them contributing to the overall release of chemicals into wastewater.

Although the central effluent treatment significantly reduces the pollution load of the wastewater, it was found inefficient to immobilize the residual chromate. As a consequence, over 20,000 $m^3$ of wastewater containing 10-15 mg/L of chromate are being discharged every day in the nearby water bodies. This issue has been threatening eco-system and human health and must be solved as soon as possible by developing innovative and sustainable methods for chromate removal.

The upcoming chapters will describe the study of innovative and sustainable methods for chromate removal that could be integrated within the CETP at the BSCIC tannery estate.

**References**


[1] G. Lofrano, E. Aydin, F. Russo, M. Guida, V. Belgiorno, S. Meric, Water, Air, Soil Pollut. Focus 8 (2008) 529–542.

[2] R.N. Saxena, G., Chandra, R. and Bharagava, in:, P. De Voogt (Ed.), Rev. Environ. Contam. Toxicol., Switzerland, (2017) 31–70.

[3] O. Tunay, I. Kabdasli, D. Orhon, E. Ates, Water Sci. Technol. 32 (1995) 1–9.

[4] K. Cooman, M. Gajardo, J. Nieto, C. Bornhardt, G. Vidal, Environ. Toxicol. 18 (2003) 45–51.

[5] B. Islam, A. Musa, E. Ibrahim, S. Sharafa, B. Elfaki, J. For. Prod. Ind. 3 (2014) 141–150.

[6] S. Dixit, A. Yadav, P.D. Dwivedi, M. Das, J. Clean. Prod. 87 (2015) 39–49.

[7] S. Saravanabhavan, P. Thanikaivelan, J.R. Rao, B.U. Nair, T. Ramasami, Environ. Sci. Technol. 38 (2004) 871–879.

[8] G. Lofrano, S. Meriç, G.E. Zengin, D. Orhon, Sci. Total Environ. 461–462 (2013) 265–281.

[9] I. Buljan, J., Kral, Introduction to Treatment of Tannery Effluents What Every Tanner Should Know about Effluent Treatment, Vienna, Austria, 2011.

[10] K.T. Sarkar, Theory and Practice of Leather Manufacture, 4th ed., pub;K. T. Sarkar, Madras, India, 1997.

[11] J.A. Wilson, The Chemistry of Leather Manufacture, Second edi, American Chemical Society Monograph Series. The Chemical Catalog Co. Inc, new york, 1929.

[12] A.D. Covington, Chem. Soc. Rev. 26 (1997) 111.

[13] K.H. Gustavson, The Chemistry of Tanning Processes, First Edit, Academic Press Inc., New York, 1956.

[14] E. Heidemann, in:, Ullmann's Encycl. Ind. Chem., Wiley-VCH Verlag GmbH & Co. KGaA, Weinheim, Germany, 2000.

[15] G. Durai, M. Rajasimman, J. Environ. Sci. Technol. 4 (2011) 1–17.

[16] G.M. Ayoub, A. Hamzeh, M. Al-Hindi, Water. Air. Soil Pollut. 224 (2013).

[17] H.L. Paul, A.P.M. Antunes, A.D. Covington, P. Evans, P.S. Phillips, SLTC J. 97 (2013) 25–32.

[18] G. Sharma, A.K. Dwivedi, Jr. of Industrial Pollution Control. 28 (2012) 1–4.

[19] Anonymous., Unione Nazionale Industria Conciaria. Environmental Report., Milan, Italy, 2009.

[20] U.N. Rai, S. Dwivedi, R.D. Tripathi, O.P. Shukla, N.K. Singh, Bull. Environ. Contam. Toxicol. 75 (2005) 297–303.

[21] D. Rameshraja, S. Suresh, Int. J. Environ. Res. 5 (2011) 349–360.

[22] G. Lofrano, V. Belgiorno, M. Gallo, a Raimo, Glob. NEST J. 8 (2006) 151–158.

[23] E.I. V. Beem, J. Oil Col. Chem. Ass. 77 (1994) 158.

[24] M. Bosnic, J.B. And, R.P. Daniels, United Nations Ind. Dev. Organ. 9 (2000) 26.

[25] M.M. Kabir, A.N.M. Fakhruddin, M.A.Z. Chowdhury, Z. Fardous, R. Islam, Pollution 3 (2017) 395–406.

[26] M. Chowdhury, M.G. Mostafa, T.K. Biswas, A. Mandal, A.K. Saha, Environ. Process. 2 (2015) 173–187.

[27] Department of Environment, The Environment Conservation Rules, Ministry of Environment and Forests, Bangladesh, Dhaka, Bangladesh, 1997.

# [Chapter 3]

# Removal of Cr(VI) from water by coprecipitation with ferrihydrite: mechanism elucidation

## 3.1 Introduction

Hexavalent chromium, Cr(VI) has been attracting researchers' attention because it is toxic, bioavailable and difficult to remove from water, especially at low concentration. Toxic anions like chromate are usually immobilized by methods such as chemical precipitation, oxidation-reduction, membrane nano-filtration, reverse osmosis, ion exchange and adsorption have been preferred in the latest years [1–6]. Among them, adsorption is considered as one of the most attractive methods due to its relatively low costs, easy implementation and high sustainability [7,8].

In general, the adsorption of toxic species onto adsorbing agents can be realized by simply adding the solid adsorbing material (adsorbent) to the solution bearing the metal ions to be removed (adsorbate). Alternatively, the adsorbing material can be also directly generated within the solution containing the species to be removed. In this case, the adsorption is said to be realized *via* coprecipitation.

Naturally available iron oxy-hydroxide, namely ferrihydrite (Fh) [$(Fe^{3+})_2O_3 \cdot 0.5H_2O$], has shown an interesting potential as adsorbing material for low concentrations of Cr(VI) [9]. Fh is a widespread hydrous ferric oxy-hydroxide mineral [10,11] that can be found in freshwater and marine systems, aquifers of hydrothermal hot springs, soils, and areas affected by mining. Due to the large surface area and high density of local defects (e.g. dangling bonds, vacancies), Fh exhibits large adsorption capacity towards many environmentally important chemical species [9]. Therefore it could play a key role in wastewater treatment and in particular in removing chromate from tannery wastewater. In addition, natural ferric oxy-hydroxide minerals are largely available and easily obtainable by precipitation from iron precursor solutions. Therefore, a hypothetical coprecipitation of chromate with Fh would be cost-effective and could be easily integrated into already established wastewater treatment processes in developing countries like Bangladesh.

The use of Fh as adsorbing agent for chromate has been widely investigated for a few decades. Most studies investigated the effect of operating parameters like pH on removal characteristics and kinetics [12–14]. As for removal mechanism, the scientific literature highlights fewer information. Based on energy dispersive analysis x-ray (EDAX) and fourier-transform infrared spectroscopy (FTIR) results Hsia et al. (1993) [15] reported that chromate was adsorbed onto iron oxide *via* inner-sphere coordination.

However, the authors mostly speculated about the specific sorption mechanism but did not actually provide any evidence [15]. Chad and Maria (2012) investigated the same aspect by in-situ ATR-FTIR spectroscopy and found monodentate and dominant bidentate coordination at pH < 6 [16]. However, $N_2$ flushed environments, freeze drying methods and washing applied in that research might lead to inner-sphere coordination at very lower Cr/Fe molar ratio. Takahashi et al. (2015), examined the Fh-chromate interaction at pH 4 by EXAFS Cr-Fe second shell fitting. Authors highlighted a coordination number as low as 0.4, thus suggesting mostly outer-sphere complexation with a lower contribution of inner sphere complexation [17]. However, when performing the EXAFS fitting, authors used a fixed value of Debye-Waller factor and this operation might have led to inaccuracies.

Given the few and often contrasting available information, it is reasonably to consider the adsorption mechanism of chromate onto Fh is not fully understood yet. In addition, whereas the above mentioned research works were based on adsorption, there are no detailed studied on chromate immobilization through coprecipitation with Fh.

Novelty of the present study includes the identification of sorption mechanism in coprecipitation based on a detailed discussion of EXAFS fitting results.

## 3.2 Materials and methods

### 3.2.1 Materials and stock solutions

All chemicals and solutions used in this work were analytical grade reagents purchased from Wako Pure Chemical Industries, Tokyo, Japan. The Cr(VI) and Fe(III) solutions to be used in adsorption and coprecipitation experiments were prepared dissolving $K_2CrO_4$ and $Fe(NO_3)_3 \cdot 9H_2O$ in ion-exchanged and distilled water. In all experiments, pH and ionic strength were adjusted by addition of 0.1 M $HNO_3$ and 0.1 M KOH.

### 3.2.2 Fh reference materials

Fh to be used as reference material in XRD and XAFS analysis was synthesized dissolving $Fe(NO_3)_3 \cdot 9H_2O$ in ion-exchanged and distilled water and by adjusting the pH to 7 through the addition of 0.1 M NaOH, as described by Cornell and Schwertmann [10]. The initial Fe(III) concentration was set at 20 mg/L in all experiments. Fh was allowed to form under magnetic stirring and controlled ion strength (0.05 M) at 25 ℃.

### 3.2.3 Coprecipitation experiments

In coprecipitation experiments, Fh was allowed to form and precipitate in the presence of Cr(VI), as elsewhere reported [18–21]. Cr(VI) concentration was fixed at 10 mg/L while the Fe(III) solution was added up to the desired Cr/Fe molar ratio (0.05, 0.1, 0.5, 1, 5, 10). The resulting solutions were mixed for 1 hour at 25°C, under controlled ionic strength (0.05 M) and pH (5, 7). After 1 hour, the suspensions were filtered through 0.1 μm membrane filters. The filtrate was directly stored for analysis while solid residues were freeze-dried at -45°C and 10 Pa for 24 h to avoid crystallization and/or mineralogical transformation. The experimental flowchart of coprecipitation is reported in Fig. 3.1. Coprecipitation experiments were performed in triplicates.

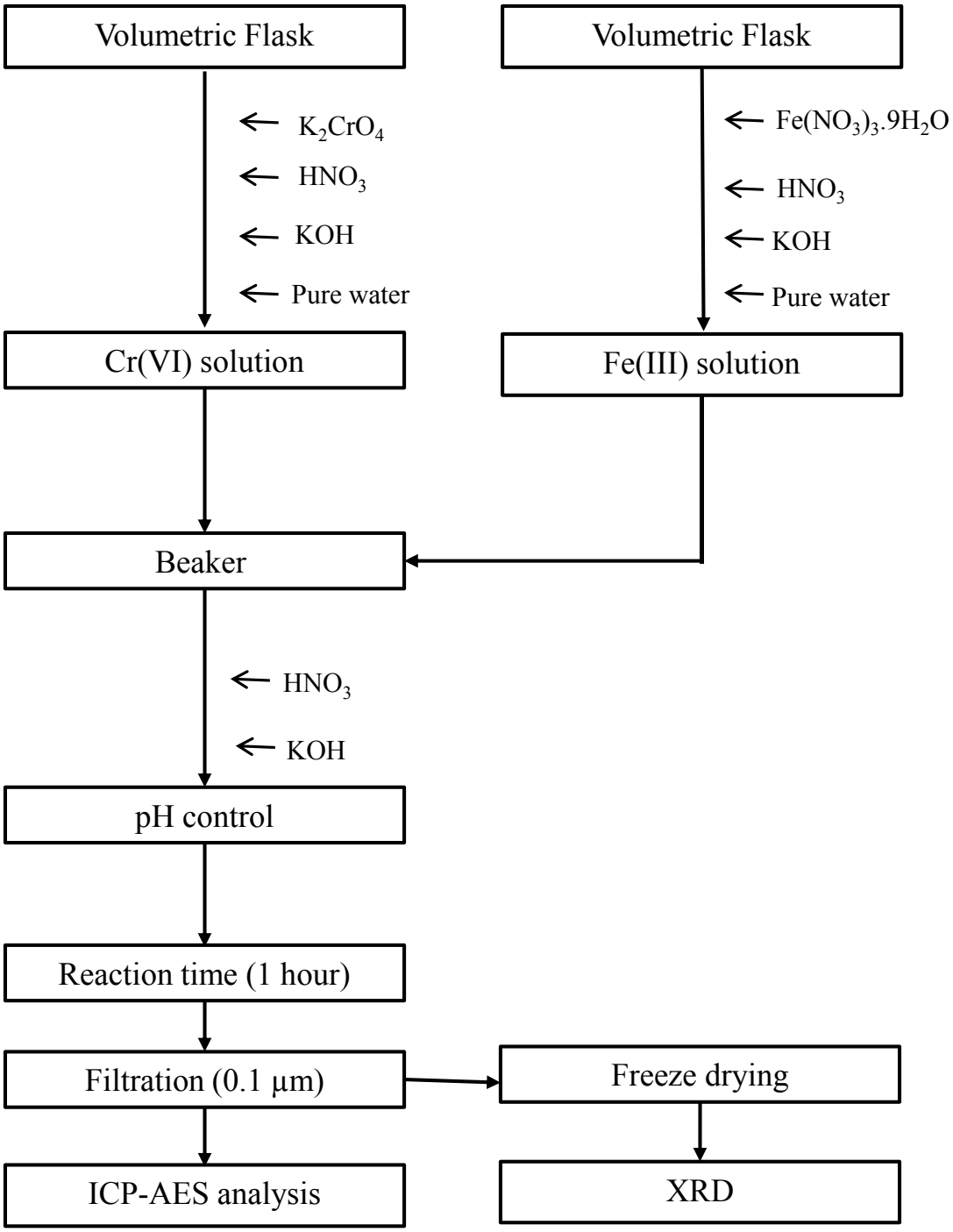


**Fig. 3.1 Flow chart of coprecipitation experiments**

### 3.2.4 Adsorption experiments

In adsorption experiments, 0.1 L of Fh suspension and 0.1 L of chromate-bearing solution were mixed up to the desired Cr/Fe molar ratio [18–21]**,** under controlled pH (5, 7) and ionic strength (0.05 M). After 1 hour under magnetic stirring at 25°C (Fig. 3.2), the suspensions were filtered through 0.1 μm membrane filters. The filtrate was directly stored for analysis while solid residues were freeze-dried at -45°C and 10 Pa for 24 h to avoid crystallization and/or mineralogical transformation. To achieve the desired concentration upon mixing, the initial concentrations of Fe(III) and Cr(VI) solutions were double than that of the targeted ones. The experimental flowchart of coprecipitation is reported in Fig. 3.2. All adsorption experiments were performed in triplicates.

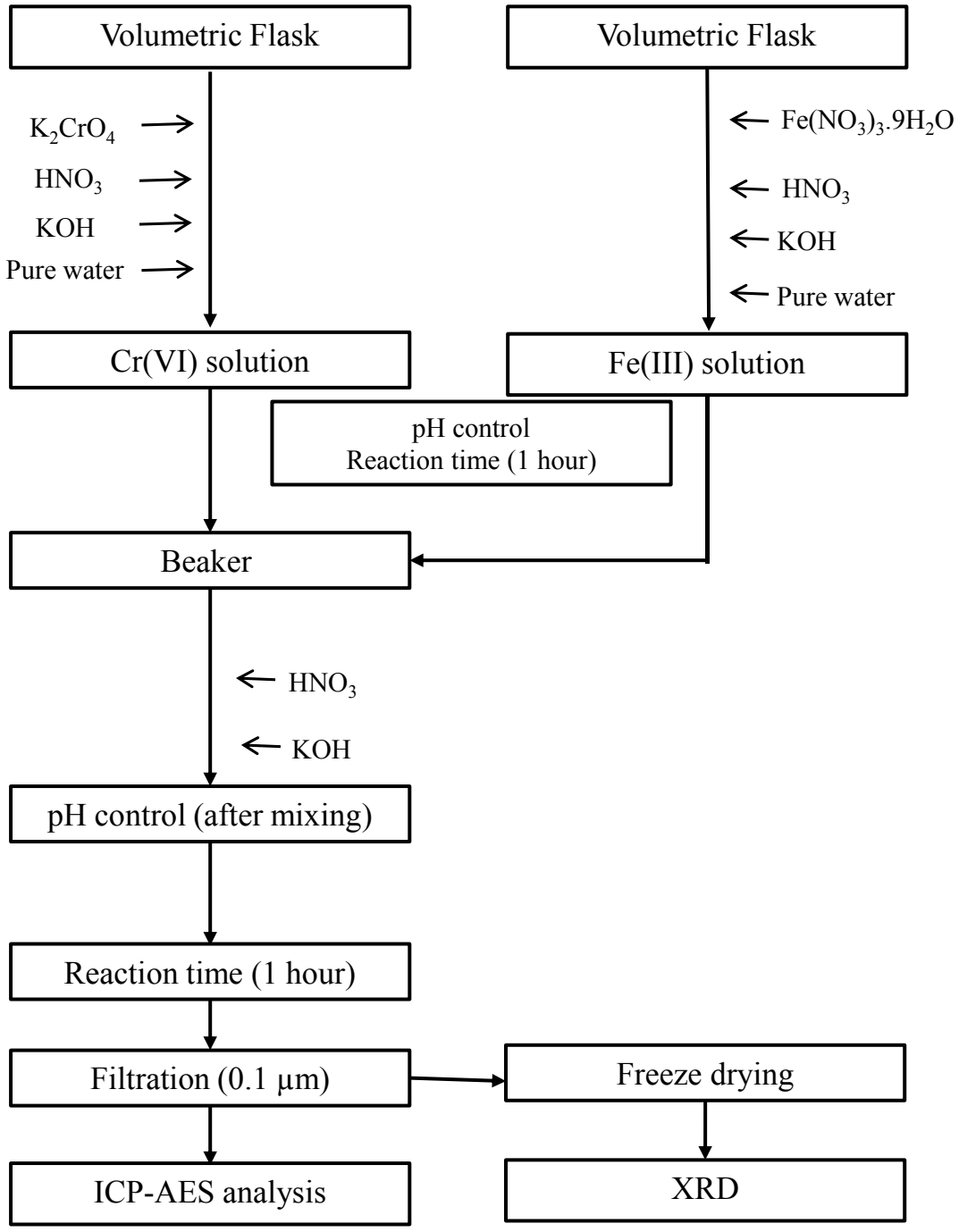


**Fig. 3.2 flow chart of adsorption experiments**

### 3.2.5 Sorption isotherms

Sorption isotherms were determined from experimental results of coprecipitation and adsorption experiments. For this purpose, the sorption density (SD) were calculated over a wide range of Cr/Fe molar ratio (0, 0.05, 0.1, 0.5, 1, 5 and 10). The sorption density represents the removal efficiency of Fh towards Cr and was calculated based on equation (1)

$$\mathrm{SD} = \frac{\mathrm{Cr(VI)_i} - \mathrm{Cr(VI)r}}{\mathrm{Fh}} \qquad (1)$$

Where $Cr(VI)_i$ $Cr(VI)_r$ are the initial and residual molar concentrations of chromate determined by ICP-AES while Fh is the molar concentration of Fe.

### 3.2.6 ICP-AES analysis

The residual Cr was measured (after filtration) by inductively-coupled plasma atomic emission spectrometry (ICP-AES, Vista-MPX ICP, Varian Technologies) using an SPS-4000 atomic emission spectrometer (Seiko Instruments Inc.) with a hydride generator accessory (HYD-10, Seiko Instruments Inc.). The detailed conditions of ICP-AES analysis are listed in Table 3.1.

**Table 3.1 ICP-AES measuring conditions**

| | |
|---|---|
| Power (kW) | 1.20 |
| Plasma (L/min) | 16.0 |
| Carrier gas flow (L/min) | 1.00 |
| Auxiliary gas flow (L/min) | 1.00 |
| View height (mm) | 10.0 |
| Resolution (nm) | 0.006 |
| Wavelength (nm) | 175-800 |
| As measurement wavelength (nm) | 228.812 |

### 3.2.7 XRD analysis

XRD analysis was performed on solid residues from coprecipitation and adsorption experiments to assess the change of crystal structure and phase composition under different Cr/Fe ratio. The analysis was carried out using an XRD diffractometer (Geiger flex RAD-IX, Rigaku Corp.) with a copper target (Cu-Kα), a crystal graphite monochromator and a scintillation detector. The X-ray source was operated at 40 kV and 30 mA with step-scanning from 2θ values of 2-80°, in increments of 0.02°. A crystal sample holder was used and the patterns were not corrected for background diffraction and a scan speed of 2°/min. The detailed conditions of XRD analysis are listed in Table 3.2.

**Table 3.2 XRD measuring conditions**

| | |
|---|---|
| X-ray | Cu/40kV/30mA |
| goniometer | UltimaIII horizontal goniometer |
| divergence slit (°] | 2/3 |
| longitudinal restriction divergence slit [mm] | 10 |
| scattered slit [°] | 2/3 |
| light receiving slit [mm] | 0.3 |
| sampling range [°] | 0.02 |
| scan speed [°/min] | 2 |
| scan range [°] | 2.0～80.0 |

### 3.2.8 Zeta potential measurements

Zeta potentials and electrophoretic measurement of the suspensions were conducted using an electrophoresis light scattering spectrophotometer (Zetasizer Nano, Malvern, Worcestershire, UK). According to the analytical procedure, the suspensions produced in coprecipitation and adsorption experiments were first dispersed in an ultrasonic bath for 5 min, and then filtered and quickly poured into a capillary cell for the measurement. The detailed conditions of zeta potential measurements are listed in Table 3.3.

**Table 3.3 Zeta potential measuring conditions**

| | |
|---|---|
| Cell | DTS1060 - Clear disposable zeta cell |
| *f*(kα) selection | Smoluchowski (Value-1.5) |
| Temperature [°C] | 25 |
| Equilibrium time [min] | 1 |
| Measurement voltage [V] | 20 |
| Measurement times | 2 |

### 3.2.9 ESR measurement

For the purpose of ESR measurements, the above-described coprecipitation experiments were scaled-up to 4 L to collect enough solid samples. Samples were loaded into a 5 mm diameter quartz sample tube and then into the X-band electron spin resonance (ESR) spectrometer (JEOL JES TE-200) operated according to the conditions described in Table 3.4. Experimental time constant was set at 0.03 seconds while sweep time was set at 4 minutes. For comparison, the spin resonance of Fh prepared at pH 5 was also measured.

**Table 3.4 ESR measuring conditions**

| | |
|---|---|
| Field modulation | 100 KHz |
| Modulation width | 0.2 mT |
| Field width | ± 500 mT |
| Center field | 335 mT |
| Microwave power | 4 mW |
| microwave frequency | 9.44 GHz |

### 3.2.10 XAFS analysis

XAFS analysis was performed at the beamline BL5S1 in Aichi Synchrotron Radiation Center, Nagoya, Japan. Both x-ray absorption near-edge structure (XANES) and extended x-ray absorption fine structure (EXAFS) analysis were performed. For the purpose of the measurement, samples were mixed with boron nitride (BN) powder and pressed to create a thin tablet shaped sample [22], in accordance with the requirements of the transmission method. The flowchart of sample preparation for XAFS analysis is shown in Fig. 3.3.

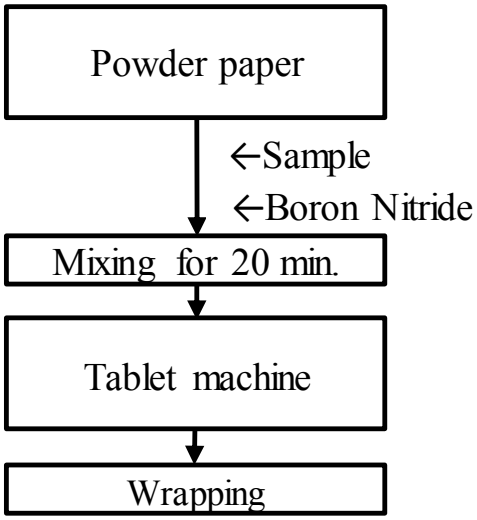


**Fig. 3.3 Flow chart of sample preparation for XAFS analysis**

For the analysis, the ionization chamber was filled with $N_2$ gas (30%) and He (Helium) gas (70%) whereas $N_2$ gas (75%) and Ar (25%) were used for the transmission beam. The beam was untuned by 30% to avoid higher-order harmonics generation in the K-edge analysis of Fe and Cr. The Fe K-edge and Cr K-edge analysis were performed with the transmission method due to the sufficient concentrations of Fe and Cr in solid samples. The detailed conditions of XAFS analysis are reported in Table 3.5.

**Table 3.5 Photonic condition and facilities at BL5S1 beam line in Aichi-SR**

| | | |
|---|---|---|
| Measurement Range | K-edge | Ti - Mo |
| | L(III)-edge | Cs - U |
| Photon Energy [keV] | | 5 - 20 |
| Wave length [nm] | | 0.25 - 0.06 |
| Beam size [mm] | | 0.50 × 0.30 |
| Dissolution (E/ΔE) at 12 keV | | 7000 |
| Equipment | | 19 element germanium detector for fluorescence measurement |
| | | Ionization chamber for transmission measurement |
| | | 7 element Silicon drift detector |
| | | Detector for conversion electron yield method |
| | | Lytle detector |

### 3.3 Results and discussion

#### 3.3.1 Fh formation and equilibrium time

To assess the time required to reach the equilibrium in coprecipitation and adsorption, Fh was precipitated in the presence of chromate (Cr/Fe molar ratio = 0.5) at pH 5. The choice of this condition arisen from previous results describing pH 5 as the best condition for chromate removal by Fh [23]. As shown in Fig. 3.4, coprecipitation reached the equilibrium within 10 minutes, whereas 20 minutes were required for adsorption.

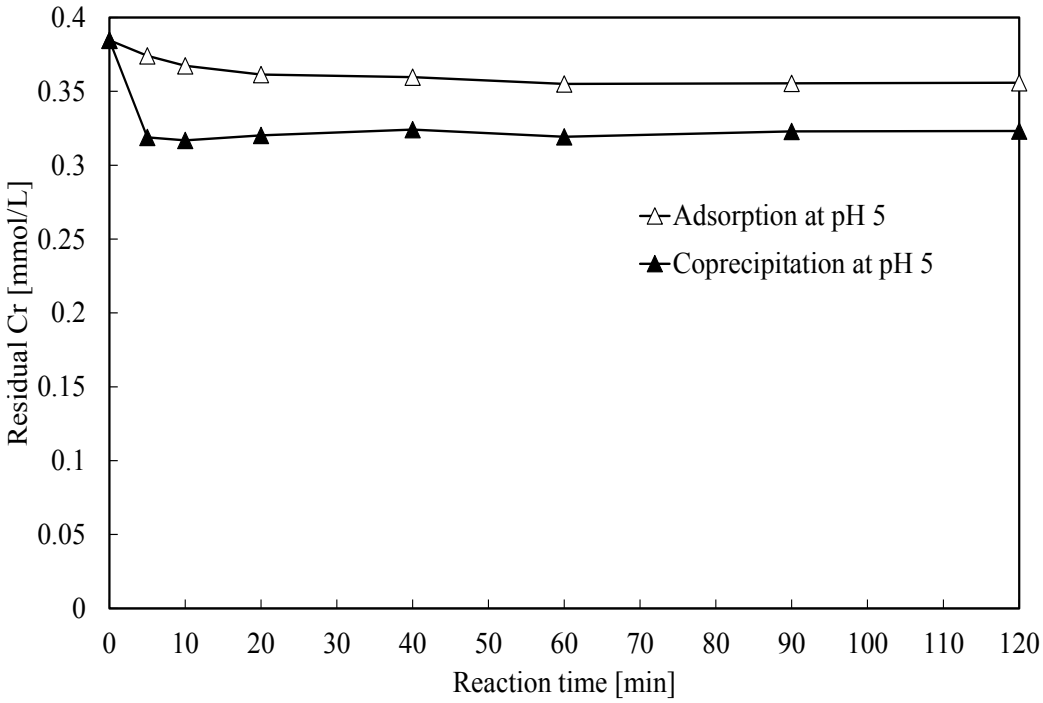


**Fig. 3.4 Equilibrium reaction time study of coprecipitation and adsorption (Cr/Fe 0.5, pH 5)**

To confirm the formation of Fh at pH 5, XRD analysis was performed on both products at pH 5 and pH 7. The obtained XRD spectra highlighting the formation of 2-line Fh at both pH values are shown in Fig. 3.5.

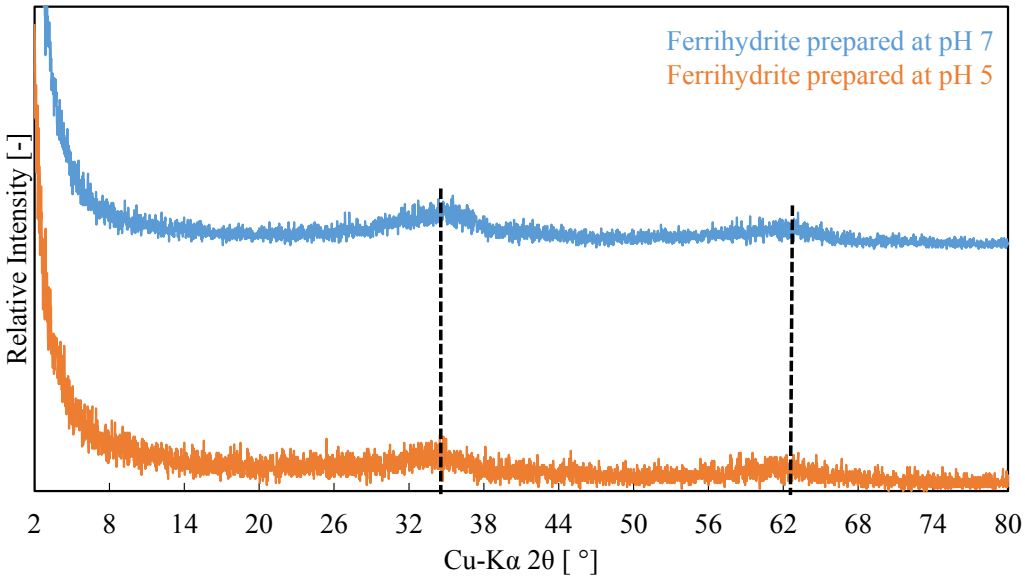


**Fig. 3.5 XRD pattern of Fh (2-line) obtained at pH 5 and pH 7**

### 3.3.2 Cr(VI) removal and sorption isotherms

Results of removal experiments at different Cr/Fe molar ratios are shown in Fig. 3.6 for coprecipitation and adsorption at pH 5 and 7. Clearly, the removal of Cr(V) at pH 5 was higher than the one obtained at pH 7, like also reported in previous investigations [22,23]. The lower removal observed at pH 7 can be explained considering the competitive adsorption of hydroxyl ions onto Fh at higher pH. In addition, at pH 5 the predominant Cr(VI) species is hydrogen chromate ($HCrO_4^-$), which can be more strongly adsorbed on the surface of iron and/or aluminium oxides [24]. The Fe dosage required to remove Cr(VI) below the effluent standard limit of most of the developed countries (0.5 mg/L or 0.0096 mmol/L) was determined as a parameter of efficiency. In coprecipitation at pH 5, Cr(VI) was removed up to 0.1215 mg/L (0.0023 mmol/L) whereas in adsorption the final concentration was 0.503 mg /L (0.0097 mmol /L) (Fig. 3.6). At pH 7, both adsorption and coprecipitation could not remove Cr(VI) below the effluent standard.

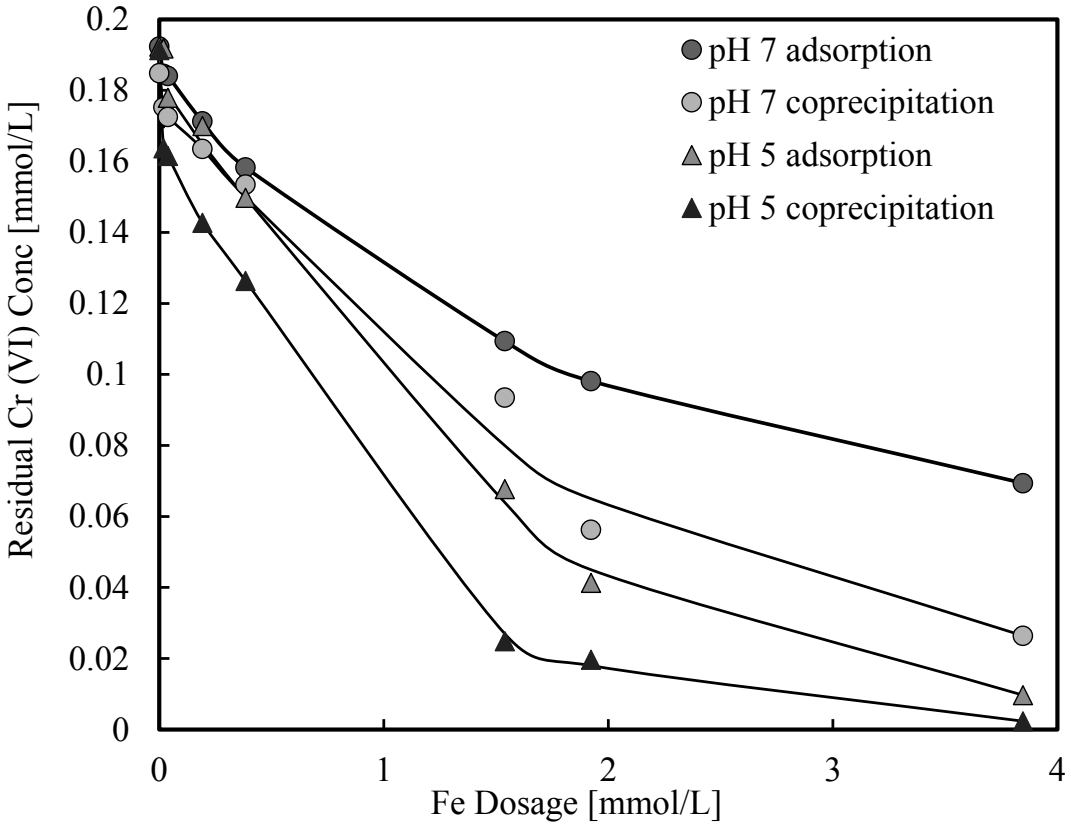


**Fig. 3.6 Cr(VI) removal by Fh in adsorption and coprecipitation experiments at pH 5 and 7 (initial Cr(VI) concentration = 0.19 mmol/L)**

By looking at the sorption isotherms in Fig. 3.7, it appears clear that the sorption density for coprecipitation at pH 5 was almost double that the one for adsorption at same pH (1.56 mol Cr/mol Fe versus 0.85 mol Cr/mol Fe). Regardless of the different sorption densities, the experimental data fitted the Brunauer–Emmett–Teller (BET)-like isotherm. This evidence suggested that the Cr(VI) sorption onto Fh might not only be a simple outer-sphere adsorption. The BET-like isotherm suggests that adsorption might have occurred by multi-layer adsorption like $SiO_4^{4-}$ and $AsO_4^{3-}$ at a higher molar ratio [25–27] or by special inner-sphere complexation like for selenite, lead, cadmium, zinc, and uranium [28–34]. Interestingly, the sorption isotherms exhibit two different trends at low and high Cr/Fe molar ratio. The sorption density increased very slowly at low Cr/Fe molar ratios and then dramatically increased. This evidence suggests a shift of removal mechanism by changing the molar ratio.

Previous works reported that the sorption of Cr(VI) onto α-$Fe_2O_3$ and α-FeOOH in simple adsorption experiments follows a Langmuir type mechanism [35,36]. The BET-

type isotherm observed in this work can be explained considering that coprecipitation and adsorption experiments were carried out with fresh Fh, which has a great activity towards Cr(VI).

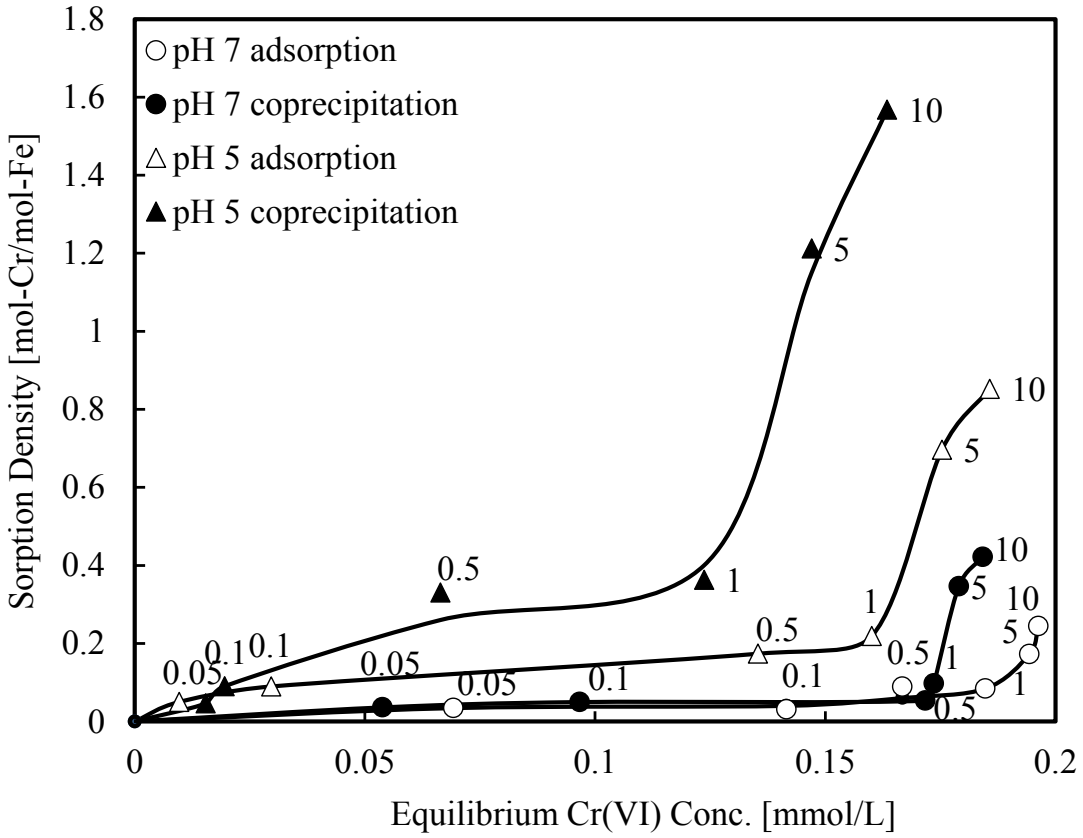


**Fig. 3.7 Sorption isotherms in coprecipitation and adsorption at pH 5 and 7 (initial concentration of Cr(VI) = 0.19 mmol/L; the numbers in the figure represent the initial molar ratio of Cr/Fe)**

As for the structural reasons determining the increase of sorption density at high Cr/Fe ratios will be discussed in details later in the XAFS section. Here, it is just worth mentioning that BET-like isotherm was a consequence of the structural change of Fh structure at different Cr/Fe ratio. At low Cr/Fe molar ratio, Fh would bind another octahedral Fh and would increase the surface area prone to adsorption [27]. By increasing the Cr/Fe ratio determined insertion of chromate into Fh and disruption of Fe-Fe correlations. As a consequence, the bidentate Cr-Fe relation could be established and more chromate could be bound by Fh with stronger interactions.

Coprecipitation and adsorption at pH 7 showed very similar results in terms of

sorption density. This result can be considered as a consequence of the lower adsorption ability of $CrO_4^{2-}$ compared to $HCrO_4^-$.

### 3.3.3 XRD analysis

The XRD pattern of the solid residue from the Cr(VI) removal by coprecipitation at pH 5, exhibited different characteristics depending on the Cr/Fe molar ratio. At Cr/Fe =0.1, the XRD pattern was similar to Fh (Fig. 3.8). By increasing the Cr/Fe molar ratio, the peak at $2\theta = 34°$ broadened up to $2\theta = 23°$, thus suggesting the structural change due to Cr(VI) inclusion into Fh. At pH 5, the peak broadening was observed from Cr/Fe = 0.5 in coprecipitation (Fig. 3.8) and from Cr/Fe 1 in adsorption (Fig. 3.9). These evidence match with results highlighted by sorption isotherms. In adsorption, a dramatic increase of sorption density was observed from Cr/Fe = 1, while in coprecipitation the sudden increase was observed between Cr/Fe 0.1 and 0.5. These evidence are supportive of a mechanism change with Cr/Fe molar ratio. Since chromate was also removed, even when the XRD pattern did not exhibit any change, it is reasonably to say that chromate is first adsorbed onto Fh surface and then included into Fh. In coprecipitation, chromate is included within Fh from low Cr/Fe molar ratio, whereas in adsorption the inclusion takes place comparatively at higher Cr/Fe molar ratio.

At pH 7, the XRD patterns for both adsorption and coprecipitation were similar as the peak shift was observed only from Cr/Fe = 5 (Fig. 3.10 and Fig. 3.11). This is probably due to the lower sorption density that does not allow to appreciate mechanism differences.

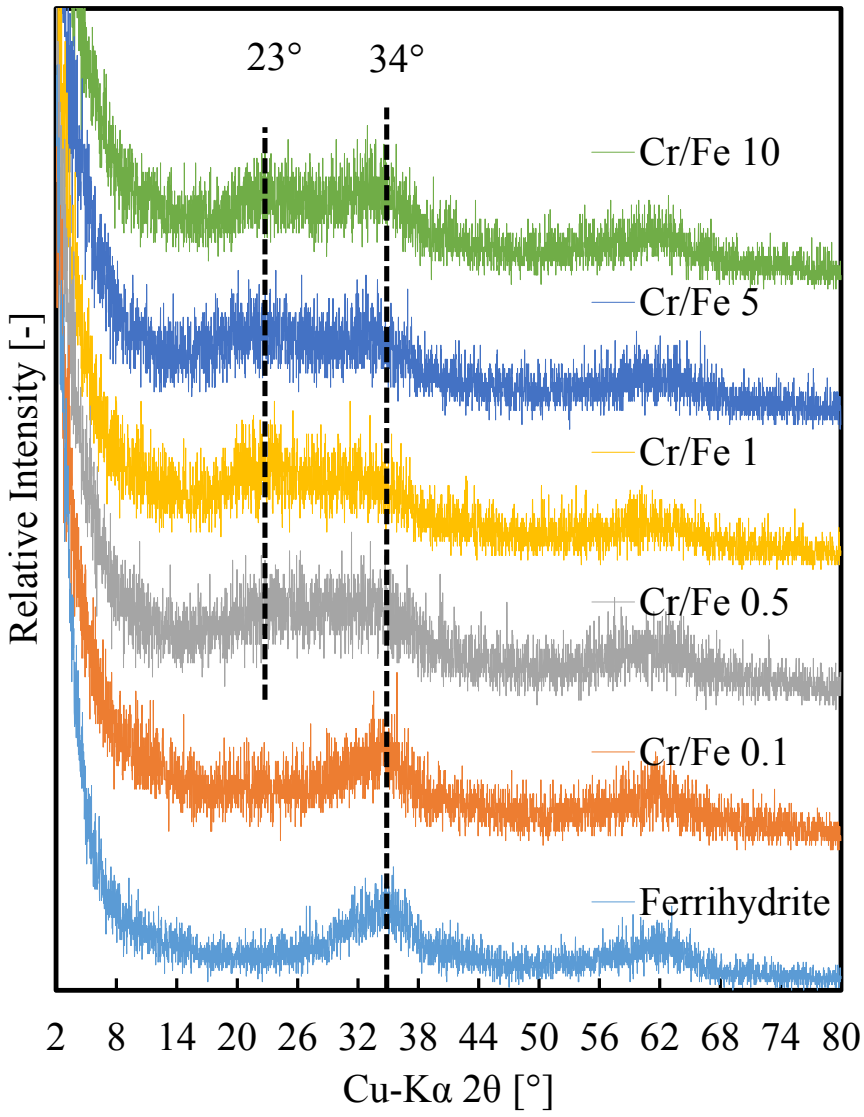


**Fig. 3.8 XRD patterns of Fh before and after chromate removal at pH 5 (coprecipitation)**

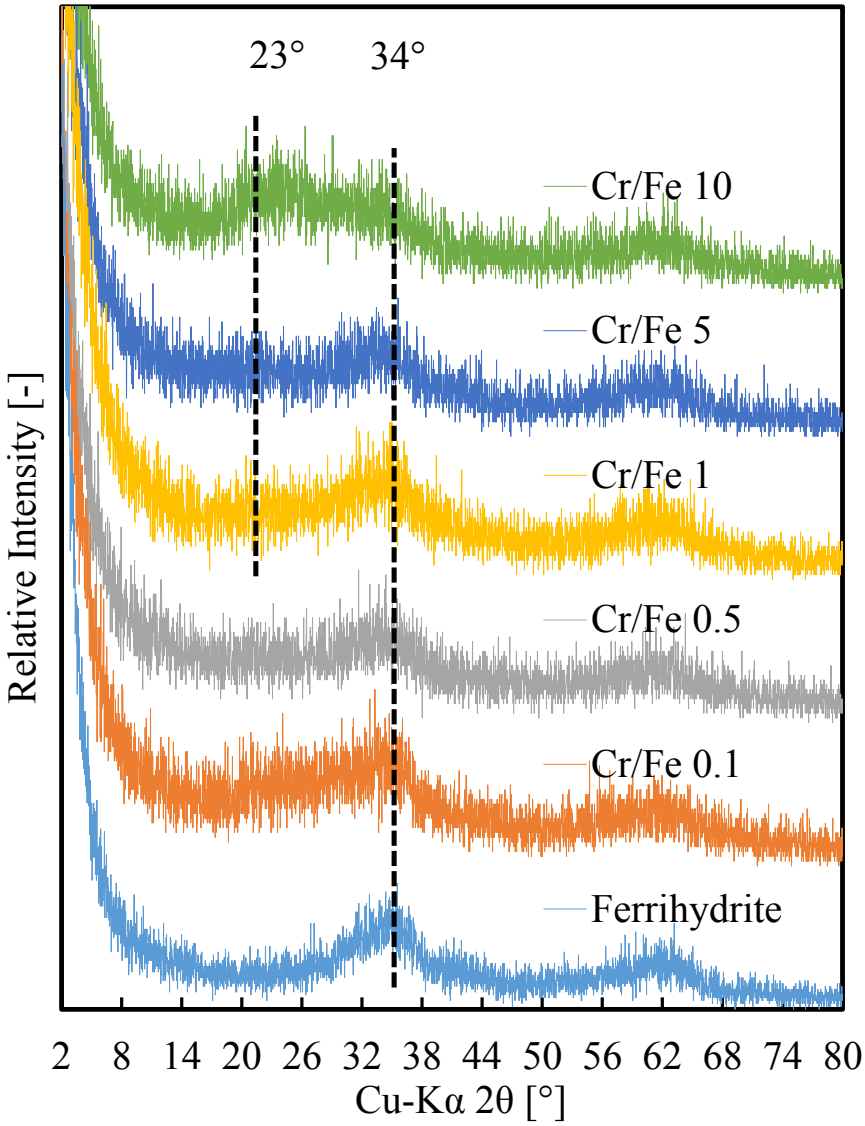


**Fig. 3.9 XRD patterns of Fh before and after chromate removal at pH 5 (adsorption)**

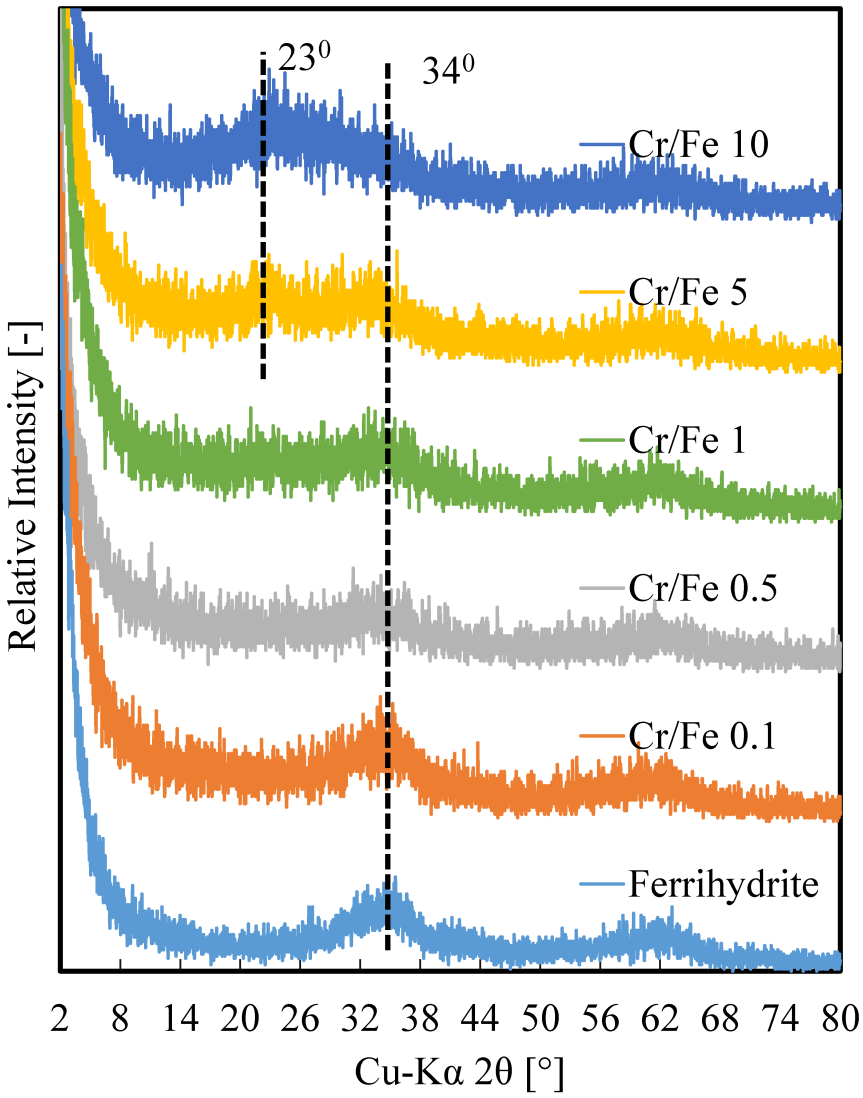


**Fig. 3.10 XRD patterns of Fh before and after chromate removal at pH 7 (coprecipitation)**

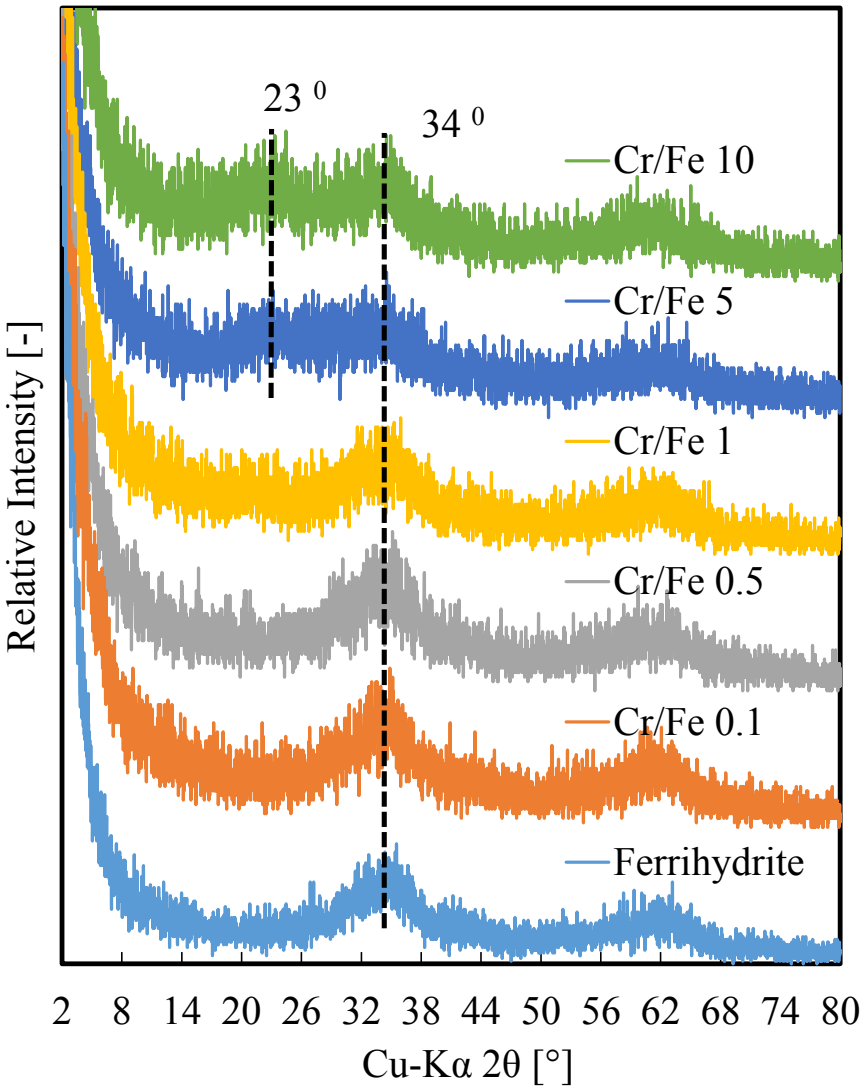


**Fig. 3.11 XRD patterns of Fh before and after chromate removal at pH 7 (adsorption)**

### 3.3.4 Zeta potential measurements

Fig. 3.12 shows the zeta potential change against the sorption density in both coprecipitation and adsorption experiments at pH 5. In the coprecipitation experiment, following a sharp decrease of zeta potential, a zeta potential plateau was reached for Cr/Fe = 0.25. On the other hand, in the adsorption experiment, the zeta potential decreases sharply up to Cr/Fe = 1 and finally, a plateau is reached.

This difference highlights the occurrence of the two different sorption behaviors [39]. Indeed, a sharp decrease in zeta potential can be associated to surface complexation

at the interface whilst the slow decrease can be considered as the result of the insertion of Cr(VI) into Fh octahedral structure. Accordingly, in coprecipitation, the surface complexation seem to take place up to Cr/Fe = 0.25 whereas in adsorption the same phenomenon occurs up to Cr/Fe = 1.

Regardless of the exact value of Cr/Fe where the change could be observed, these evidence are consistent with previous results. The sorption density in coprecipitation increased between Cr/Fe ratio of 0.1~0.5, where XRD patterns shifts and zeta potential reaches the plateau. In adsorption, the same phenomena take place from Cr/Fe = 1. These results highlight that coprecipitation enhances the removal of chromate by promoting its inclusion into Fh from lower Cr/Fe molar ratios.

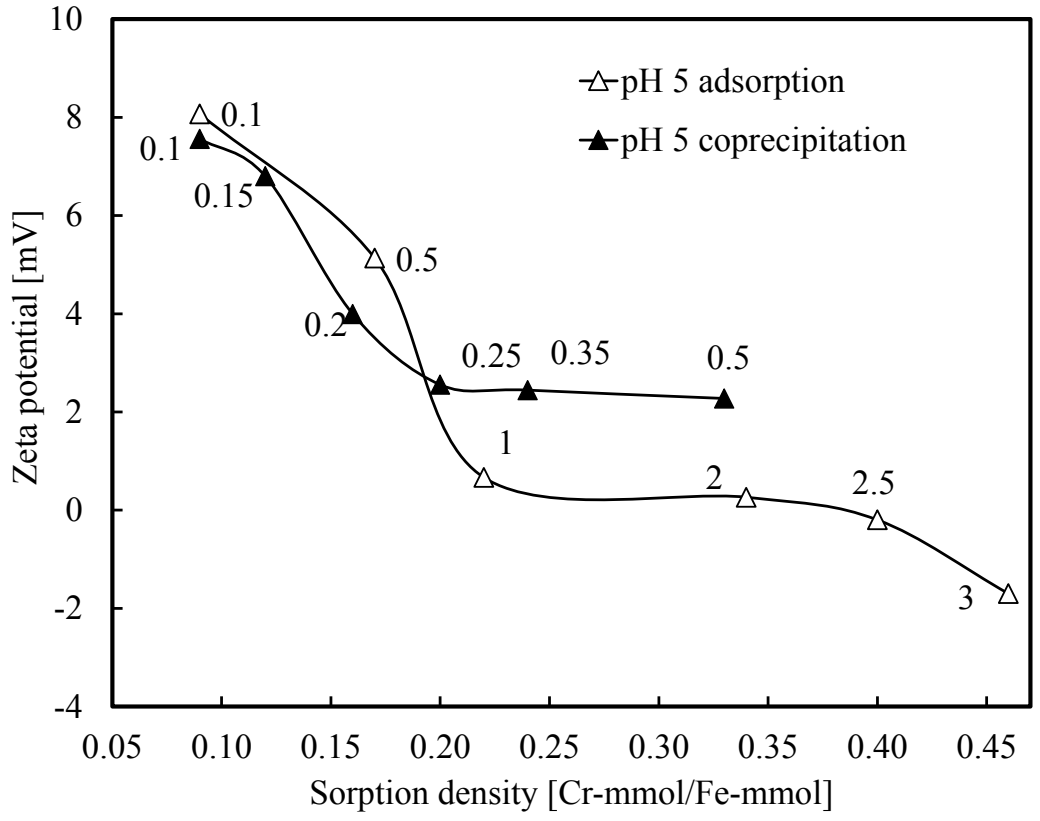


**Fig. 3.12 Relationship between sorption density and zeta potential during adsorption and coprecipitation at pH 5 (the numbers in the figure represent the initial molar ratio of Cr/Fe)**

### 3.3.5 ESR analysis

The magnetic properties of unpaired electron spins resonance from coprecipitated Fh with/without chromate at different Cr/Fe ratio can be observed in Fig. 3.13. The most stable Cr form, namely Cr(III), gave positive ESR due to the contained unpaired electrons. In contrast, chromate has no unpaired electrons and exhibited a negative ESR [40].

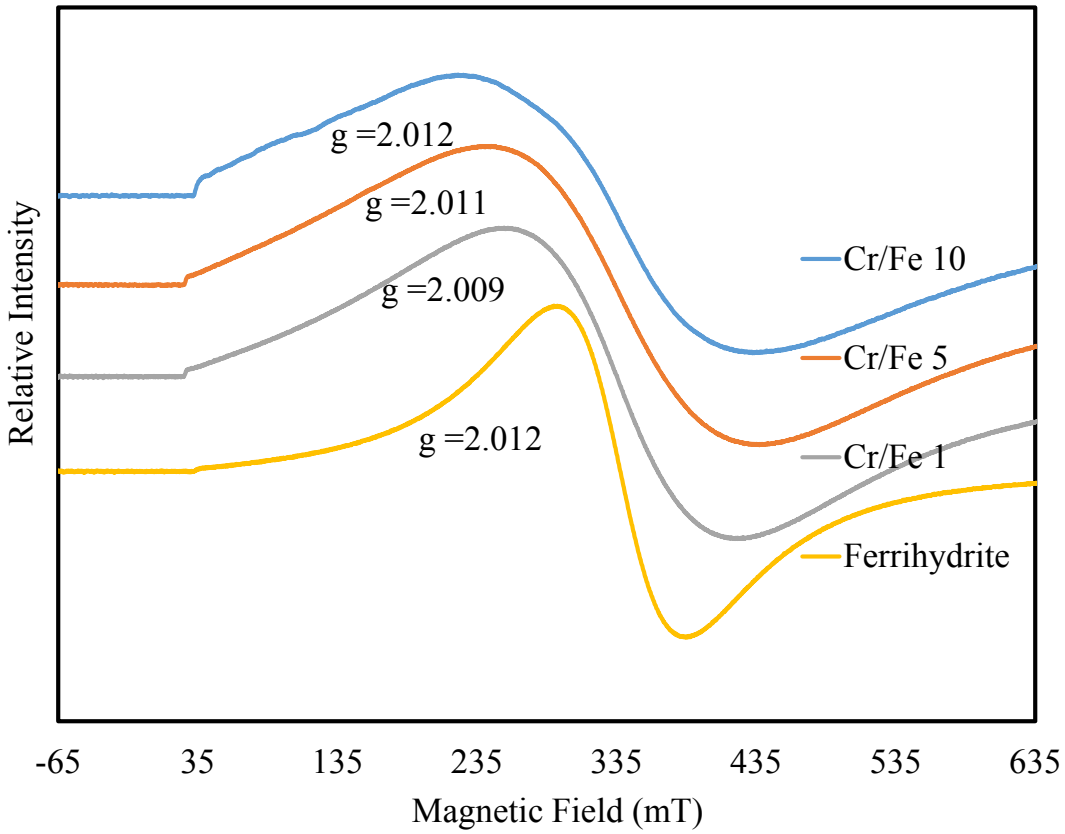


**Fig. 3.13 ESR spectra of Fh at different Cr/Fe molar ratio at pH 5 (coprecipitation)**

In these experiments, it can be clearly observed as the ESR spectra did not change considerably upon chromate adsorption, thus suggesting an unaltered magnetic state of chromate and Fh. The *g*-value of each sample was just above 2, like for low-spin Fe(III) (1 unpaired electron), which usually exhibit sharp spectra and the *g*-values ≥2.00. Indeed, high spin states (5 unpaired electrons) would exhibit broad spectra and *g*-values in the range 4.0-4.5 whilst Cr(III) would results in g-value ≤ 2 [11]. A gradual slight peak decrease was observed by increasing the Cr/Fe ratio. This evidence suggests an increase of Cr substitution in the Fe framework, most likely due to the inclusion of chromate into Fh structure.

### 3.3.6 XAFS analysis

**(i) XANES results**

Fe K-edge and Cr K-edge spectra were studied at different Cr/Fe molar ratios. The XANES pattern upon chromate removal highlighted unaltered oxidation states (Fig. 3.14 and Fig. 3.15) under all investigated Cr/Fe ratios. Therefore the EXAFS spectra were analyzed to reveal the sorption nature of Cr(VI).

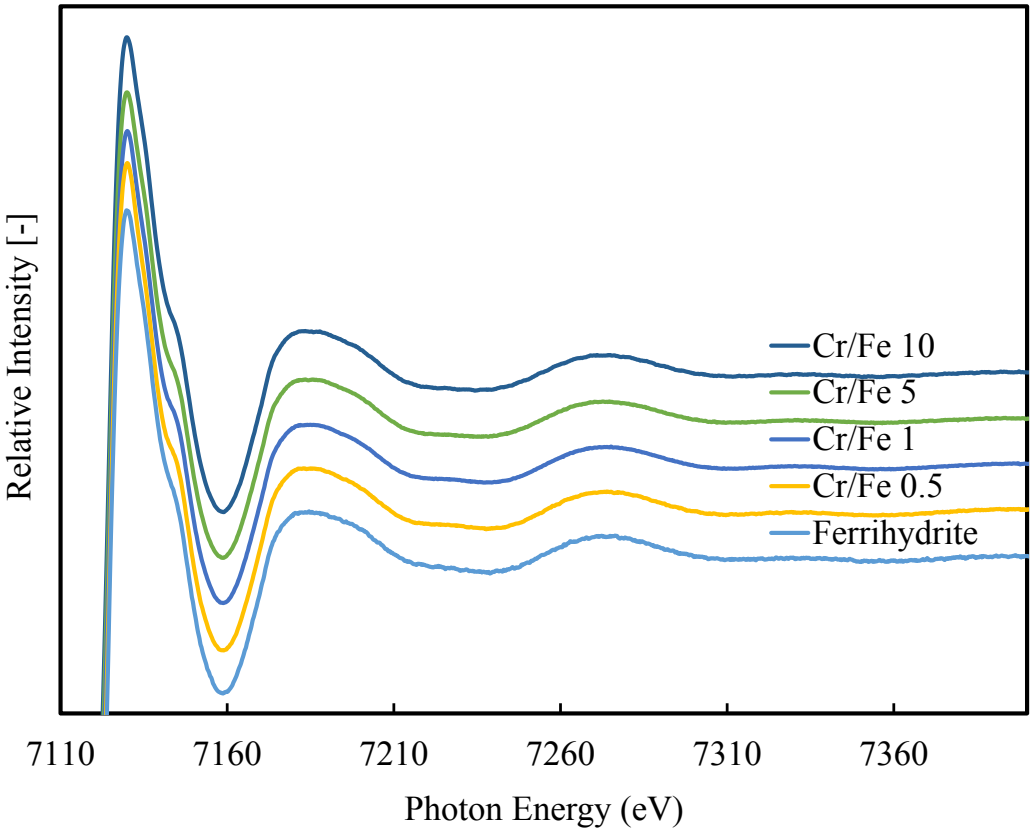


**Fig. 3.14 Fe K edge XANES spectra of precipitates obtained by coprecipitation at pH 5**

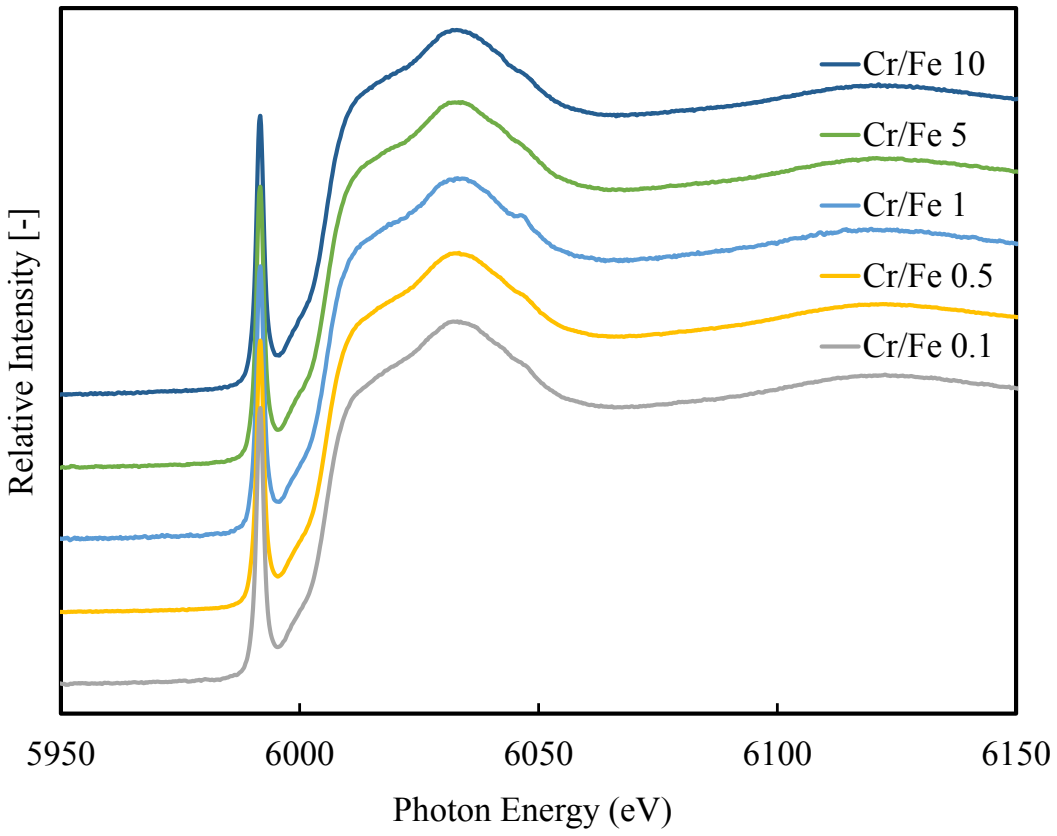


**Fig. 3.15 Cr K edge XANES spectra of precipitates obtained by coprecipitation at pH 5**

**(ii) Fe K-edge EXAFS analysis**

The Fe K-edge EXAFS spectra of Fh did not show any visible difference upon coprecipitation with Cr(VI) (Fig. 3.16). In order to highlight possible differences, the $K^3$-weighted EXAFS fitting was performed using goethite (α-FeOOH) to obtain the initial values of the fitting parameters [41]. The radial distribution function (RDF) fitting obtained from Fourier-transformed (FT) EXAFS spectra are shown in Table 3.6 and Fig. 3.17. As it can be observed in Table 3.6, Fe–O showed the coordination number around 6, which represents an almost octahedral geometry. However, at Cr/Fe = 0.5, Fe–O and Fe–Fe interatomic distances slightly decreased compared to the initial Fh. Besides, interatomic distances gradually increased by increasing the Cr/Fe molar ratio. This evidence represents an additional suggestion of the mechanism shift or modification of the local microstructure between Cr/Fe = 0-0.5. This result matches with previously described results from zeta potential measurements, where a mechanism shift was suggested for Cr/Fe = 0.25.

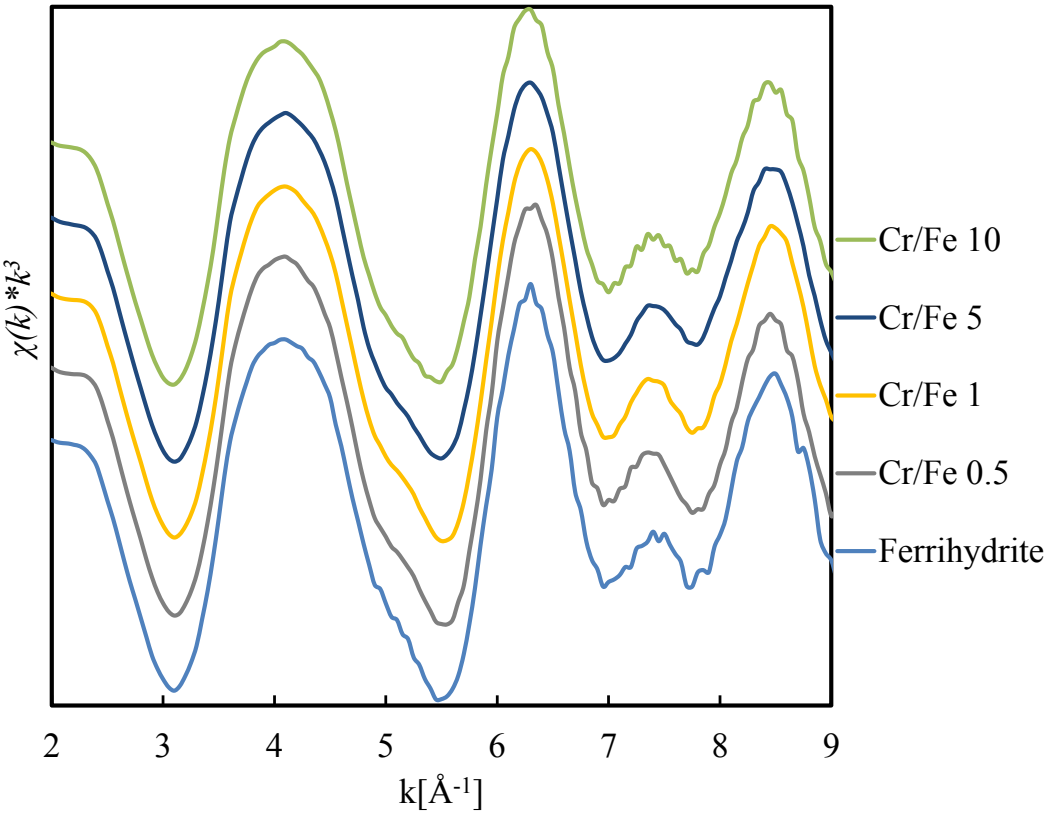


**Fig. 3.16 $K^3$ weighted Fe edge EXAFS spectra of precipitates obtained by coprecipitation at pH 5**

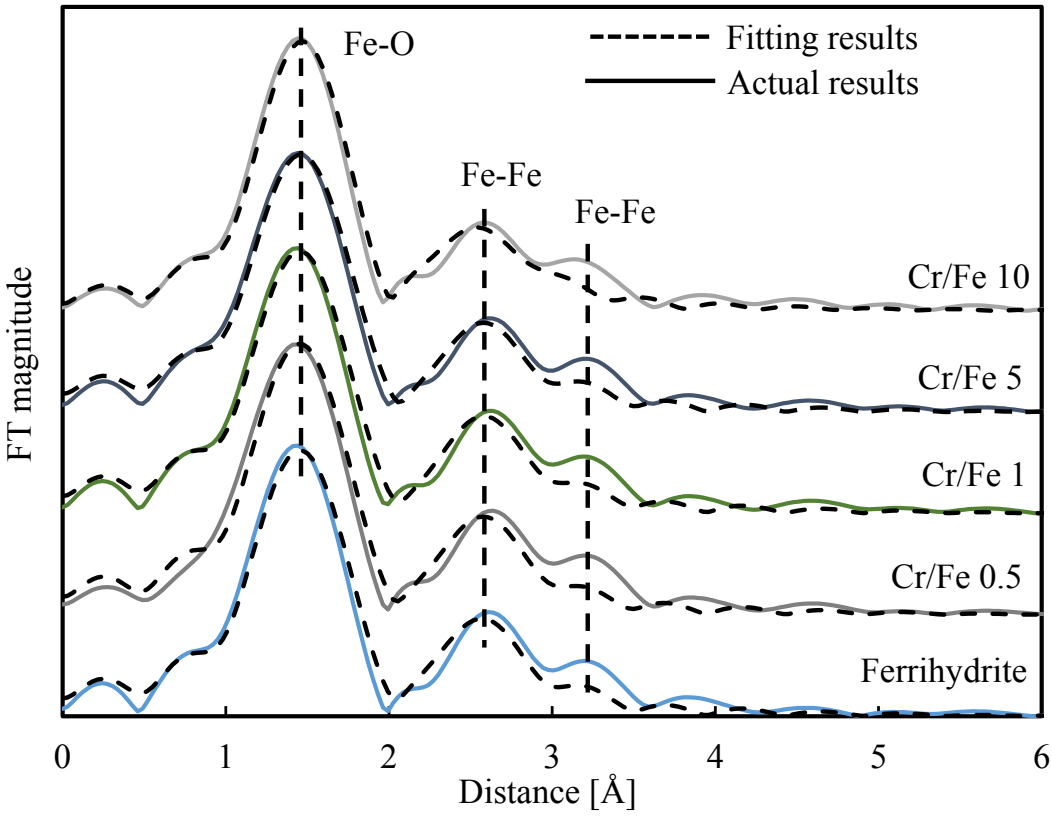


**Fig. 3.17 Fourier-transformed unfiltered spectra and fitting results of Fe K-edge at different Cr/Fe molar ratio in coprecipitation at pH 5**

In general EXAFS results, and in particular the observed Fe–O interatomic distance lower than 1.99 Å, suggests that Fh might contain 20–30% of tetrahedrally coordinated Fe(III) [42]. Although the ionic strength might affect the nature of the crystal structure, the gradual increase of interatomic distance Fe–O by increasing the Cr/Fe ratio from 0 to 1 suggests that a small amount of tetrahedral Fe(III) might exist in the Fh chain. This evidence could be reasonably explained considering that tetrahedral Fe(III) might have rearranged into octahedral structure due to chromate inclusion. Nevertheless, it is worth mentioning that Manceau and Gates (1997) suggested that large portions of tetrahedral Fe(III) in Fh chain could be the result of over drying [43].

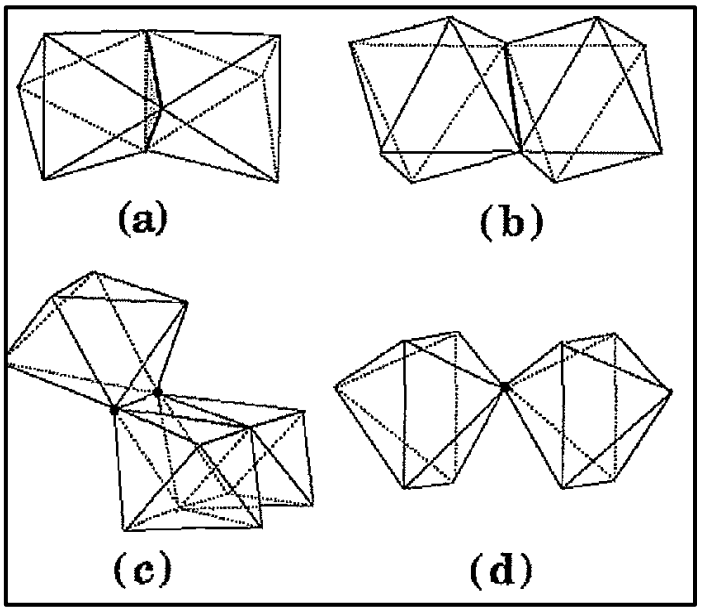


**Fig. 3.18 Schematic illustration of the local arrangements of the $FeO_6$ octahedral in the Fh and oxides**[44]**;**

**(a) face sharing linkage: Fe-Fe (2.89 Å)**

**(b) edge sharing linkage: Fe-Fe (2.97−3.08 Å)**

**(c) double-corner sharing linkage: Fe-Fe (3.37−3.70 Å)**

**(d) single-corner sharing linkage: Fe-Fe (3.90 Å)**

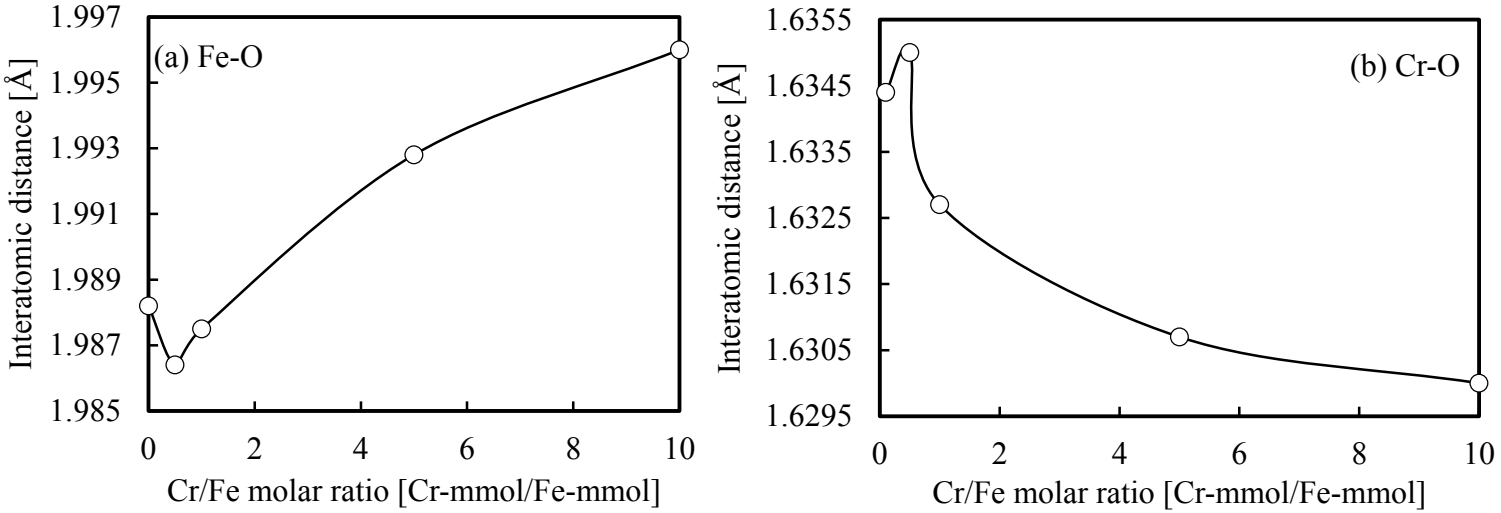


**Fig. 3.19 Interatomic distances obtained from RDF fitting of FT-EXAFS spectra: (a) Fe K-edge Fe–O inter-atomic distance, (b) Cr K-edge Cr–O inter-atomic distance**

**Table 3.6 Fe K-edge RDF fitting of EXAFS area with changing Cr/Fe molar ratio at 0.05 M ionic strength and pH 5**

| sample | Fe-O | | | Fe-$Fe_1$ | | | Fe-$Fe_2$ | | | $E_0$ (eV) | R factor |
|---|---|---|---|---|---|---|---|---|---|---|---|
| | $N$ | $R$ (Å) | $\sigma^2$ (Å$^2$) | $N_1$ | $R$ (Å) | $\sigma^2$ (Å$^2$) | $N_2$ | $R$ (Å) | $\sigma^2$ (Å$^2$) | | |
| Fh | 6.14 | 1.9882 | 0.01 | 1.89 | 3.0578 | 0.02 | 1.63 | 3.3508 | 0.02 | -0.77 | 0.01 |
| Cr/Fe 0.5 | 6.27 | 1.9864 | 0.01 | 1.58 | 3.0560 | 0.01 | 1.00 | 3.3490 | 0.02 | -0.82 | 0.02 |
| Cr/Fe 1 | 6.10 | 1.9875 | 0.01 | 1.38 | 3.0571 | 0.01 | 0.93 | 3.3501 | 0.03 | -0.71 | 0.02 |
| Cr/Fe 5 | 6.17 | 1.9928 | 0.01 | 1.45 | 3.0624 | 0.01 | 1.26 | 3.3554 | 0.02 | -0.42 | 0.01 |
| Cr/Fe 10 | 5.74 | 1.9960 | 0.01 | 1.43 | 3.0656 | 0.01 | 1.00 | 3.3586 | 0.02 | -0.43 | 0.01 |

$N$: coordination number, $\sigma^2$: Debye-Waller factor, $E_0$: threshold shift in electron volts, $R$: interatomic distance.

Fh usually shows two Fe–Fe shell configurations: edge sharing and double-corner sharing (Fig. 3.18). According to literature, the edge sharing of $Fe(O, OH)_6$ octahedra shows an interatomic distance from 2.99 Å to 3.07 Å, with a wide range of coordination numbers from 1.4 to 3.5 [43]. Xie et al. (2015) reported that the Fe–Fe distance in double-corner sharing was in the range 3.12–3.15 Å, whereas most researchers agreed on the range 3.4–3.5 Å [45]. In this work, the Fe-Fe interatomic distance was found to be 0.5~0.15 Å lower than that mostly reported (3.4–3.5 Å). This might be due to the ionic strength adjustment to 0.05 M [45]. Fe–Fe shell fittings evidenced an interatomic distance of 3.05 ± 0.01 Å (edge sharing) and 3.35 ± 0.003 Å (double-corner sharing).

The EXAFS fitting results (Table 3.6) highlighted irregularities of Fe–Fe coordination numbers and a gradual increase of interatomic distances by increasing the Cr/Fe molar ratio (Fig. 3.19a). This trend is a further suggestion that a larger inclusion of chromate into the inner sphere of the Fh [26] produced a change of structure geometry of Fh from tetrahedral to octahedral.

**(iii) Cr K-edge EXAFS analysis**

Since Cr K-edge EXAFS results (Fig. 3.20) showed no visible differences by changing the Cr/Fe molar ratio, the RDF fitting from the Fourier-transformed EXAFS spectra (Table 3.7 and Fig. 3.21) was produced for further evaluations. The crystal structure of $Fe_2(CrO_4)_3 \cdot 3H_2O$ by Bonnin [46] was used as a reference to obtain the initial fitting parameters for $K^3$-weighted EXAFS fitting. The fitting parameters in Table 3.7 highlighted that Cr was tetrahedrally coordinated with an oxygen atom and that the Cr–O bond distance was ~1.63 Å. These results match with those reported by Bonnin (1978) who reported a tetrahedrally coordinated Cr with Cr–O distance ranging from 1.566 Å to 1.747 Å [46]. The Cr–Fe interatomic distance slightly increased along with Cr/Fe molar ratio change from 0.1 to 0.5, whilst it decreased above Cr/Fe 0.5 (Fig. 3.19b). For Cr/Fe between 0.1 and 0.5, the Cr–Fe might be coordinated via oxygen atoms [46] and the direct coordination was increased gradually by decreasing the Cr–Fe interatomic distance above Cr/Fe molar ratio 0.5. The obtained results confirm that more inner-sphere surface complexation occurred at higher Cr/Fe molar ratios. This interpretation support that when high surface coverage at higher Cr/Fe molar ratio in pH below 6, the bidentate Cr–Fe relationship is more likely to be established [16].

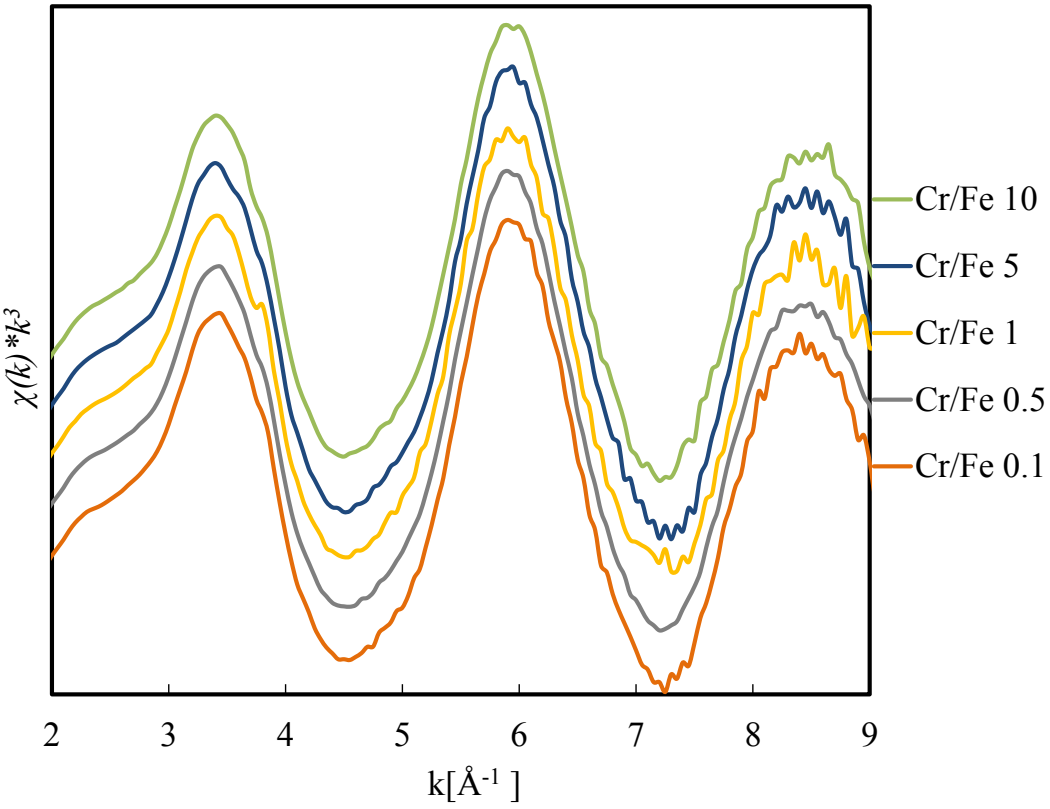


**Fig. 3.20 $K^3$ weighted Cr edge EXAFS spectra of precipitates obtained by coprecipitation at pH 5**

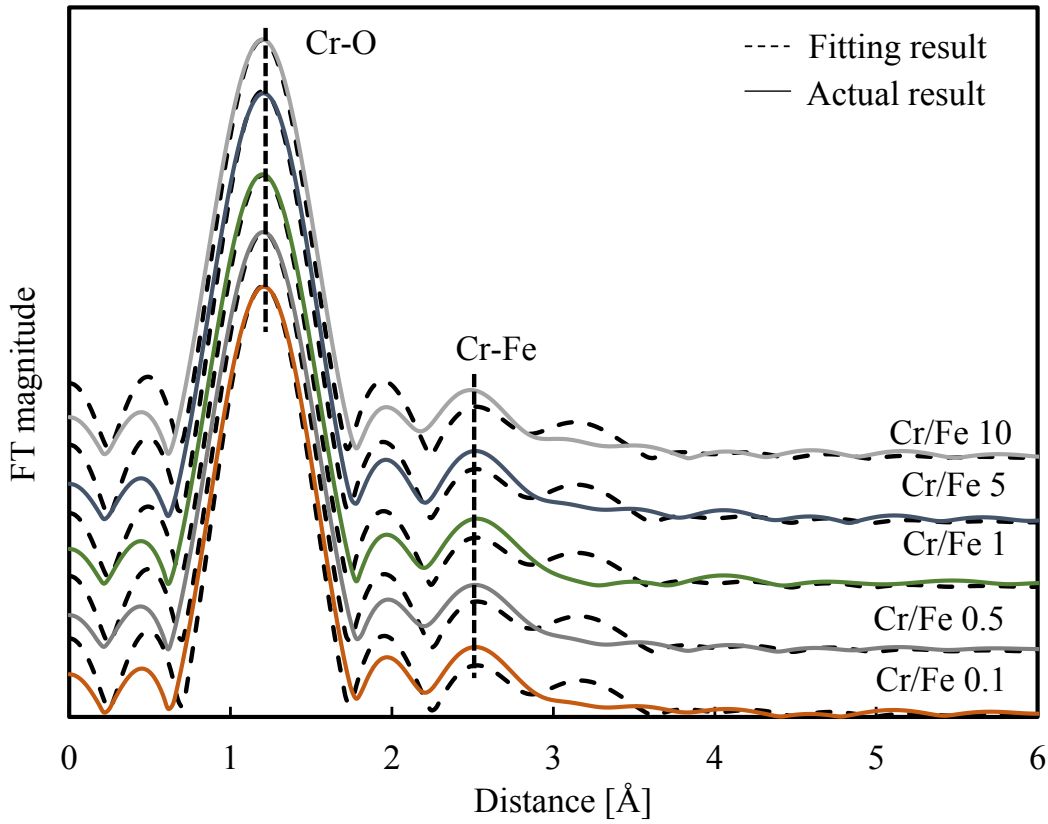


**Fig. 3.21 Fourier-transformed unfiltered spectra and fitting results of Cr K-edge at different Cr/Fe molar ratio at pH 5 (coprecipitation)**

**Table 3.7 Cr K-edge RDF fitting of EXAFS area (coprecipitation at pH 5)**

| Sample | Cr-O | | | Cr-Fe | | | $E_0$ (eV) | R Factor |
|---|---|---|---|---|---|---|---|---|
| | $N$ | $R$ (Å) | $\sigma^2$ (Å$^2$) | $N$ | $R$ (Å) | $\sigma^2$ (Å$^2$) | | |
| Cr/Fe 0.1 | 4.03 | 1.6344 | 0.0012 | 1.40 | 3.3808 | 0.0477 | 8.72 | 0.01 |
| Cr/Fe 0.5 | 4.04 | 1.6350 | 0.0015 | 1.47 | 3.3814 | 0.0483 | 8.59 | 0.01 |
| Cr/Fe 1 | 4.04 | 1.6327 | 0.0018 | 1.60 | 3.3791 | 0.0502 | 8.22 | 0.01 |
| Cr/Fe 5 | 3.99 | 1.6307 | 0.0011 | 1.61 | 3.3771 | 0.0487 | 8.26 | 0.01 |
| Cr/Fe 10 | 4.08 | 1.6300 | 0.0017 | 1.68 | 3.3764 | 0.0501 | 8.02 | 0.01 |

$N$: coordination number, $\sigma^2$: Debye-Waller factor, $E_0$: threshold shift in electron volts, $R$: interatomic distance.

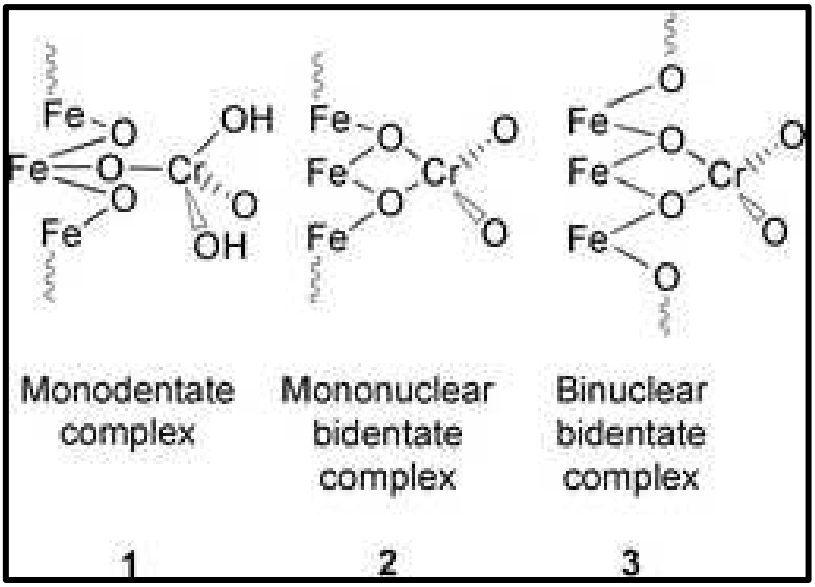


**Fig. 3.22 potential Cr-Fe bonding** [47]

Xie et al. (2015) [45] assessed the portions of inner and outer sphere complexation and coordination geometry by using Fh proxy; goethite. Their results evidenced that chromate was immobilized *via* inner-sphere complexation with bidentate predominance (Fig. 3.22) at low pH (pH <6.5), and monodentate predominance at higher pH (pH>6.5). In a previous study, Scott et al. (1997) reported that, at pH 5, goethite forms bidentate binuclear (3.29 Å) and bidentate mononuclear complexes (2.91 Å) with Cr at low surface coverage [39].

In comparison, this study exhibited a close Cr–Fe surface complexation (Fig. 3.23 and Fig. 3.24) as the bidentate binuclear complex formed at ~3.378 Å in Fh [48]. This difference might be explained considering that goethite contains more protonation sites than Fh [16]. Therefore, the higher ability of protonation sites at displacing water molecules compared to hydroxyl groups would result in a closer bonding.

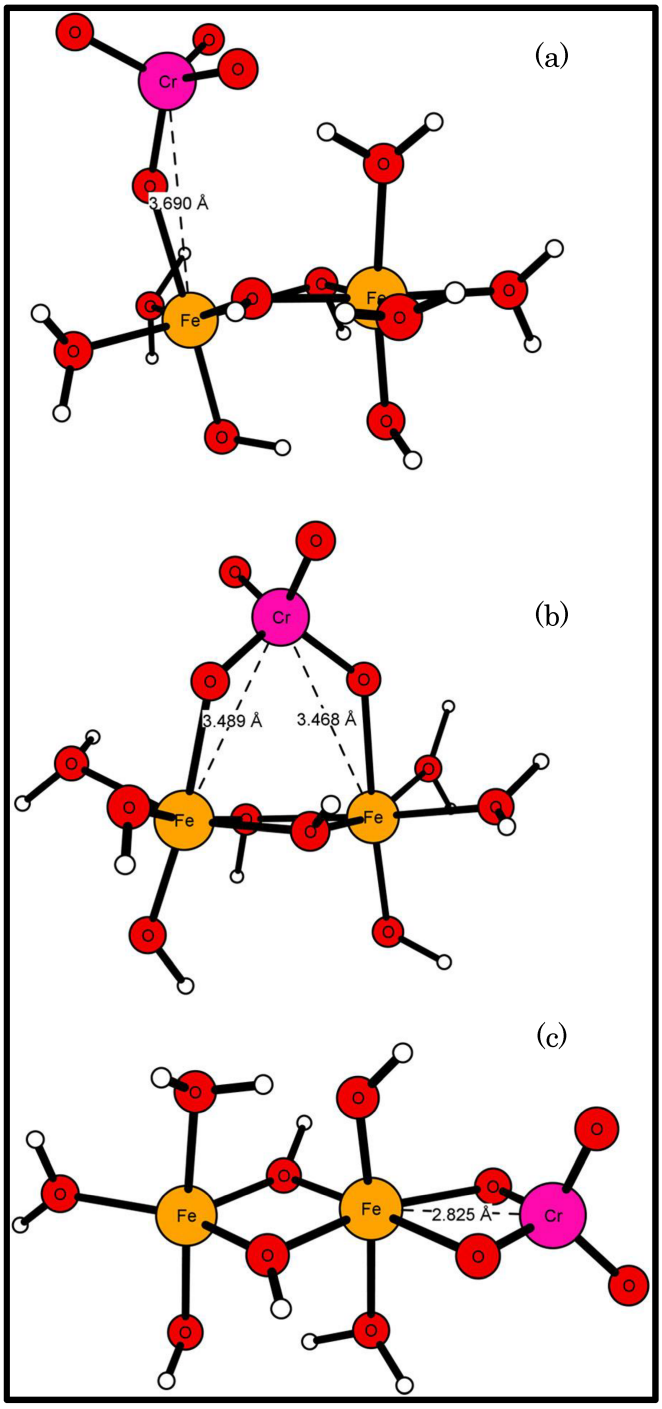


**Fig. 3.23 Model inner-sphere structures of chromate coordinated to iron hydroxide dimers and theoretical Cr–Fe distances (Å ) corresponding to (a) monodentate, (b) corner-sharing bidentate, and (c) edge sharing- bidentate surface complexes** [49]

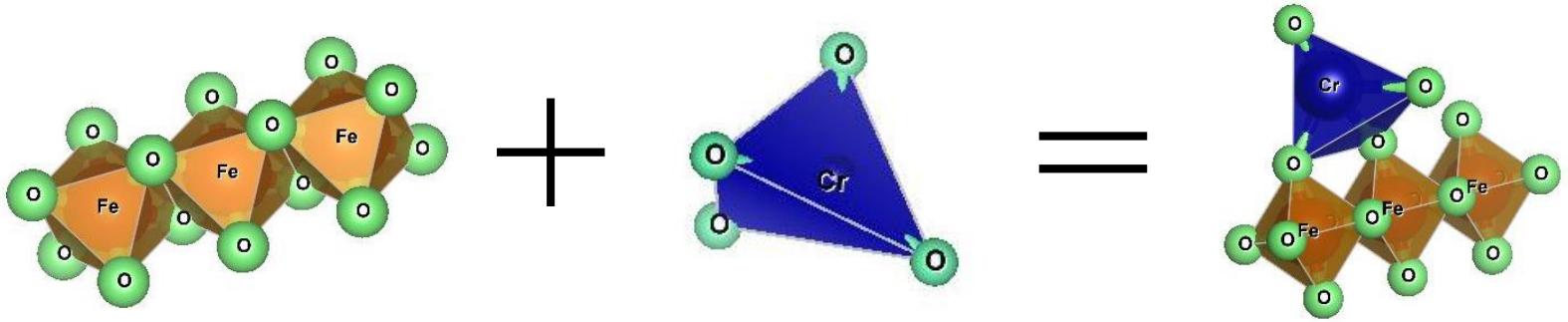


Fh | Chromate | Inner-sphere bidentate binuclear surface complexation comprising with tetrahedral Cr with octahedral Fe bonding brings Fh expansion

**Fig. 3.24 Graphical representation of final sorption product of chromate coprecipitated with Fh at pH 5. Figure is drawn using the VESTA 3** [48]

### 3.4 Summary

The chromate adsorption onto Fh could be described by a BET-type sorption isotherm with shape dependent on the operating conditions (e.g. pH, coprecipitation/adsorption). Coprecipitation at pH 5 exhibited a higher sorption density than adsorption and a change of slope for lower Cr/Fe molar ratio (Cr/Fe = 0.50). At the same molar ratio, the XRD peak at 34° broadened and an increase of interatomic distance Fe-O with partial rearrangement tetrahedral-octahedral was confirmed by XAFS analysis. In addition, the zeta potential stabilized at Cr/Fe = 0.25 and the ESR confirmed unaltered magnetic properties. All these evidence highlighted a mechanism shift from outer-sphere to inner-sphere complexation from Cr/Fe = 0.25. In other words, chromate is adsorbed onto ferrihydrite up to Cr/Fe 0.25 and then it is included into Fh. In adsorption, similar phenomena were observed but from higher Cr/Fe molar ratios (Cr/Fe = 1).

The obtained results confirmed that the predominant sorption mechanism is outer-sphere complexation in adsorption and inner-sphere complexation in coprecipitation. In addition, bidentate binuclear Cr–Fe bonds were well established upon chromate removal at high Cr/Fe molar ratios. This information is important for the purpose of chromium recovery since complexation geometry affects the ease of chromate release. In this view, the stronger Cr-Fe bonding resulting from the bidentate binuclear coordination might impede an efficient Cr recovery but also might provide more stabilization in case of disposing in landfills.

**References**


[1] J.H. Kim, V. Bokare, E.J. Kim, Y.Y. Chang, Y.S. Chang, J. Nanoparticle Res. 14 (2012).

[2] J.S. Hu, L.S. Zhong, W.G. Song, L.J. Wan, Adv. Mater. 20 (2008) 2977–2982.

[3] R. H. Li, Q. LI, J. Am. Ceram. Soc. 94 (2011) 584.

[4] L.C.A. Oliveira, D. I . Petkowicz, Water Res. 38 (2004) 3699.

[5] N.N. Nassar, Can. J. Chem. Eng. 90 (2012) 1231–1238.

[6] R. Wu, J. Qu, Y. Chen, Water Res. 39 (2005) 630–638.

[7] F. Mou, J. Guan, Z. Xiao, Z. Sun, W. Shi, X.-A. Fan, J. Mater. Chem. 21 (2011) 5414.

[8] Z. Wu, W. Li, P.A. Webley, D. Zhao, Adv. Mater. 24 (2012) 485–491.

[9] T. Ren, P. He, W. Niu, Y. Wu, L. Ai, X. Gou, Environ. Sci. Pollut. Res. 20 (2013) 155–162.

[10] R.M. Cornell, U. Schwertmann, The Iron Oxides: Structure, Properties, Reactions, Occurrences and Uses, John Wiley & Sons, 2006.

[11] J.L. Jambor, J.E. Dutrizac, Chem. Rev. 98 (1998) 2549–2586.

[12] I. Garcia-Sosa, A. Cabral-Prieto, N. Nava, J. Navarrete, M.T. Olguin, L. Escobar, R. Lopez-Castanares, O. Olea-Cardoso, Hyperfine Interact. 232 (2015) 67–75.

[13] C.C. Fuller, J.A. Dadis, G.A. Waychunas, Geochim. Cosmochim. Acta (1993).

[14] H. Wang, J. Zhu, Q. Fu, H. Hu, J. Soils Sediments (2015) 1500–1509.

[15] Hsia, T. H., S. L. Lo, C. F. Lin, D.Y.L. Chemosphere 26 (1993) 1897–1904.

[16] C.P. Johnston, M. Chrysochoou, Environ. Sci. Technol. 46 (2012) 5851–5858.

[17] Y. Takahashi, D. Ariga, Q. Fan, T. Kashiwabara, in:, J. Ishibashi, K. Okino, M. Sunamura (Eds.), Subseafloor Biosph. Linked to Hydrothermal Syst., Springer Japan, Tokyo, 2015, pp. 39–48.

[18] C. Tokoro, S. Suzuki, D. Haraguchi, S. Izawa, Materials (Basel). 7 (2014) 1084–1096.

[19] C. Tokoro, T. Sakakibara, S. Suzuki, Chem. Eng. J. 279 (2015) 86–92.

[20] C. Tokoro, Y. Yatsugi, H. Sasaki, S. Owada, Resour. Process. 8 (2008) 3–8.

[21] D. Haraguchi, C. Tokoro, Y. Oda, S. Owada, J. Chem. Eng. Japan 46 (2013) 173–180.

[22] C. Tokoro, H. Koga, Y. Oda, S. Owada, Y. Takahashi, J. MMIJ 127 (2011) 213–

218.

[23] S. Leckie, J. O. Benjamin, M. M., Hayes, K., Kaufman, G., Altman, Adsorption/Coprecipitation of Trace Elements from Water with Iron Oxyhydroxide, Palo Alto, CA, 1980.

[24] J.M. Zachara, C.E. Cowan, R.L. Schmidt, C.C. Ainsworth, Clays Clay Miner. 36 (1988) 317–326.

[25] A.C. Cismasu, F.M. Michel, A.P. Tcaciuc, G.E. Brown, Geochim. Cosmochim. Acta 133 (2014) 168–185.

[26] E. Doelsch, J. Rose, A. Masion, J.Y. Bottero, D. Nahon, P.M. Bertsch, Langmuir 16 (2000) 4726–4731.

[27] G.A. Waychunas, B.A. Rea, C.C. Fuller, J.A. Davis, Geochim. Cosmochim. Acta 57 (1992) 2251–2269.

[28] S. Das, M. Jim Hendry, J. Essilfie-Dughan, Appl. Geochemistry 28 (2013) 185–193.

[29] P. Trivedi, J.A. Dyer, D.L. Sparks, Environ. Sci. Technol. 37 (2003) 908–914.

[30] M. Kawser Ahmed, M.A. Baki, G.K. Kundu, M. Saiful Islam, M. Monirul Islam, M. Muzammel Hossain, Springerplus 5 (2016) 1697.

[31] G.A. Waychunas, C.C. Fuller, J.A. Davis, J.J. Rehr, Geochim. Cosmochim. Acta 67 (2003) 1031–1043.

[32] T.D. Waite, J.A. Davis, T.E. Payne, G.A. Waychunas, N. Xu, Geochim. Cosmochim. Acta (1994).

[33] K. Kameda, Y. Hashimoto, S. Wang, Y. Hirai, J. Hazard. Mater. 327 (2017) 171–179.

[34] V. Veselska, R. Fajgar, S. Cihalova, R.M. Bolanz, J. Gottlicher, R. Steininger, J.A. Siddique, M. Komarek, J. Hazard. Mater. 318 (2016) 433–442.

[35] H.I. Adegoke, F. AmooAdekola, O.S. Fatoki, B.J. Ximba, Korean J. Chem. Eng. 31 (2013) 142–154.

[36] Y. Wang, J. Ma, K. Chen, Phys. Chem. Chem. Phys. 15 (2013) 19415.

[37] A. Al Mamun, M. Morita, M. Matsuoka, C. Tokoro, J. Hazard. Mater. 334 (2017) 142–149.

[38] C. Tokoro, Resour. Process. 62 (2015) 3–9.

[39] S. Fendorf, M.J. Eick, P. Grossl, D.L. Sparks, Environ. Sci. Technol. 31 (1997)

315–320.

[40] P. Suksabye, A. Nakajima, P. Thiravetyan, Y. Baba, W. Nakbanpote, J. Hazard. Mater. 161 (2009) 1103–1108.

[41] Y. Hexiong, L. Ren, R.T. Downs, G. Costin, Acta Crystallogr. Sect. E Struct. Reports Online 62 (2006).

[42] F. Maillot, G. Morin, Y. Wang, D. Bonnin, P. Ildefonse, C. Chaneac, G. Calas, Geochim. Cosmochim. Acta 75 (2011) 2708–2720.

[43] A. Manceau, W.P. Gatest, Clay Clay Miner. 45 (1997) 448–460.

[44] Y. Shinoda, Kozo., Matsubara, Eiichiro., Muramatsu, Atsushi., Waseda, Mater. Res. Bull. 35 (1994) 394–398.

[45] J. Xie, X. Gu, F. Tong, Y. Zhao, Y. Tan, J. Colloid Interface Sci. 455 (2015) 55–62.

[46] P.A.R.E.A. Bonnin, Acta Cryst. 2 (1978) 706–709.

[47] D.M. Roundhill, H.F. Koch, Chem. Soc. Rev. 31 (2002) 60–67.

[48] K. Momma, F. Izumi, J. Appl. Crystallogr. 44 (2011) 1272–1276.

[49] C.P. Johnston, M. Chrysochoou, Geochim. Cosmochim. Acta 138 (2014) 146–157.

# [Chapter 4]

# Cr(VI) removal mechanism through pH-dependent LDH (Layer Double Hydroxide) of sulfate green rust

## 4.1 Introduction

Cr(VI) has become a major concern because of carcinogenicity and removal difficulty [1]. Recently, several forms of iron oxides showed an interesting ability towards the immobilization of the predominant Cr(VI) species, i.e. chromate in a wide range of pH. Among them, ferrihydrite [$(Fe^{3+})_2O_3 \cdot 0.5H_2O$] was described in the previous chapter as efficient but not enough for real processes due to slow kinetics, large production of sludge and difficult chromate recovery from the sludge [2].

An interesting alternative to ferrihydrite was found in green rust (GR), an iron-based compound composed by Fe(II) and Fe(III) hydroxide units intercalated with water molecules and anions such as chloride, carbonate and sulfate ions [3]. GR exhibits a layer double hydroxide (LDH) structure where positively charged hydroxide units occupy surface positions whilst anions and water molecules are intercalated in the resulting interlayer [5]. GR can be described through the general formula $[Fe(II)_{6-x}Fe(III)_x(OH)_{12}]^{x+}[(A)_{x/n}.yH_2O]^{x-}$, where *A* is the anion and *n* is the anion charge (Fig. 4.1). Accordingly, the Fe(II)/T-Fe ratio ranges between 0.8 and 0.3 [4,5]. GR is also described through another generalised formula, namely $[M(II)_{1-x}M(III)_x(OH)_2]^{x+}A^{y-}_{x/y} \cdot mH_2O$, where M= Fe and *x* ranges from 0.25 to 0.33 [6]. Accordingly, the Fe(II)/T-Fe ratio would lie between 0.66 and 0.75 [7,8].

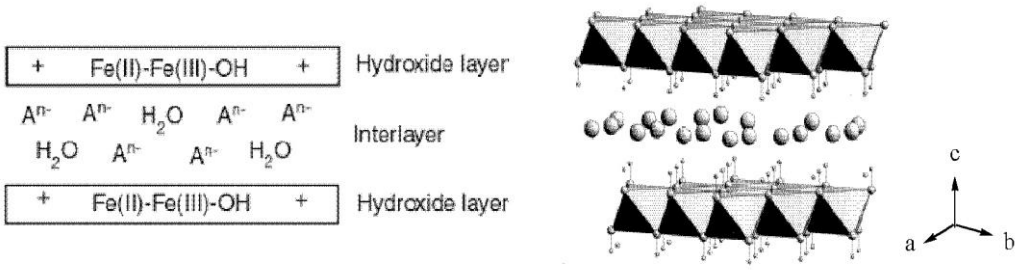


**Fig. 4.1 Simplified Layer double hydroxide** [9]

Among GRs, the ones containing sulfate ions in the interlayer are the most studied [10–12]. This is because the sulfate ion can be naturally found in both engineered and natural geo-environmental systems like seawaters and oxic-anoxic interfaces in hydromorphic soils [13].

GR has been recently proven capable to reduce and immobilize oxidized organic pollutants and heavy metal anions such as chromate, arsenate and selenate [4,14,15].

Therefore it could be potentially utilized in the treatment of tannery wastewater. GR's ability to remove oxidized species arisen mainly from the presence of surface Fe(II). Indeed, Fe(II) can reduce oxidized species by oxidizing itself to Fe(III). In addition, the interlayer between the double hydroxide chains contains anions (e.g. sulfate) that can be exchanged with the toxic anions to be removed [11,16].

Although GR's ability to remove chromate has been confirmed, implementing real processes requires a full understanding of removal mechanism. Most research works on chromate removal with GR addressed only performances and kinetic aspects [5,8,17] whereas the available information about the mechanism is scarce and often conflicting [1,11,18,19]. In particular, it is not clear yet whether GR immobilizes chromate through surface sorption [10] or intercalation [11,12]. The discrepancies may arise from differences in the experimental setup and from the low stability of GR, which is very prone to oxidation. Depending on the operating conditions, the oxidation of GR can result in the formation of different kinds of iron oxides with different oxidation states, from magnetite to ferrihydrite, up to goethite [1,11,18–22]. The type of final product may affect the solid-liquid separability of the sludge. In addition, the formation of chromium compounds upon removal still needs to be elucidated to prove the ability of Cr recovery from the final sludge.

As for the final product, the only available information in literature was reported by Bond and Fendorf (2003). They discussed about the formation of a chromium-intercalated iron oxide product like $Cr_xFe_{1-x}(OH)_3.nH_2O$ [1]. Although authors confirmed the chromate insertion through XAFS, they did not show any information about Fe edge. In addition, they did not provide any detailed information about Cr-Fe and Cr-O bonding, which is a crucial aspect aiming to recover Cr.

In general, the still required information are not only related to removal mechanism. Understanding the conditions to confer specific properties and removal abilities to GR is also very important. Ahmed et al. (2010) reported that sulfate-GR undergoes structural changes depending on the pH during preparation [14]. However, authors did not assess whether this change affects removal properties and behaviour. In this view, further studies where the properties are related to chromate removal are required.

This chapter addresses the use of sulfate-GR to remove chromate from water and

provides details about removal performance and removal mechanism at different pH. The objective of the research was to investigate the role of pH in GR preparation and chromate removal. For this purpose, two different types of sulfate-GR were prepared at pH 8.75 and 7.50 (hereafter referred to as $GR_{8.75}$ and $GR_{7.50}$, respectively) and tested at pH 5 and pH 9. The role of pH during GR preparation was elucidated determining GR's structural properties by XRD and XAFS. The obtained information was related to GR's behaviour and chromate removal.

The correlation between preparation pH, GR properties and chromate removal mechanism represents a novelty aspect of this work and will lay the foundations for the use of GR in real wastewater treatment processes.

## 4.2 Materials and methods

### 4.2.1 Materials and stock solutions

All chemicals used during the experimental campaign were analytical grade reagents from Wako Chemical Industries (Japan). All solutions were prepared in deionized-distilled water. The Cr(VI) stock solution was prepared dissolving $K_2CrO_4$ in water while the Fe(II)-Fe(III) solutions used for the precipitation of GRs were prepared dissolving in water pre-defined amounts of $FeSO_4 \cdot 7H_2O$ and $Fe_2(SO_4)_3 \cdot nH_2O$.

### 4.2.2 Preparation of GR

The preparation of GR was carried out within a glove box under argon atmosphere. For the batch experiments, a gas displacement type acrylic glove box equipped with pass box and oxygen meter (As-One, Japan) was used. GR was prepared *via* coprecipitation method by titrating a mixture solution of Fe(II)–Fe(III) with 8 M NaOH, as described by Hayashi et al. (2009) (Fig. 4.2) [10]. The solution was kept under magnetic stirring and argon bubbling by using a glass diffuser for 5 hours while continuously monitoring pH (Thermo Scientific) and ORP (Horiba Scientific). Finally, the olive green coloured precipitate was collected by centrifugation at 12000 rpm for 10 min (Himac CR21, Hitachi, Japan). Since Fe ions and electrolytes could adsorb on the surface of GR precipitates, the product was washed by argon-flushed deionized water with vigorous shaking. The GR precipitate was collected after a second centrifugation and was suspended again in argon-flushed deionized water to perform the batch experiments.

To investigate the role of pH, two different types of sulfate-GR were prepared by titrating at pH 7.5 ($GR_{7.50}$) and 8.75 ($GR_{8.75}$). The total concentration of iron (T-Fe) in the Fe(II)–Fe(III) solution was 0.4 M while the [Fe(II)]/[T-Fe] ratio was 0.75.

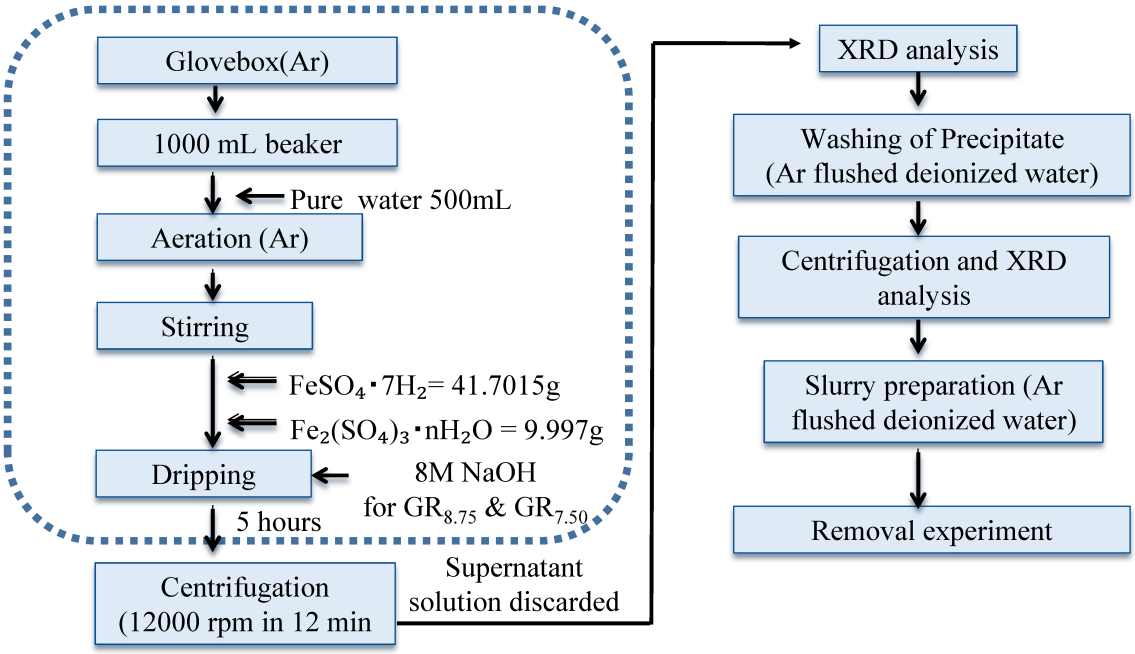


**Fig. 4.2 Flow chart of GR preparation (dotted box represent operations within glove box)**

### 4.2.3 Batch chromate removal experiments

The batch tests for chromate removal were carried out for 1 hour under the same Cr/T-$Fe_{GR}$ ratio (where T-$Fe_{GR}$ means total Fe molar of GR) of 0.5. The total iron in the GR slurry was measured to ensure equal inputs in solution. For the investigation of the role of pH on chromate removal, the pH of the slurry was continuously monitored and kept constant at 5 or 9 through the addition of 0.1 M $HNO_3$ and 0.1 M KOH. The ORP was also kept constant by flushing argon gas throughout the experiment. The desired amount of GR suspension was added to 500 ml of Ar-flushed deionized water and then the previously prepared Cr(VI) solution was injected up to reach the desired Cr/T-$Fe_{GR}$ ratio.

Samples of the suspension were taken at regular intervals and filtered using 0.1μm membrane filters. Both filtrate and solid residues were stored for analysis.

### 4.2.4 Analysis

**(i) ICP-AES and IC analysis**

The filtrates from the removal experiments were analysed by inductively coupled plasma-atomic emission spectrometry (ICP-AES, SPS 7800 - Seiko Instruments Inc., Japan) to quantify the residual Cr concentration (Table 3-1; chapter 3). The concentration of sulfate was determined by ion chromatography (IC) with an electric conductive detector (ICS 2100, Thermofisher Scientific, USA). The measurements were conducted according to the conditions described in Table 4.1.

**Table 4.2 IC measuring conditions**

| | |
|---|---|
| A separation column | IonPac AS19 |
| A guard column | IonPac AG19 |
| Eluent | 3.2 mM-$Na_2CO_3$/1.0 mM-$NaHCO_3$ |
| Flow [mL/min] | 0.7 |
| Injecting amount | 25 μL |
| Column temperature | 35°C |

**(ii) Absorption spectroscopy**

The concentrations of dissolved Fe(II) and T-Fe were measured by absorption spectroscopy (HACH DR 500) upon dissolution in HCl. The analysis of Fe(II) was performed through the 1-10 Phenanthroline method by measuring the absorbance at 510 nm [23]. The total concentration of iron (T-Fe) was measured by reducing Fe(III) to Fe(II) with hydroxylamine hydrochloride, before Fe(II) analysis.

**Table 4.2 Measuring condition of absorption spectroscopy**

| | |
|---|---|
| Measurement mode | fraction transmitted, absorbance, concentration |
| Lighting the lamp | visible light ; tungsten,<br>ultraviolet light ; deuterium |
| Wave length | 510 nm |
| Wavelength accuracy | Wavelength 200 ～ 900 nm±1 nm |
| Wavelength repeatability | < 0.5 nm |
| Wavelength resolution | 0.1 nm |
| Wavelength option | Automatic, Base on the measurement method |
| Spectrum band | 2 nm |
| Photometric length | Wavelength 200～900 nm±3.0 Abs ; 1 % |

**(iii) XRD analysis**

Information on phase composition and crystal structure of the solid phases ($GR_{8.75}$ and $GR_{7.50}$) before and after chromate removal were obtained by XRD (Geiger flex RAD-IX, Rigaku Corp. Japan). To preserve samples from oxidation, the collected pastes were mixed with glycerol and transferred into the XRD chamber [24]. The XRD measuring conditions are given in Table 3-2 (chapter 3). The crystallite size related to XRD peaks was estimated by the PDXL XRD-software based on the Scherer equation.

**(iv) XPS analysis**

The surface of collected solid samples was analysed by x-ray photoelectron spectroscopy (XPS) (PHI5000 Versa Probe II, ULVAC-PHI, Physical electronics Inc. USA) using adventitious hydro-carbon reference with a charge of 284.8eV. To prevent the oxidation of solid samples, the specimens for XPS and XAFS analysis were prepared within a glove box (UNICO, Japan) equipped with pass box (SUS 304, UNICO, Japan) supporting vacuum drying below 0.1 MP. For the analysis, samples were loaded in the

micro XPS sample holder directly from the glove box.

**Table 4.3 XPS measuring conditions**

| | |
|---|---|
| Incident lens | 3-step cylindrical electrostatic lens |
| Energy sweep system | Energy sweep system |
| Pressure | 7×10-8 Pa or less |
| Fe | 2p3/2 |
| Cr | 2p3/2 |
| C | 1s |
| S | 1s |
| O | 1s |

The Cr 2p3/2 spectra were fitted with symmetric peaks (70% Gaussian and 30% Lorentzian) using also Cr 2p3/2 multiplets to account for Cr oxides. The 5 peak-multiplet was constrained by fixed spin-orbit splitting of 1.01, 0.78, 1.00 and 0.41 eV and area ratio of 36, 35, 19, 8 and 5%.

**(v) XAFS analysis**

XANES and EXAFS analysis was performed at the beam line BL5S1 at Aichi Synchrotron Radiation Center, Aichi, Japan. For the transmission method, samples were blended with boron nitride powder and pressed at 20 kN to create XAFS thin tablet-shaped samples within the glove box (Fig. 3-3; chapter 3). The beam was untuned by 30% to avoid higher-order harmonics generation in the K-edge analysis of Fe and Cr (Table 3-5; chapter 3). $GR_{8.75}$ and $GR_{7.50}$ without chromate were analysed as a reference material of Fe K-edge.

**(vi) Surface area measurement**

The BET surface area of both GR determined through the adsorption of $N_2$ gas based on JIS8830 and ISO 9277 (ASAP 2010, Shimadzu, Japan).

## 4.3 Results and discussion

### 4.3.1 Characterisation of $GR_{8.75}$ and $GR_{7.50}$

According to literature, sulfate-GR can be prepared by oxidation method only in the redox potential (vs SHE) range from -550 to -100 mV and in the pH range 7-11 [25]. The experimental Eh and pH during the preparation of GR are shown in Fig. 4.3. During preparation (Fig. 4.4), schwertmannite ($Fe_8O_8(OH)_6(SO_4)\cdot nH_2O$) was formed first at pH 2-3 (dark straw colour), and then it was rearranging to brownish goethite (FeOOH) at pH 3-7. Finally, the formation of GR(II) sulfate took place beyond pH 7, as reported by Imad et al. 2010 [14]. The GR was initially reported as stable within the range of pH 6–7.5, whereas magnetite preferentially forms between pH 9.8 and 10.3. However, recent researches proved that stable GRs could be formed at pH 10 as well [14].

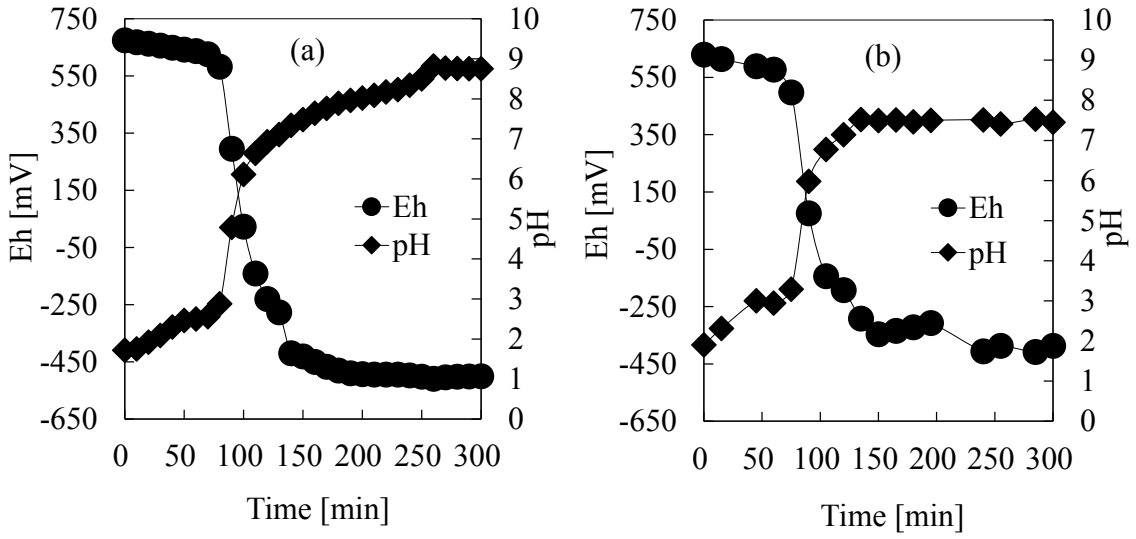


**Fig. 4.3 Eh (vs SHE) and pH during the preparation of (a) $GR_{8.75}$ and (b) $GR_{7.50}$**

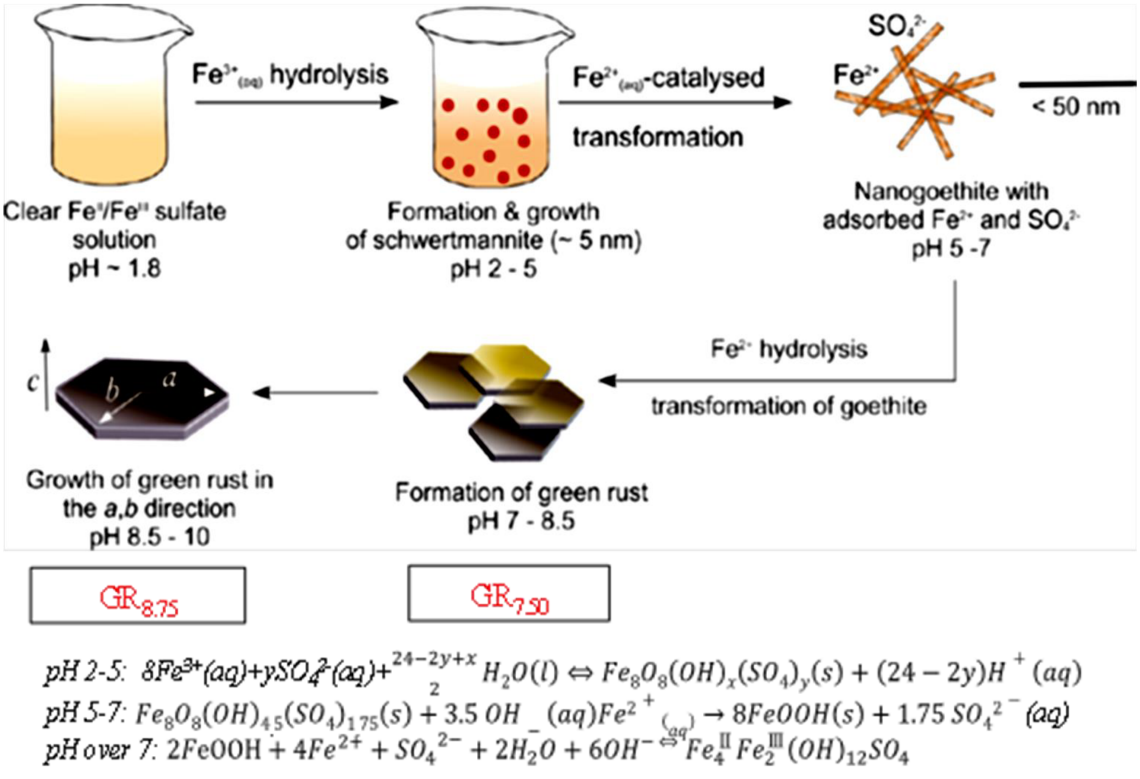


$$pH\ 2\text{-}5:\ 8Fe^{3+}(aq)+ySO_4^{2-}(aq)+\frac{24-2y+x}{2}H_2O(l) \Leftrightarrow Fe_8O_8(OH)_x(SO_4)_y(s)+(24-2y)H^+(aq)$$

$$pH\ 5\text{-}7:\ Fe_8O_8(OH)_{4.5}(SO_4)_{1.75}(s)+3.5\ OH^-(aq)Fe^{2+}{}_{(aq)} \rightarrow 8FeOOH(s)+1.75\ SO_4{}^{2-}(aq)$$

$$pH\ over\ 7:\ 2FeOOH+4Fe^{2+}+SO_4{}^{2-}+2H_2O+6OH^- \Leftrightarrow Fe_4^{II}Fe_2^{III}(OH)_{12}SO_4$$

**Fig. 4.4 Formation of green rust in coprecipitation** [14]

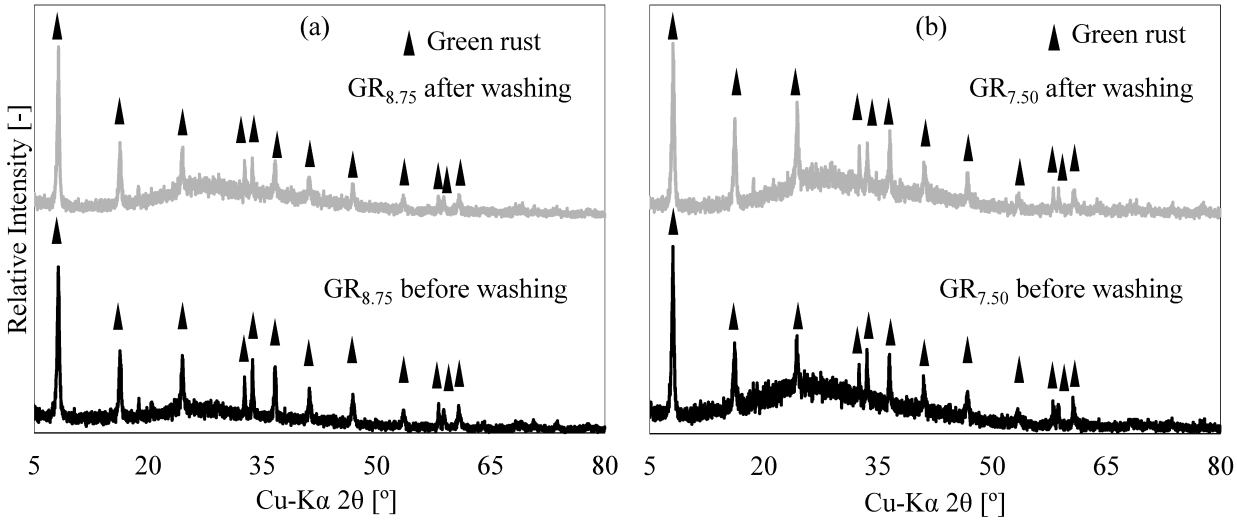


**Fig. 4.5 XRD pattern of (a) $GR_{8.75}$ and (b) $GR_{7.50}$ before and after washing**

The Fe(II) ion in solution could adsorb on GR surface. Therefore, since a large Fe(II)/Fe(III) ratio was used in the preparation of sulfate-GR, the obtained GR product was washed to remove the adsorbed ion and increase the purity. Previous researchers

reported that the sulfate-based LDH of GR could collapse by alkali-free washing [13]. However, in this research work, the produced GR exhibited the same XRD pattern before and after washing, thereby highlighting a successful GR formation at both pH 8.75 and pH 7.50 (Fig.4.5). This result is in agreement with Refait et. al. (2003), who had reported that anaerobic conditions could prevent the alteration of the crystal structure for one week [26]. In addition, the washed GRs exhibited an ideal Fe(II)/T-Fe ratio compared to the unwashed GRs.

To elucidate the effect of washing on $GR_{8.75}$ functionality, washed and non-washed GR samples were used in chromate removal experiments at pH 5, 7 and 9. The experimental results are shown in Fig. 4.6. Results highlighted that non-washed $GR_{8.75}$ removed significantly more chromate than its washed equivalent counterpart. The higher removal of Cr(VI) can be considered as a consequence of the adsorbed Fe ions providing additional reducing power. This result confirmed also the importance of washing GR to obtain meaningful and non-misleading sorption results.

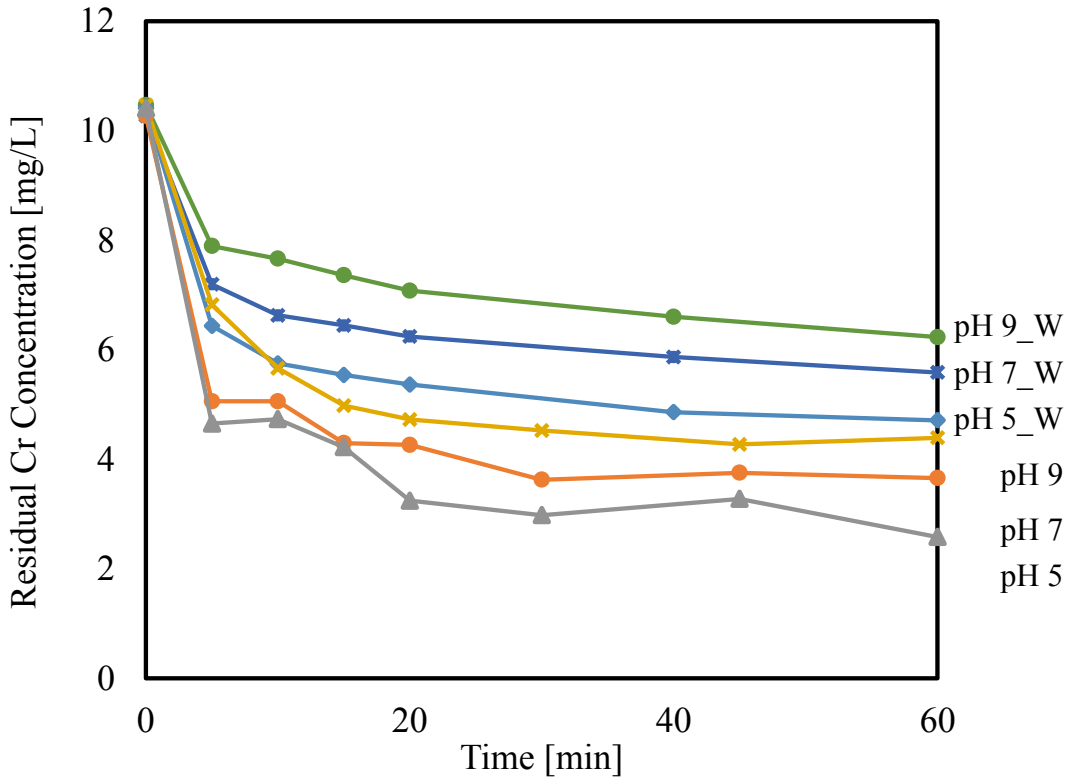


**Fig. 4.6 Effect of washing on chromate removal by $GR_{8.75}$ ('W' = washed)**

The significantly lower full-width at half-maximum (FWHM) of XRD peaks [001], [003] and [100] obtained for $GR_{8.75}$, highlight the horizontal and vertical expansion of GR (Table 4.4). This phenomenon could be reasonably considered as the consequence of a larger intercalation of $SO_4^{2-}$ and $Na^+$ in the interlayer of $GR_{8.75}$. Unlike Ahmad et al. (2010) who confirmed only the horizontal expansion beyond pH 8.5, we observed both horizontal and vertical expansion. This difference might be explained considering that prepared GR exhibited different Fe(II)/Fe(III) molar ratios. Ahmed et al. (2010) produced GR at Fe(II)/Fe(III) = 2 [14], whereas in this research the Fe(II)/Fe(III) = 3. The higher proportion of Fe(II) might have determined a larger inclusion within GR's structure, thereby promoting the enlargement of [001] and [003] lattices. An alternative explanation for the expansion could be given in terms of charge balance. Christiansen [27] revealed that cations like $Na^+$ are necessary for green rust to achieve stability. Accordingly, when the surface charge of GR switches from positive to negative at pH higher than 8.3 [28], a larger inclusion of $Na^+$ within the interlayer is required to achieve the charge balance [13]. Therefore, the vertical expansion might take place as a consequence of the enhanced inclusion of $Na^+$

The as-prepared $GR_{8.75}$ and $GR_{7.50}$ were analysed by XAFS to obtain information on their local crystal structures. XAFS results evidenced a higher Fe-Fe coordination for edge-sharing and double-corner sharing in $GR_{8.75}$ (Table 4.5). This result could be explained considering that an increase of T-Fe concentration might have promoted the edge and double corner sharing. Alternatively, the increase of monodentate/single corner sharing via oxygen might have occurred due to the larger amount of $Na^+$ and $SO_4^{2-}$ included within the interlayer of $GR_{8.75}$ compared to $GR_{7.50}$.

As a further confirmation of the enhanced inclusion of $Na^+$ and $SO_4^{2-}$ at higher pH, $GR_{8.75}$ released about 1.7 times the $Na^+$ and 1.6 times the $SO_4^{2-}$ than $GR_{7.50}$ upon dissolution in aqua regia. Moreover, the T-Fe concentration in $GR_{8.75}$ was about 33% higher than in $GR_{7.50}$. Since the sulfate oxygen is bound to the beneath layer $OH^-$ though hydrogen bonding, the inclusion of more $Na^+$ and $SO_4^{2-}$ might have determined a change of the oxygen position, which in turn produced a shift of $OH^-$ and resulted in the change of Fe position as well.

For both $GR_{8.75}$ and $GR_{7.50}$, the Fe(II)/T-Fe ratio was in the range 0.63-0.68, which is very close to the theoretical ratio 0.66 [29–31]. Therefore, the electro-neutrality of

$GR_{8.75}$ and $GR_{7.50}$ would be achieved with the following formulas;

$$Na_{0.17}Fe(II)_{0.49}Fe(III)_{0.25}(OH)_{1.24}(SO_4)_{0.33}\ (s) \approx GR_{8.75} \qquad (1)$$

$$Na_{0.10}Fe(II)_{0.32}Fe(III)_{0.16}(OH)_{0.80}(SO_4)_{0.21}\ (s) \approx GR_{7.50} \qquad (2)$$

$GR_{8.75}$ exhibited a higher specific surface area (49.66 $m^2/g$) compared to $GR_{7.50}$ (25.76 $m^2/g$), thus suggesting a higher degree of crystallinity of $GR_{7.50}$. This evidence might be the result of the larger inclusion of $Na^+$ and $SO_4^{2-}$, which resulted in an increased disorder of the crystal structure. A similar finding was confirmed by Rogers et al. (2013) who confirmed an increase of surface area of GR due to Zn substitution into GR structure [32] when adding $Zn^{2+}$ to the Fe(II) and Fe(III) solutions.

**Table 4.4 XRD data output of $GR_{8.75}$ and $GR_{7.50}$ (after washing)**

| $GR_{8.75}$ | | | $GR_{7.50}$ | | | |
|---|---|---|---|---|---|---|
| **2-theta(deg)** | **FWHM(deg)** | **Size(Å)** | **2-theta(deg)** | **FWHM(deg)** | **Size(Å)** | **Phase name** |
| 8.2 | 0.3289 | 253 | 8.1 | 0.3906 | 213 | Green Rust II(0,0,1) |
| 16.23 | 0.3052 | 275 | 16.2 | 0.3816 | 220 | Green Rust II(0,0,2) |
| 24.48 | 0.311 | 273 | 24.3 | 1.7599 | 48 | Green Rust II(0,0,3) |
| 32.60 | 0.1455 | 594 | 32.6 | 2.3475 | 37 | Green Rust II(1,0,0) |
| 33.63 | 0.1357 | 639 | 33.6 | 0.1162 | 746 | Green Rust II(1,0,1) |
| 36.63 | 0.2305 | 379 | 36.6 | 0.2373 | 368 | Green Rust II(1,0,2) |
| 41.19 | 0.2627 | 337 | 41.1 | 0.3083 | 287 | Green Rust II(1,0,3) |
| 46.91 | 0.2583 | 350 | 46.7 | 0.1997 | 453 | Green Rust II(1,0,4) |
| 53.50 | 0.1377 | 675 | 53.4 | 0.1889 | 492 | Green Rust II(1,0,5) |
| 58.12 | 0.1686 | 563 | 58.1 | 0.1825 | 520 | Green Rust II(1,1,0) |
| 58.69 | 0.1992 | 478 | 58.7 | 0.1582 | 602 | Green Rust II(1,1,1) |
| 60.77 | 0.5422 | 177 | 60.7 | 0.3266 | 294 | Green Rust II(1,1,2) |

FWHM: Full-Width at Half-Maximum

### 4.3.2 Cr(VI) removal

A comparison of chromate removal by $GR_{8.75}$, $GR_{7.50}$ and ferrihydrite at pH 5 for different Cr/Fe molar ratio is shown in Fig. 4.7. Although aspects related to ferrihydrite have been already discussed in the previous chapter, the removal by ferrihydrite was included in the figure to highlight the high efficiency of GR. The pH was set to 5 since both sulfate-GR and ferrihydrite showed the best removal performance at this pH [2]. Zero-valent iron was deliberately excluded from the comparison because it was proven to be not efficient in chromate removal under alkaline condition [5]. Both GRs could remove efficiently chromate below the Japanese wastewater standard. However, $GR_{8.75}$ was found 6.7 times more efficient than ferrihydrite and around 1.7 times more efficient than $GR_{7.50}$ in terms of the required amount of iron to obtain the same performance. Accordingly, $GR_{7.50}$ showed 4 times higher removal efficiency than ferrihydrite. When using $GR_{8.75}$, 0.57mmol/L T-Fe were required to remove 0.19 mmol/L of chromate from the initial 0.20 mmol/L (95% removal). In contrast, 0.96 mmol/L T-Fe from $GR_{7.50}$ and 3.84 mmol/L of T-Fe from ferrihydrite were required to achieve the same performance. This is an important information aiming to implement real processes because a smaller amount of sludge would be produced when using lower amounts of Fe.

The higher removal performances of $GR_{8.75}$ compared to $GR_{7.50}$ could be explained through different factors. First, $GR_{8.75}$ surface area was almost double than $GR_{7.50}$, and this might have determined a higher exposure of Fe(II) to chromate. Rogers et al. (2013) also reported a faster reaction rate for GR-$ZnCO_3$ due to a larger surface area [5]. In addition, higher amounts of $Na^+$, $SO_4^{2-}$ as well as Fe-Fe coordination (formula 1 and 2) might stabilize the LDH structure of $GR_{8.75}$, thereby prolonging its activity [33].

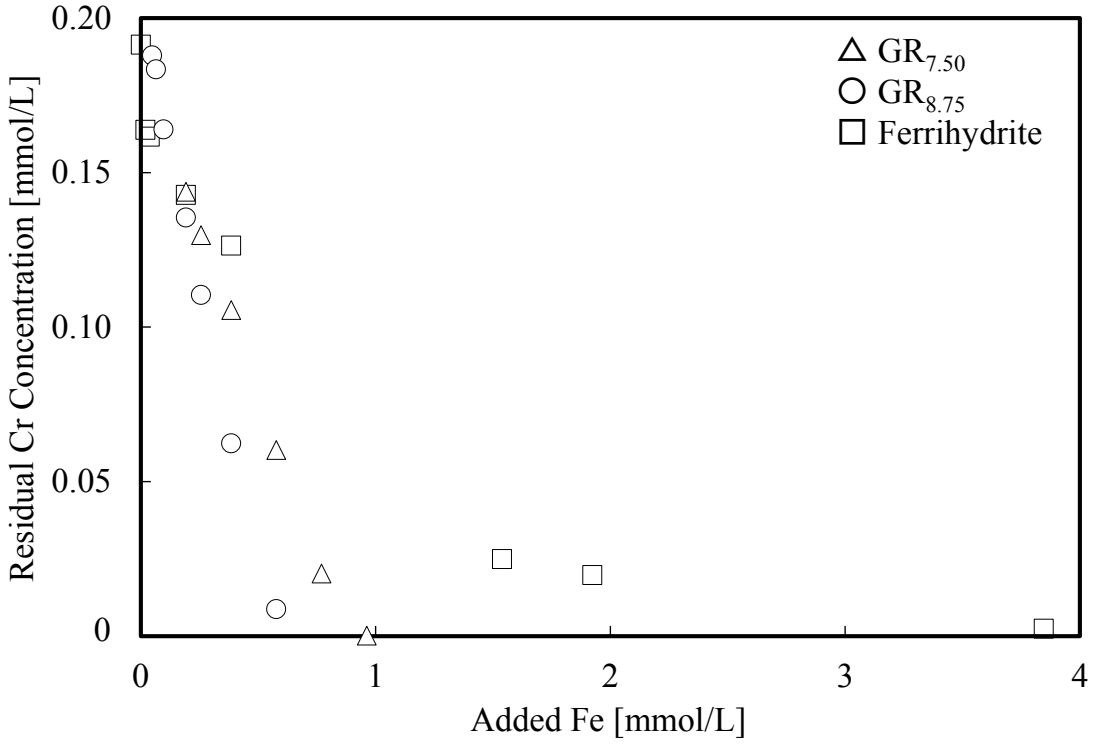


**Fig. 4.7 Chromate removal by $GR_{8.75}$, $GR_{7.50}$ and ferrihydrite at pH 5**

The chromate removal by $GR_{8.75}$ and $GR_{7.50}$ was found to be strongly dependent on pH (Fig. 4.8). Both $GR_{8.75}$ and $GR_{7.50}$ showed the best removal efficiency at pH 5, in agreement with previous findings [10,15,34].

$GR_{8.75}$ removed 55% of the initial chromate at pH 5 and 41% at pH 9 whereas $GR_{7.50}$ removed 47% and 36% respectively. The lower removal under alkaline conditions can be reasonably considered as a consequence of an increased competition between chromate and hydroxyl ions for the adsorption sites of GR. Furthermore, the lower pH might have favoured the redox reaction between chromate and green rust.

Unlike in the experiments for the optimization of the removal performance (where the concentration of GR must be set in excess to Cr) for the elucidation of the removal mechanisms the experiments were operated with a lower amount of GR. The purpose of this investigation was elucidation of the fate of GR and its evolution up to exhaustion. In other words, an excess of GR would determine a complete removal of chromate but would not allow elucidating the GR behaviour through the reaction.

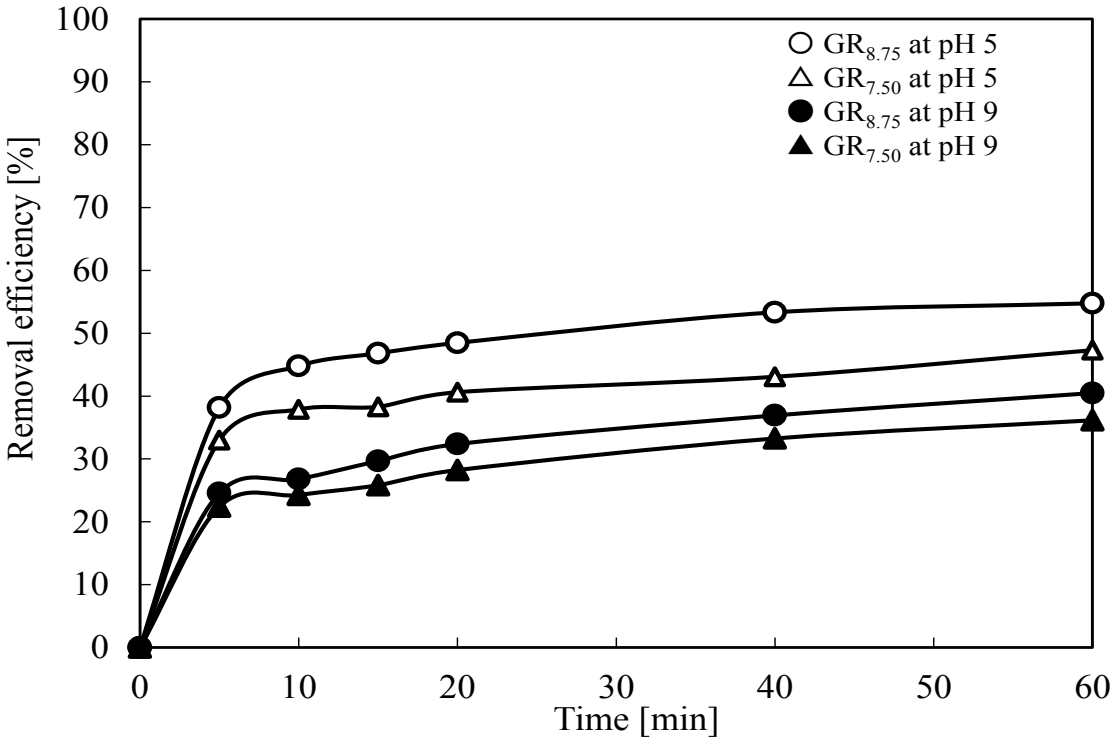


**Fig. 4.8 pH dependent chromate removal efficiency of $GR_{8.75}$ and $GR_{7.50}$ at pH 5 and 9**

### 4.3.3 Sulfate release

The sulfate release from GRs upon adsorbing chromate was found to be dependent on pH. The lower the pH, the lower the sulfate release and vice-versa. A possible explanation for the larger release at high pH is based on the increased dissolution of $Fe(OH)_2$.

The sulfate release by $GR_{8.75}$ and $GR_{7.50}$ (with or without chromate) at pH 5 and pH 9 is shown in figure 4.9. Because chromate can replace the sulfate in the interlayer [12] one might expect a larger sulfate release in the presence of Cr(VI). Nevertheless, the experimental evidence was opposite, as the sulfate release was significantly lower in the presence of chromate for both $GR_{8.75}$ and $GR_{7.50}$. This evidence suggests that the adsorption of chromate onto GR can suppress the sulfate release. In the presence of chromate, the sulfate release by $GR_{7.50}$ was higher, not only as percentage (%) but also as mg/L (5.78 mg/L *vs* 8.40 mg/L at pH 5; 5.91 mg/L *vs* 9.92 mg/L at pH 9). Interestingly, even though $GR_{8.75}$ removed more chromate than $GR_{7.50}$, it released significantly less sulfate. Therefore, we can speculate that $GR_{7.50}$ released more sulfate due a more

pronounced ion-exchange with chromate (Fig. 4.10) from the interlayer.

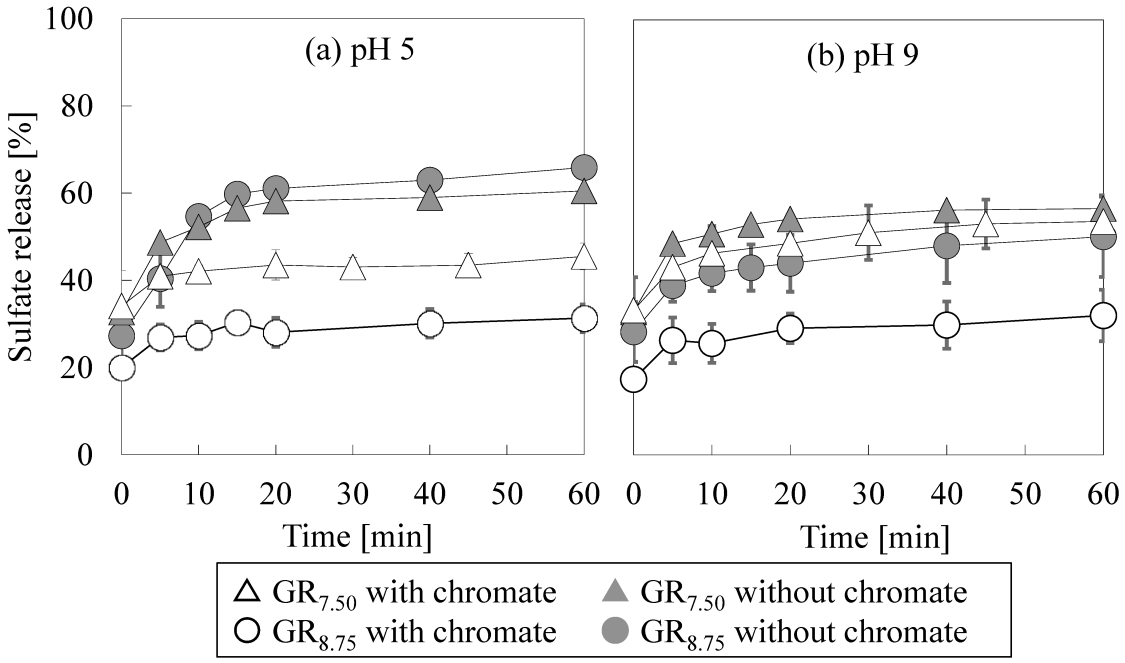


**Fig. 4.9 Sulfate release by $GR_{8.75}$ and $GR_{7.50}$, with and without chromate, at (a) pH 5 and (b) pH 9**

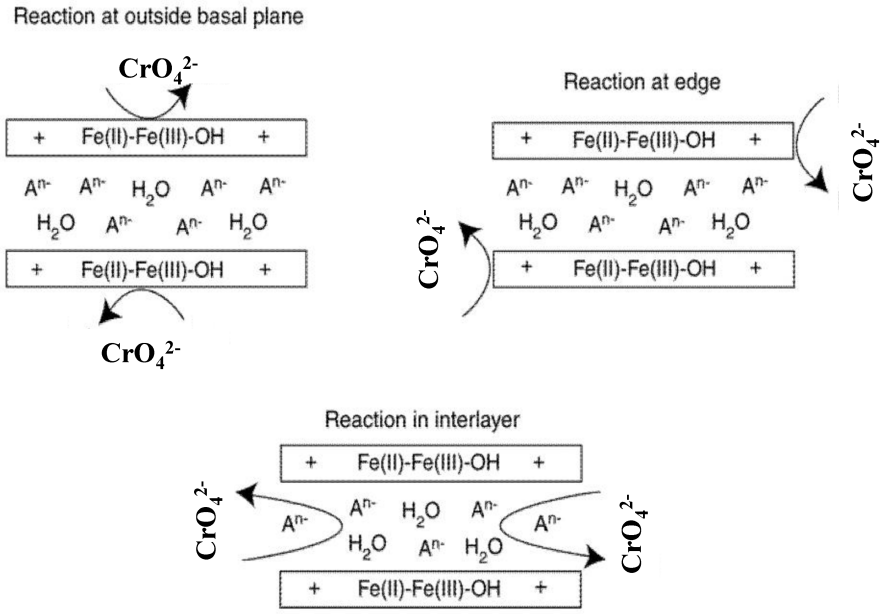


**Fig. 4.10 Reaction at basal planes, at edges and in the interlayer of GR** [9]

### 4.3.4 Solid phase analysis

The XRD spectra of the solid residues from removal experiments with $GR_{8.75}$ and $GR_{7.50}$ are shown in Fig. 4.11 and 4.12. Upon chromate removal by $GR_{8.75}$ at pH 5, the XRD spectra exhibited goethite, magnetite and chromite ($FeCr_2O_4$) peaks. On the other hand, the removal at pH 9 resulted in the formation of magnetite and chromite. Clearly, the higher removal at pH 5 was strongly related to the more efficient electron exchange between GR and chromate which resulted in a more efficient oxidation of GR to goethite. The obtained results are in agreement with Ruby et al. (2010), who reported that oxidation state and phase composition of the end-product after chromate removal varies with removal performances [7]. This implies that the end-product depends on pH during both GR preparation and chromate removal. The authors also stated that, the 20% of oxidation would favour the formation of goethite whereas the 2% of oxidation would favour the formation of magnetite (Fig. 4.13).

The analysis of the XRD spectra by PDXL software [36] revealed that chromite and magnetite deposited on the same lattice (e.g. [311], [400], [422], [511], [440] of $GR_{8.75}$). This implies that the higher the magnetite content, the lower the chromite deposition. This result supports the hypothesis that lower pH enhances the Cr removal.

In the removal experiments with $GR_{7.50}$ at pH 5, the XRD spectra (Fig. 4.12) exhibited a sharp hematite peak and a weak and broad signal in the range 23°-36°, which can be attributed to amorphous chromium-inserted ferrihydrite [2,12]. The same peak was observed in the removal experiment at pH 9, where the hematite peak was much weaker.

Although we refrain from any particular considerations about the broad and weak peak in the range 23°-36° because it could be misleading, it is interesting to observe the differences between the XRD spectra of $GR_{7.50}$ and $GR_{8.75}$. Such differences clearly suggested that $GR_{7.50}$ and $GR_{8.75}$ removed chromate through two different mechanisms. The larger sulfate release and the presence of inserted chromium phases for $GR_{7.50}$ suggest that chromate is removed mainly *via* replacement of sulfate in the interlayer. In contrast, $GR_{8.75}$ removes chromate mainly *via* surface reduction.

According to this hypothesis, upon insertion of the chromate into the LDH interlayer of $GR_{7.50}$, the electrons for the reduction of chromate became available and transferred very fast from the adjacent sheets containing Fe(II) [35]. Therefore, $GR_{7.50}$ would release sulfate, reduce chromate and oxidize itself to ferrihydrite. As a consequence,

the final product would be Cr(III) inserted into ferrihydrite structure. Conversely, with $GR_{8.75}$ the removal takes place from the surface, where Cr(VI) is reduced to Cr(III) upon monolayer formation [15,35,37].

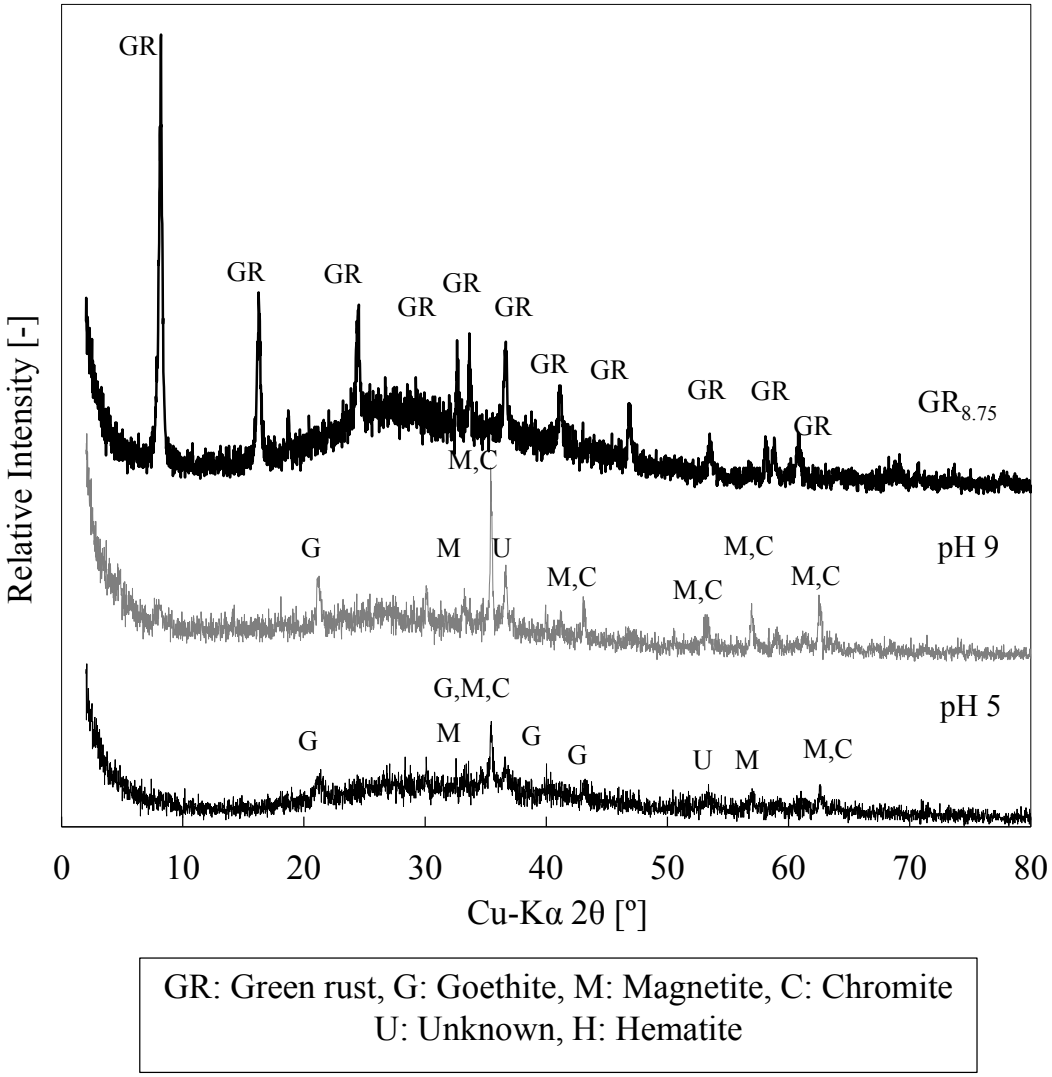


**Fig. 4.11 XRD spectra of $GR_{8.75}$ before and after chromate removal**

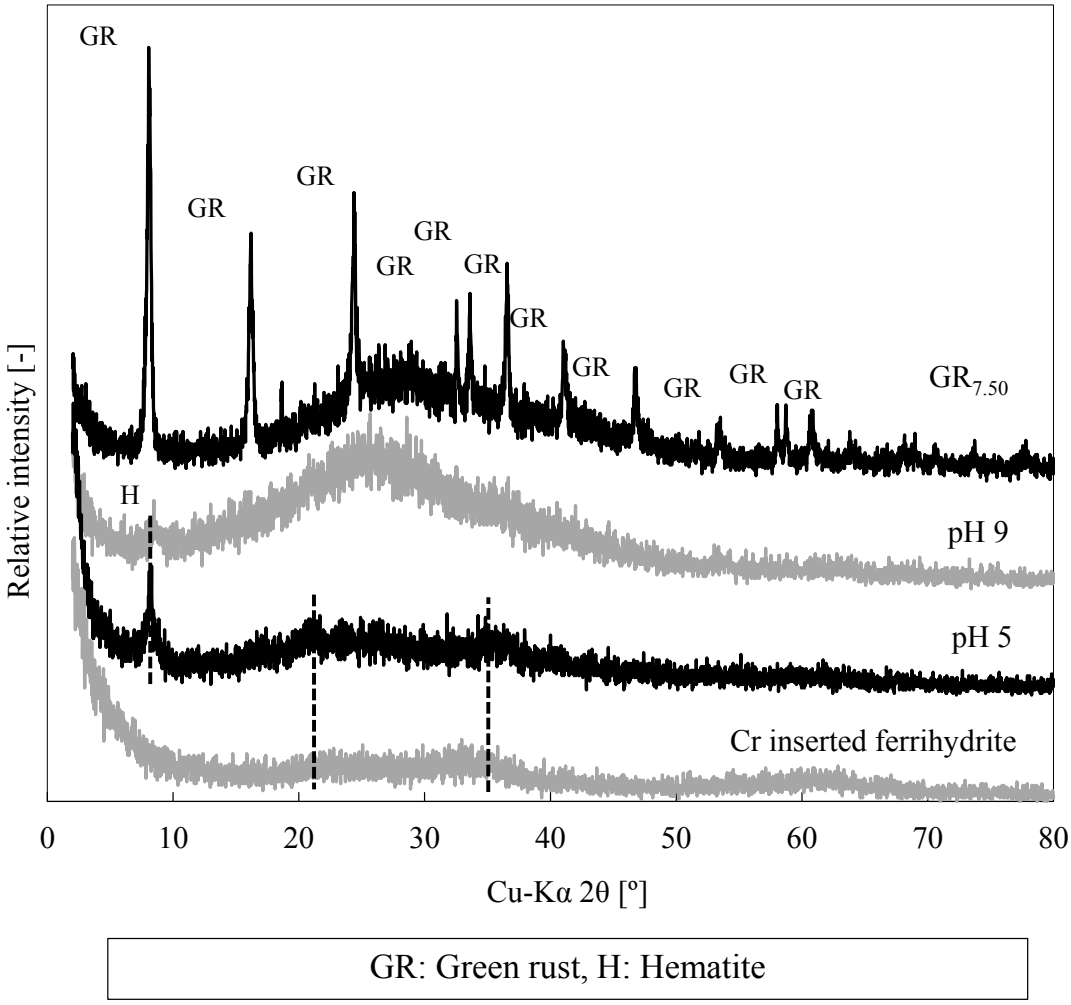


**Fig. 4.12 XRD spectra of $GR_{7.50}$ with chromate at different pH**

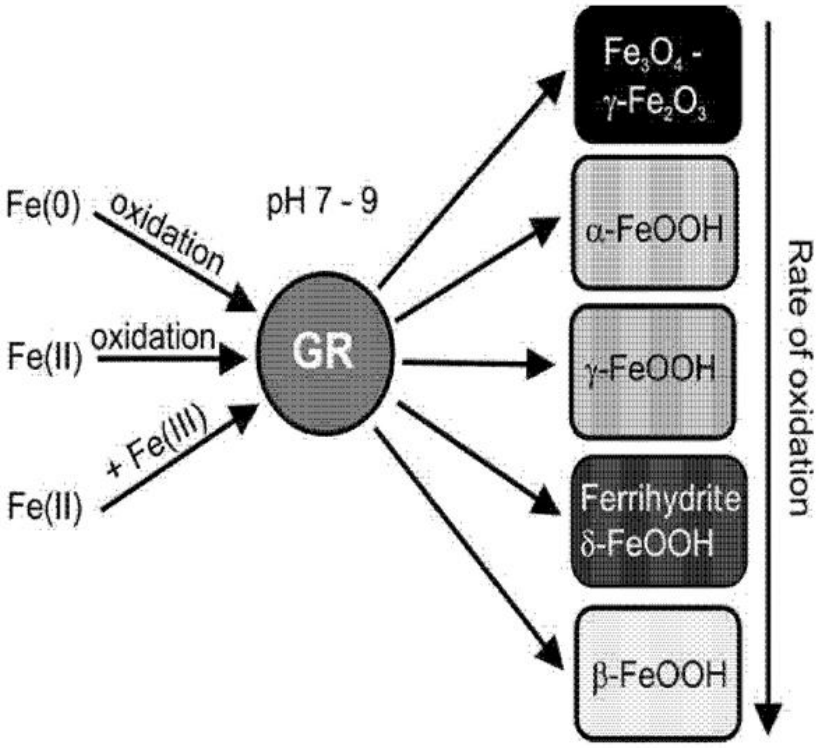


**Fig. 4.13 Formation and transformation of GRs to magnetite ($Fe_3O_4$), maghemite ($\gamma$-$Fe_2O_3$), goethite ($\alpha$-FeOOH), lepidocrocite ($\gamma$-FeOOH) and akageneite ($\beta$-FeOOH)** [9]

The XRD spectra of the solid residue after 12 hours showed that the ultimate product at pH 5 was Cr-inserted ferrihydrite for both $GR_{8.75}$ and $GR_{7.50}$ (Fig. 4.14). Since Cr adsorb onto goethite surface (Fig. 4.11), the Cr insertion might be facilitated further by the oxidation towards metastable ferrihydrite [30,38], whose formation requires exhaustive oxidation.

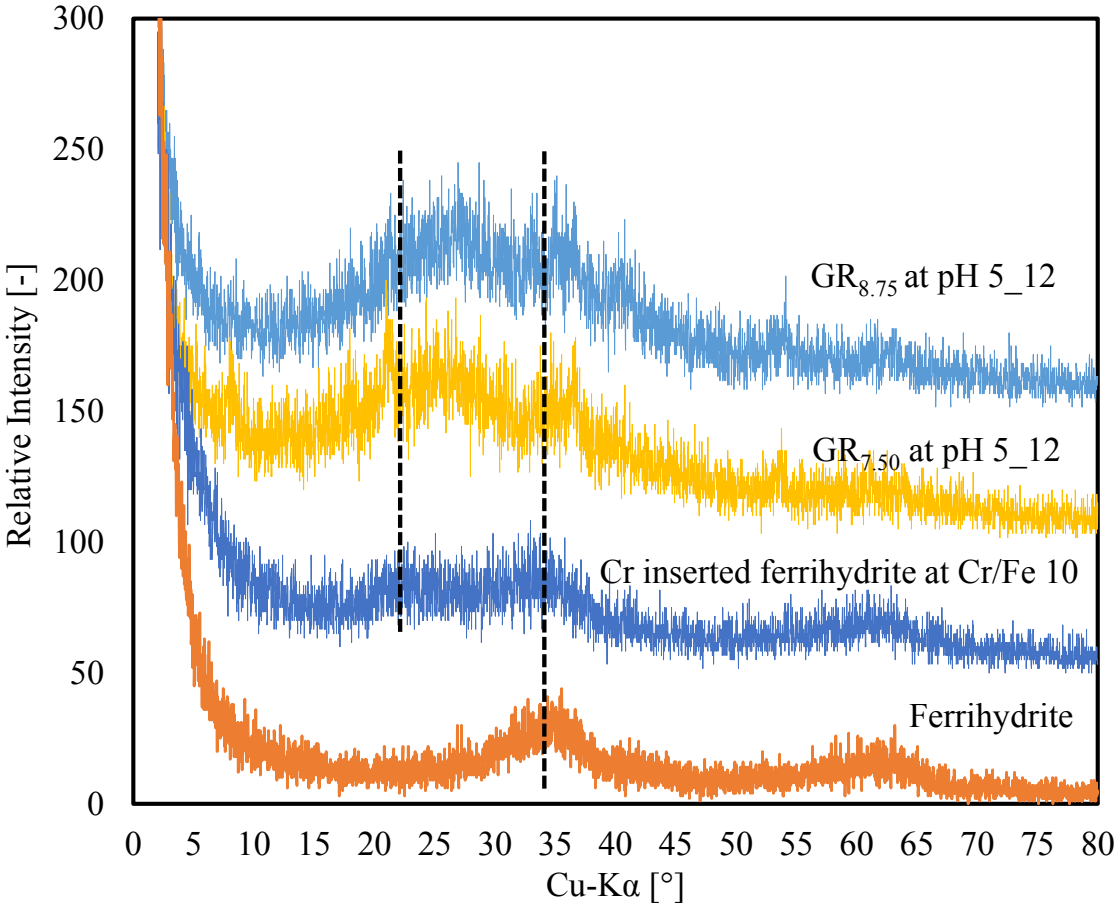


**Fig. 4.14 XRD patterns of $GR_{8.75}$ and $GR_{7.50}$ at pH 5 after 12 hours**

### 4.3.5 Surface oxidation state

The XPS narrow scan spectra of $GR_{8.75}$ highlighted a slight shift of the Fe 2p3/2 peak to a higher binding energy at pH 5, thereby confirming the previous speculation about the surface reduction mechanism (Fig. 4.15(a)). In particular, the deconvolution of the multiplets Fe peak in the 2p3/2 region performed by Gaussian fitting (Fig. 4.16(a)) revealed the presence of about 41% of Fe(II) and 59% of Fe(III) upon chromate removal by $GR_{8.75}$ at pH 5. The Fe(II) peak was most likely due to FeO [39] while the Fe(III) peak was assigned to $Fe_2O_3$ [40]. At pH 9 (Fig. 4.16(b)), the surface of $GR_{8.75}$ exhibited 52% Fe(II), most likely due to FeO [39] and 48% Fe(III), probably due to $Fe_2O_3$ [41].

In the experiments with $GR_{7.50}$, at both pH 5 and pH 9 (Fig. 4.17) the surface of the residue solid consisted respectively of 66% and 81% FeO [42]. This lower oxidation state of the surface supports the previous consideration about the predominance of a surface-redox mechanism for $GR_{8.75}$ and an intercalation mechanism with $GR_{7.50}$. The

generally higher concentrations of FeO at pH 9 can be considered as a consequence of the lower chromate removal, in turn determining a lower oxidation of GR's surface.

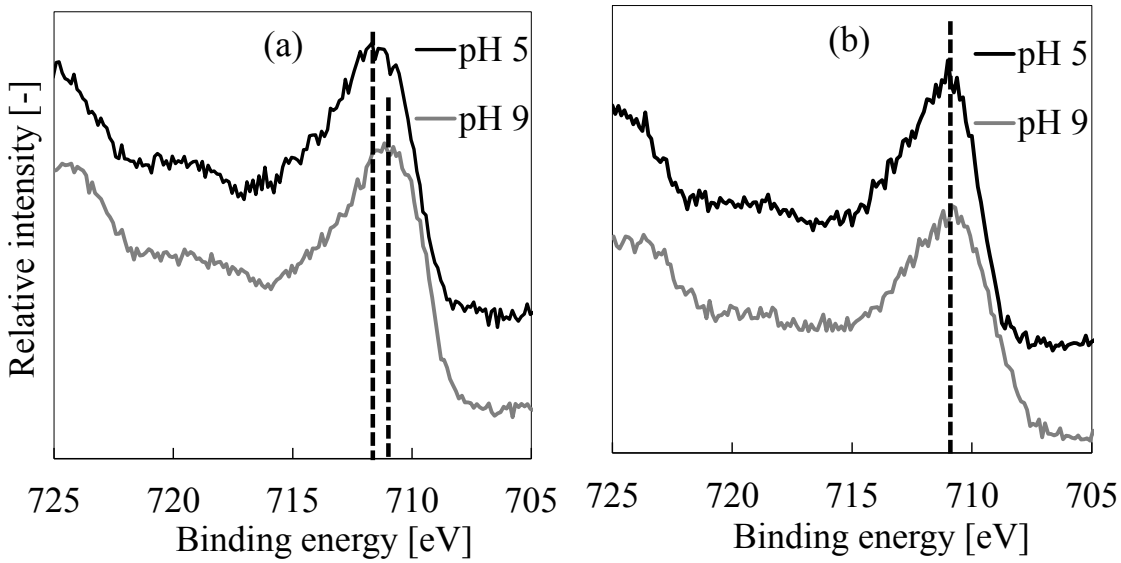


**Fig. 4.15 Fe 2p3/2 peak of (a) $GR_{8.75}$ and (b) $GR_{7.50}$ upon chromate removal**

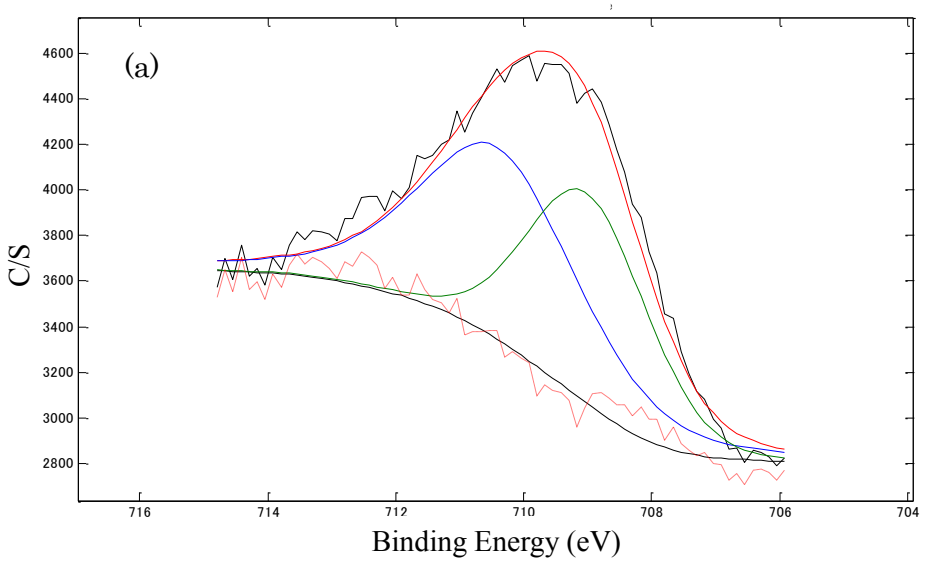


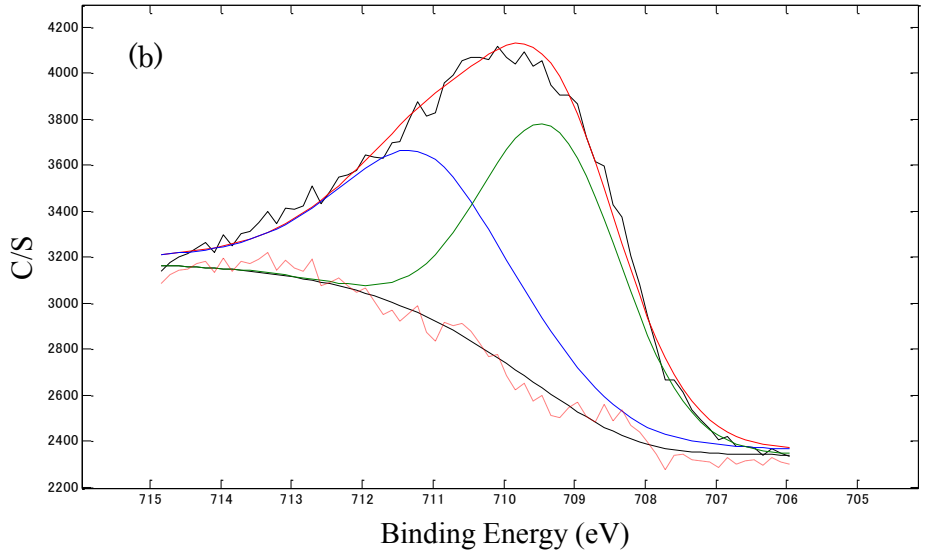


**Fig. 4.16 Fe-edge XPS fitting of $GR_{8.75}$ at (a) pH 5 and (b) pH 9**

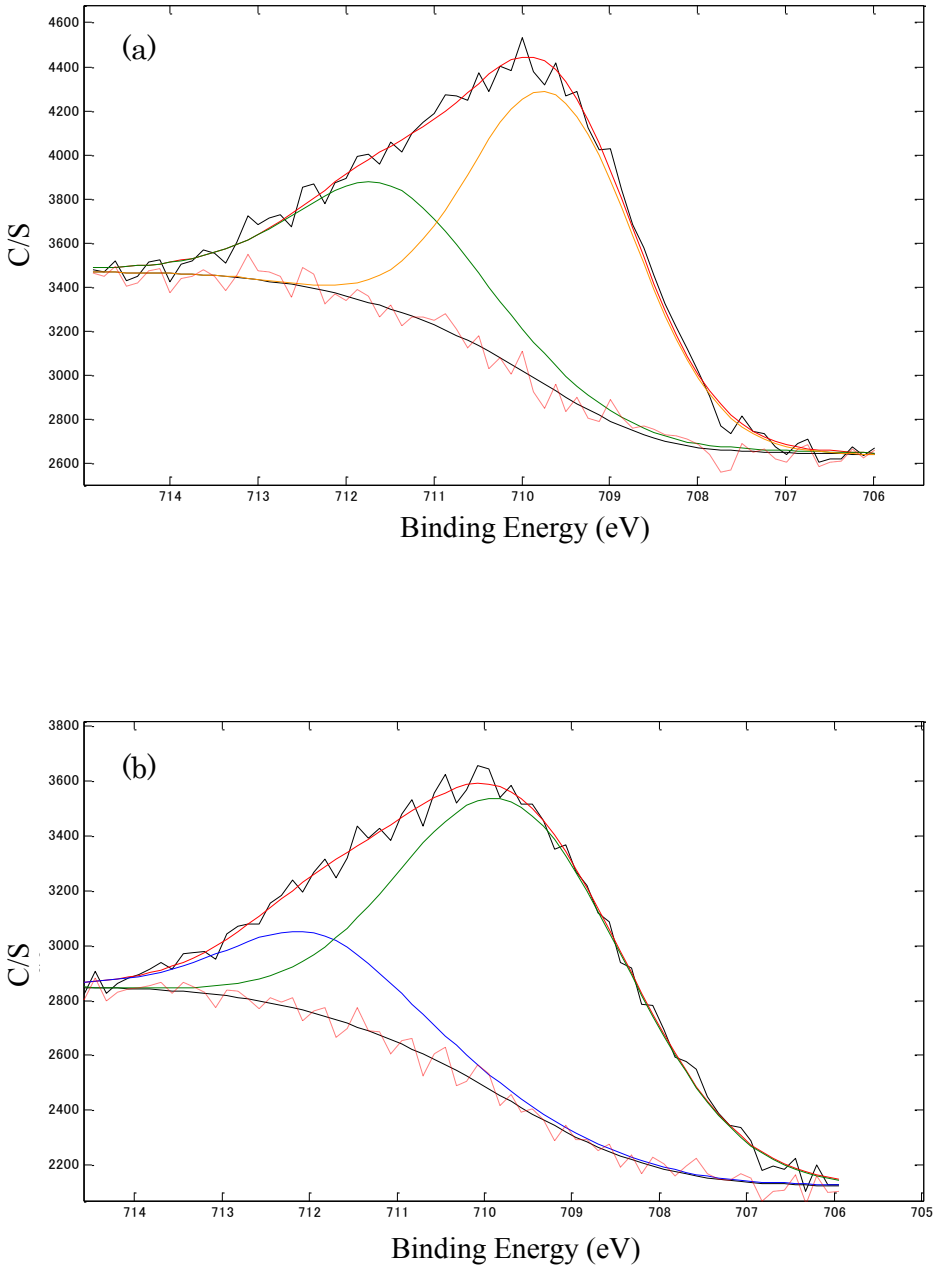


**Fig. 4.17 Fe-edge XPS fitting of $GR_{7.50}$ at (a) pH 5 and (b) pH 9**

For both GRs, the Cr-edge (Fig. 4.18) revealed that the only chromium species on the surface was $Cr(OH)_3$ [11,16,43]. As for the Cr-edge, a slight shift (0.5 eV) of the Cr 2p3/2 peak towards higher binding energies seems to have occurred by lowering the removal pH from 9 to 5 with $GR_{8.75}$ (Fig. 4.19). The deconvolution of the Cr 2p3/2 multiplet (Fig. 4.20) suggested a decrease in $Cr(OH)_3$ concentration from 90 to 76 % to the advantage of $Cr_2O_3$ [44]. However, given the very slight shift, we refrain from further speculations on this aspect.

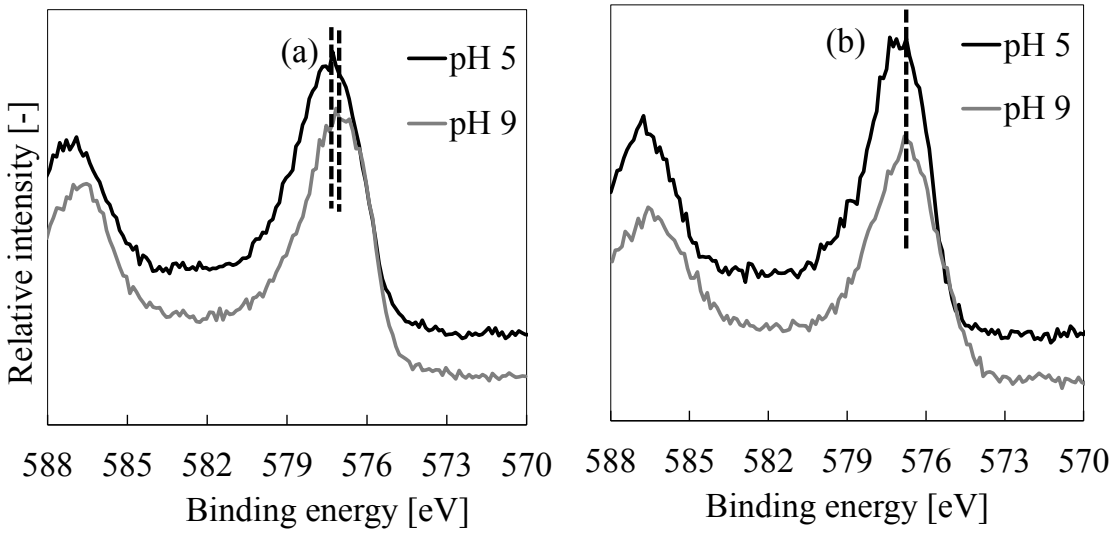


**Fig. 4.18 Cr edge XPS spectra of (a) $GR_{8.75}$ and (b) $GR_{7.50}$ upon chromate removal**

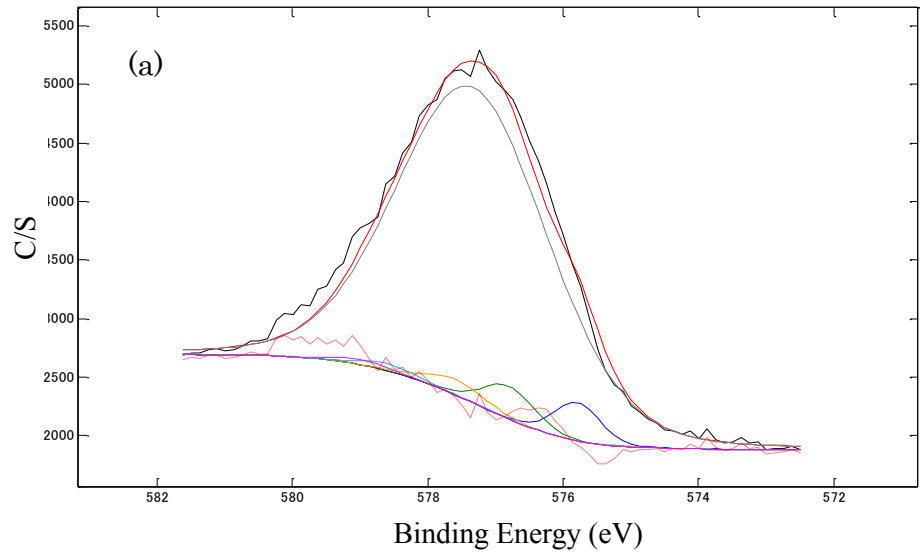


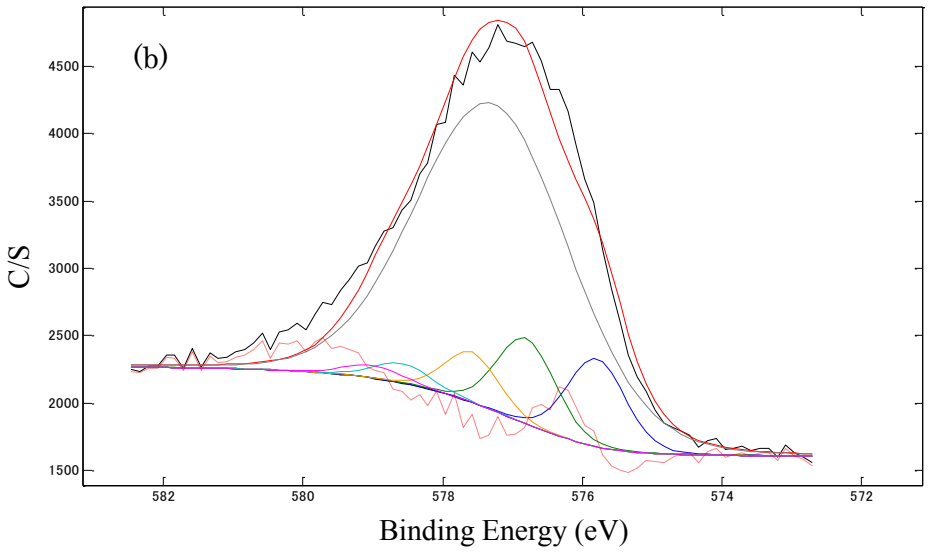


**Fig.4.19 Cr-edge XPS fitting of $GR_{8.75}$ at (a) pH 5 and (b) pH 9**

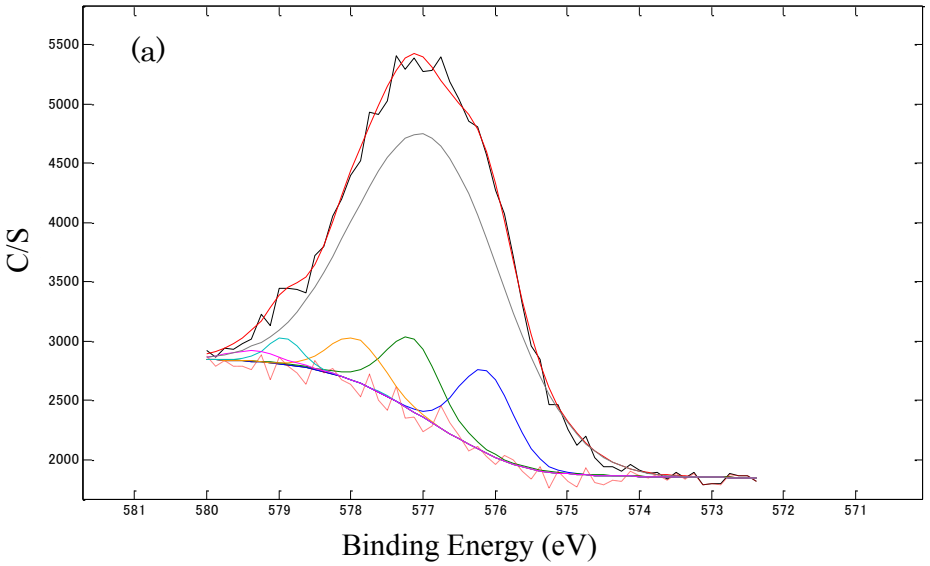


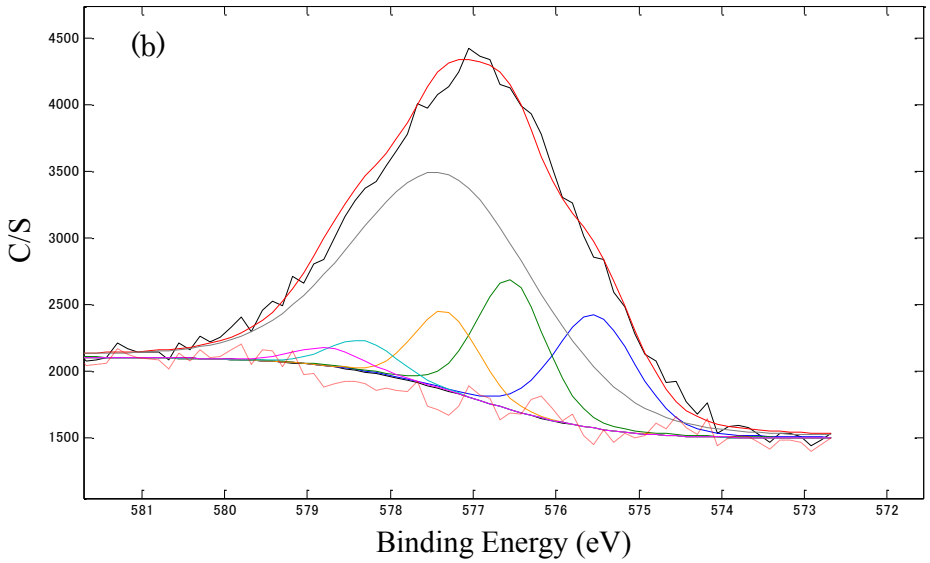


**Fig. 4.20 Cr-edge XPS fitting of $GR_{7.50}$ at (a) pH 5 and (b) pH 9**

### 4.3.6 Quantification of oxidation by absorption spectroscopy

Two types of redox reactions might have occurred between GR and chromate: (i) homogeneous redox reaction between aqueous Fe(II) and chromate, and (ii) heterogeneous redox reaction between chromate and Fe(II) from solid green rust. The presence of both homogeneous and heterogeneous reactions was previously reported. However, authors described this aspect only qualitatively based on the poor crystallinity of the formed chromium(III)-iron(III) oxyhydroxide [45].

Results of this work highlighted that at pH 5 the reduction occurred mostly as heterogeneous reaction (~77%), whereas the homogenous reaction was significant at pH 9 (~35%). This can be understood by looking at results in Fig. 4.21 and Fig. 4.22. Both $GR_{8.75}$ and $GR_{7.50}$, released about 40% of Fe(II) upon contact with the Cr-bearing solution. Following the release, the Fe(II) concentration decreased due to oxidation to Fe(III). These trends were used to quantify the Fe(II) used for the reduction of GR from solution based on the stoichiometric ratio Fe(II)-$CrO_4^{2-}$ 3:1. For both GRs, about 30-40% of the electrons used to reduce chromate were donated by Fe(II) in solution. More importantly, the high pH produced a larger release and consumption of Fe(II). This result is in agreement with previous qualitative findings highlighting that the homogeneous reaction is more favoured in alkali condition pH >8 [35].

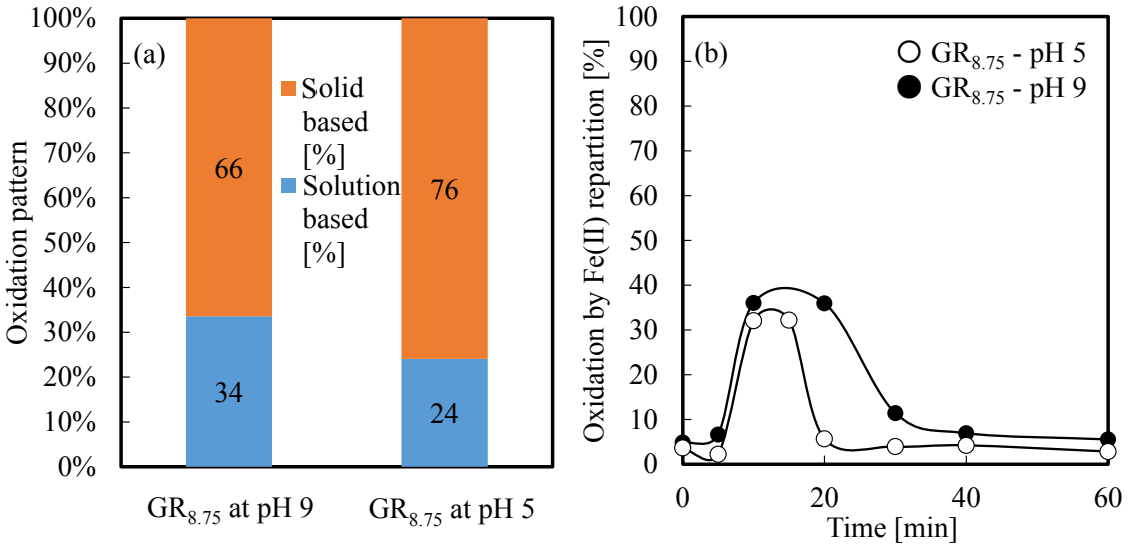


**Fig. 4.21 (a) Heterogeneous-homogeneous repartition of Fe(II)-chromate redox reaction and (b) dissolved Fe(II) with $GR_{8.75}$**

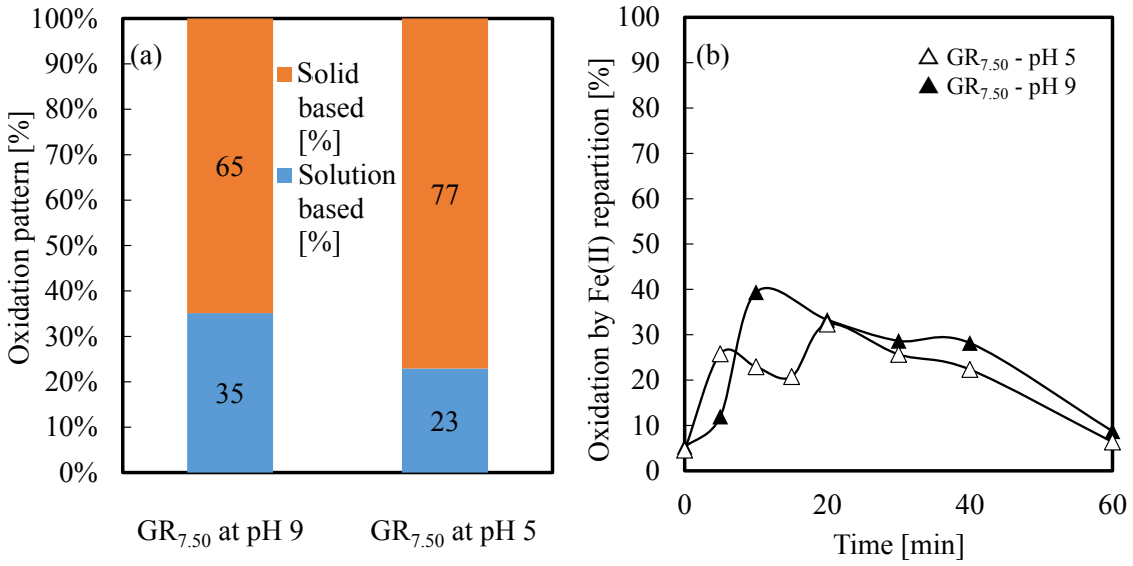


**Fig. 4.22 (a) Heterogeneous-homogeneous repartition of Fe(II)-chromate redox reaction and (b) dissolved Fe(II) with $GR_{7.50}$**

### 4.3.7 XAFS analysis

XAFS analyses were performed in order to elucidate the structural changes of GR upon chromate immobilization. At the time when this experimental work was done, there was no detailed information about XAFS (both Fe edge and Cr edge) in literature.

The XANES pattern of Fe K-edge did not exhibit any visible differences under the different experimental conditions (Fig. 4.23). On the other hand, EXAFS spectra showed several differences between the end-products of $GR_{8.75}$ and $GR_{7.50}$ (Fig. 4.24). The $K^3$ weighted EXAFS spectra were fitted against reference ferrihydrite, goethite, magnetite, hematite and GR to identify possible differences (Fig.4.25). Results confirmed an enhanced formation of magnetite (25%) and goethite (45%) respectively at pH 9 and 5 for $GR_{8.75}$ and a predominant formation of goethite/ferrihydrite and hematite (10-15%) hematite for $GR_{7.50}$ (Table 4.6).

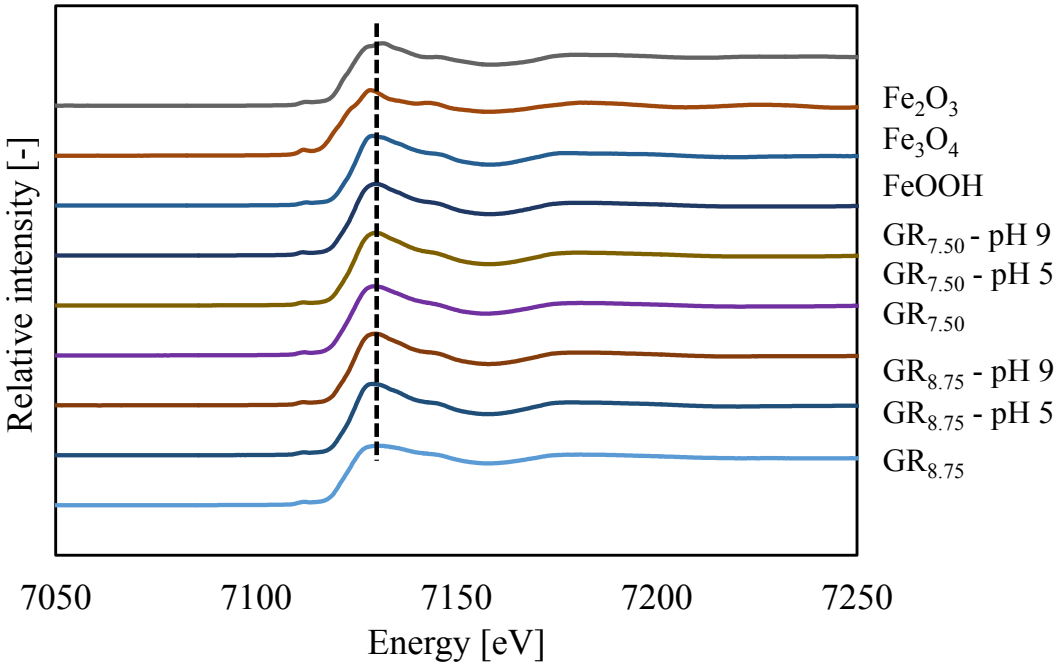


**Fig. 4.23 Fe K-edge XANES spectra of solid residues upon chromate removal**

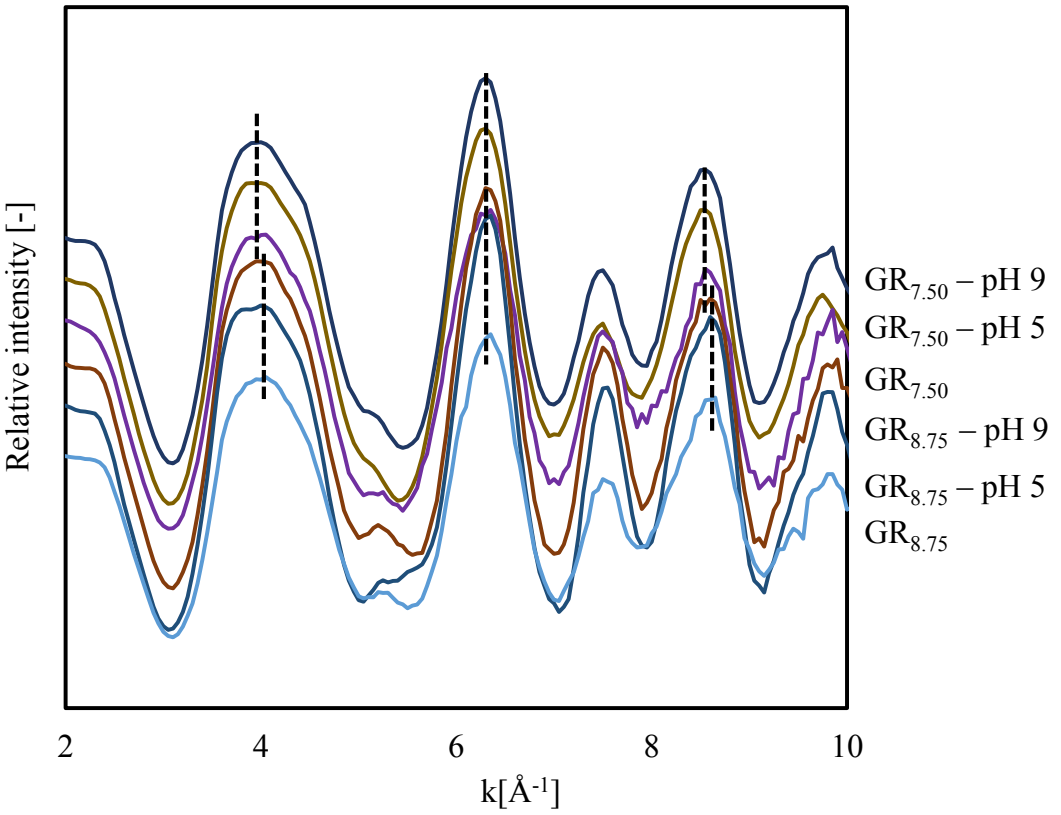


**Fig. 4.24 $K^3$-weighted Fe-edge EXAFS spectra of solid residues upon chromate removal**

XANES results (Cr-edge) revealed the presence of Cr(III) for both $GR_{8.75}$ and $GR_{7.50}$, irrespective of the pH. Interestingly, the end-product of $GR_{7.50}$ at pH 5 exhibited also a minor amount of residual Cr(VI) [46] (Fig.4.26). Because the XPS analysis did not reveal any Cr(VI) on the surface of $GR_{7.50}$, the one detected by XANES must be located in the interlayer. This evidence, along with previous results, is a further confirmation that $GR_{7.50}$ reduced chromate to Cr(III) preferentially from the interlayer, upon replacement of sulfate. Whereas this phenomenon was significant at pH 5, at pH 9 the replacement occurred to a lower extent due to the excess of negative charge on the surface of GR [28]. Thus, the lower amount of Cr(VI) inserted at pH 9 could be quantitatively reduced to Cr(III).

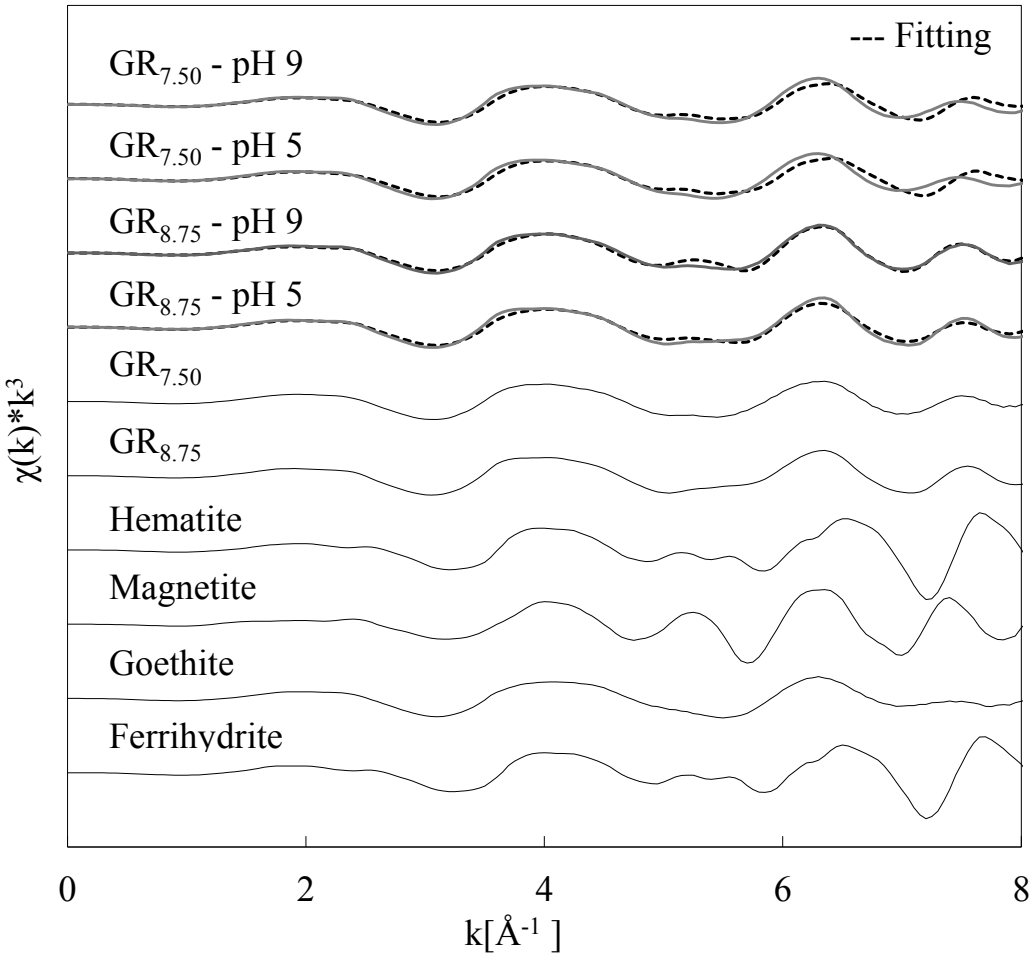


**Fig. 4.25 Fitting of $K^3$ weighted Fe K-edge EXAFS spectra with ferrihydrite, goethite, magnetite, hematite and GR**

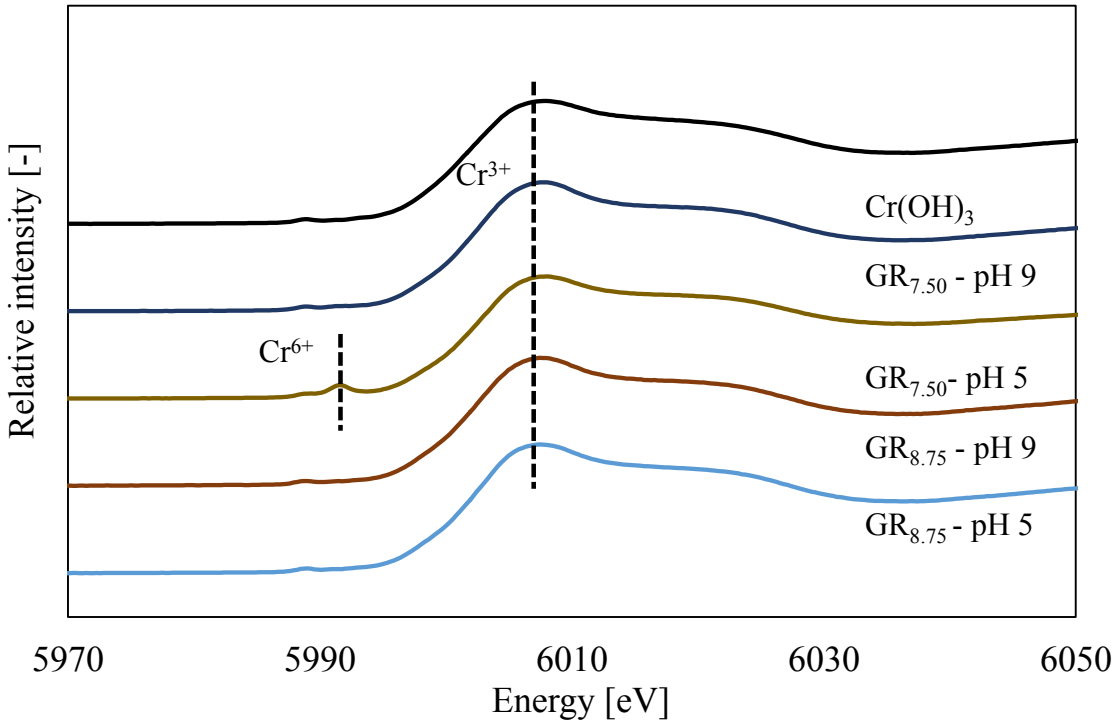


**Fig. 4.26 Cr K-edge XANES spectra of solid residues**

**Table 4.5 Fe K-edge RDF fitting of EXAFS area of $GR_{8.75}$ and $GR_{7.50}$ with/without chromate at different pH**

| Sample | Fe-O | | | Fe-$Fe_1$ | | | Fe-$Fe_2$ | | | Fe-$Fe_3$-O | | | $E_0$ | R factor |
|---|---|---|---|---|---|---|---|---|---|---|---|---|---|---|
| | $N$ | $R$ (Å) | $\sigma^2$ (Å$^2$) | $N_1$ | $R$ (Å) | $\sigma^2$ (Å$^2$) | $N_2$ | $R$ (Å) | $\sigma^2$ (Å$^2$) | $N_3$ | $R$ (Å) | $\sigma^2$ (Å$^2$) | (eV) | |
| **$GR_{8.75}$** | 1.88 | 1.98 | 0.01 | 3.38 | 3.05 | 0.01 | 2.45 | 3.35 | 0.01 | 1.20 | 4.28 | 0.006 | -3.56 | 0.01 |
| **$GR_{8.75}$ - chromate pH 5** | 2.56 | 1.99 | 0.01 | 5.17 | 3.06 | 0.01 | 4.29 | 3.35 | 0.01 | 2.25 | 4.29 | 0.01 | -4.13 | 0.02 |
| **$GR_{8.75}$ - chromate pH 9** | 2.55 | 2.00 | 0.01 | 5.90 | 3.07 | 0.01 | 4.48 | 3.36 | 0.01 | 1.30 | 4.29 | 0.01 | -2.46 | 0.02 |
| **$GR_{7.50}$** | 2.17 | 1.99 | 0.01 | 2.94 | 3.06 | 0.01 | 1.81 | 3.36 | 0.01 | 0.62 | 4.54 | 0.01 | -3.10 | 0.01 |
| **$GR_{7.50}$ - chromate pH 5** | 2.27 | 1.99 | 0.01 | 2.55 | 3.06 | 0.01 | 1.43 | 3.35 | 0.01 | 6.64 | 4.28 | 0.02 | -3.00 | 0.01 |
| **$GR_{7.50}$ - chromate pH 9** | 2.25 | 1.99 | 0.01 | 3.30 | 3.06 | 0.01 | 2.13 | 3.35 | 0.01 | 3.97 | 4.29 | 0.01 | -3.38 | 0.02 |

$N$: coordination number, $\sigma^2$: Debye–Waller factor, $E_0$: threshold shift in electron volts, *R(Å)*: interatomic distance.

**Table 4.6 Fe K-edge ($GR_{8.75}$ and $GR_{7.50}$ with chromate) EXAFS fitting with ferrihydrite, goethite, magnetite, hematite and concerned GR at different pH**

| | $GR_{8.75}$ - pH 5 | $GR_{8.75}$ - pH 9 | $GR_{7.50}$ - pH 5 | $GR_{7.50}$ - pH 9 |
|---|---|---|---|---|
| **Ferrihydrite (%)** | 5 | 5 | 10 | 10 |
| **Goethite (%)** | 45 | 20 | 35 | 30 |
| **Magnetite (%)** | 10 | 25 | - | 5 |
| **Hematite (%)** | - | - | 15 | 10 |
| **GR (%)** | 40 | 50 | 40 | 45 |
| **R-factor (%)** | 98 | 98 | 93 | 96 |

**Table 4.7 Cr K-edge RDF fitting of EXAFS area of $GR_{8.75}$ and $GR_{7.50}$ with chromate at different pH**

| sample | Cr-O | | | Cr-Fe | | | Cr-Cr | | | O-Cr-O | | | $E_0$ | R |
|---|---|---|---|---|---|---|---|---|---|---|---|---|---|---|
| | $N$ | $R$ (Å) | $\sigma^2$ (Å$^2$) | $N_1$ | $R$ (Å) | $\sigma^2$ (Å$^2$) | $N_2$ | $R$ (Å) | $\sigma^2$ (Å$^2$) | $N_2$ | $R$ (Å) | $\sigma^2$ (Å$^2$) | (eV) | factor |
| $Cr(OH)_3$ | 1.95 | 1.98 | 0.004 | - | - | - | 0.43 | 2.99 | 0.008 | 8.27 | 3.94 | 0.004 | -1.80 | 0.012 |
| $GR_{8.75}$ - chromate pH 5 | 1.97 | 1.98 | 0.003 | 1.70 | 2.96 | 0.01 | - | - | - | 8.96 | 3.94 | 0.007 | -4.17 | 0.01 |
| $GR_{8.75}$ - chromate pH 9 | 1.82 | 1.98 | 0.003 | 1.48 | 2.96 | 0.01 | - | - | - | 7.12 | 3.95 | 0.004 | -3.57 | 0.008 |
| $GR_{7.50}$ - chromate pH 5 | 1.45 | 1.98 | 0.001 | 1.35 | 2.96 | 0.001 | - | - | - | 10.44 | 3.94 | 0.001 | -4.57 | 0.009 |
| $GR_{7.50}$ - chromate pH 9 | 1.99 | 1.98 | 0.004 | 1.95 | 2.96 | 0.01 | - | - | - | 9.92 | 3.95 | 0.009 | -3.66 | 0.009 |

*N*: coordination number, $\sigma^2$: Debye-Waller factor, $E_0$: threshold shift in electron volts, *R(Å)*: interatomic distance.

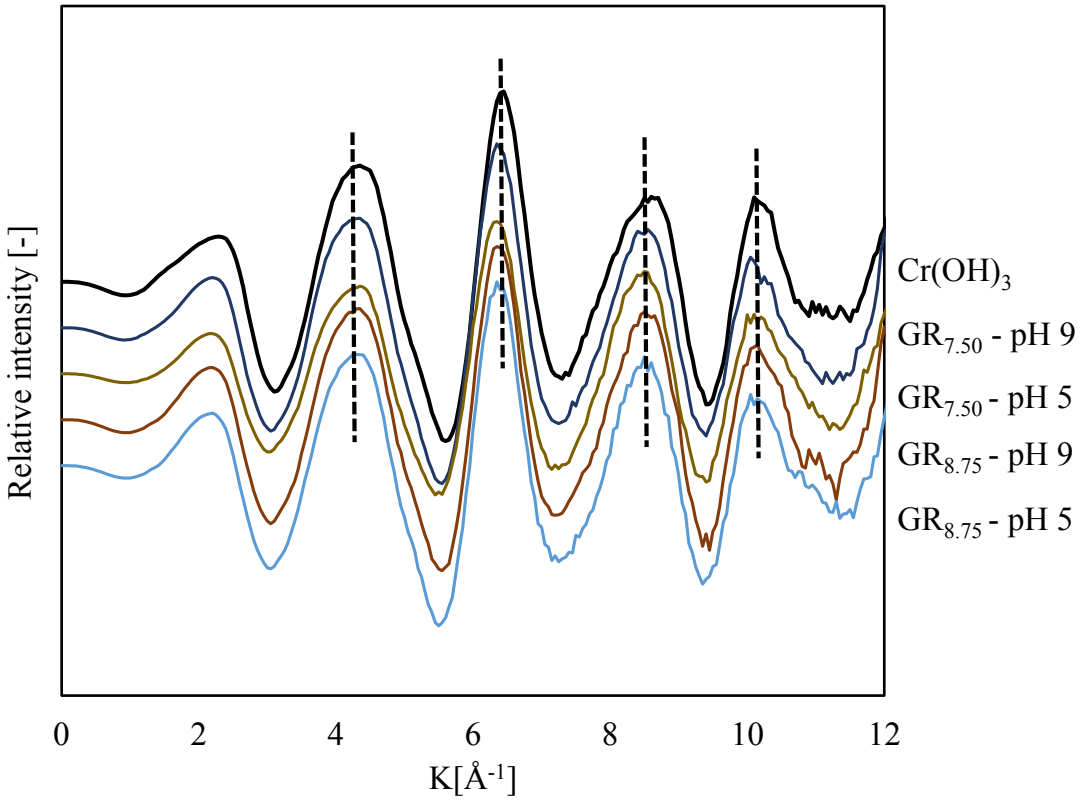


**Fig.4.27 $K^3$-weighted Cr-edge EXAFS spectra of solid residues**

The Cr edge EXAFS spectra (Fig. 4.27) showed a similar trend as in Fe edge EXAFS spectra. The peak position and peak intensity were different compared to each other, thus supporting the hypothesis of two different sorption mechanisms.

The Fourier-transformed spectra corresponding to the $K^3$ weighted EXAFS spectra of Fe-K edge as well as Cr-K edge were fitted to determine the change of interatomic distances and coordination numbers (Figs. 4.28 and 4.29). To highlight the differences, the fitting was carried out using goethite (α-FeOOH) [47] and hematite ($Fe_2O_3$) [48] as reference materials to obtain the initial values of fitting parameters. For all conditions, the Fe K-edge RDF fitting results (Fig. 4.28 and Table 4.5) also revealed the presence of Fe-Fe edge sharing and double corner sharing bonds [2] along with Fe-Fe monodentate single corner sharing *via* oxygen bonding [49]. For $GR_{8.75}$ upon reaction with chromate, the Fe-Fe edge sharing and double corner sharing coordination almost doubled, increasing from 2.45 to 4.48 and from 3.38 to 5.90, respectively. This change is thought to be due to a redox reaction taking place from the surface of GR. In comparison, $GR_{7.50}$ showed a great affinity towards the corner sharing coordination that increased by

6.5 to 10.70 times upon reaction with chromate, thereby suggesting the lateral insertion of chromate with sulfate replacement.

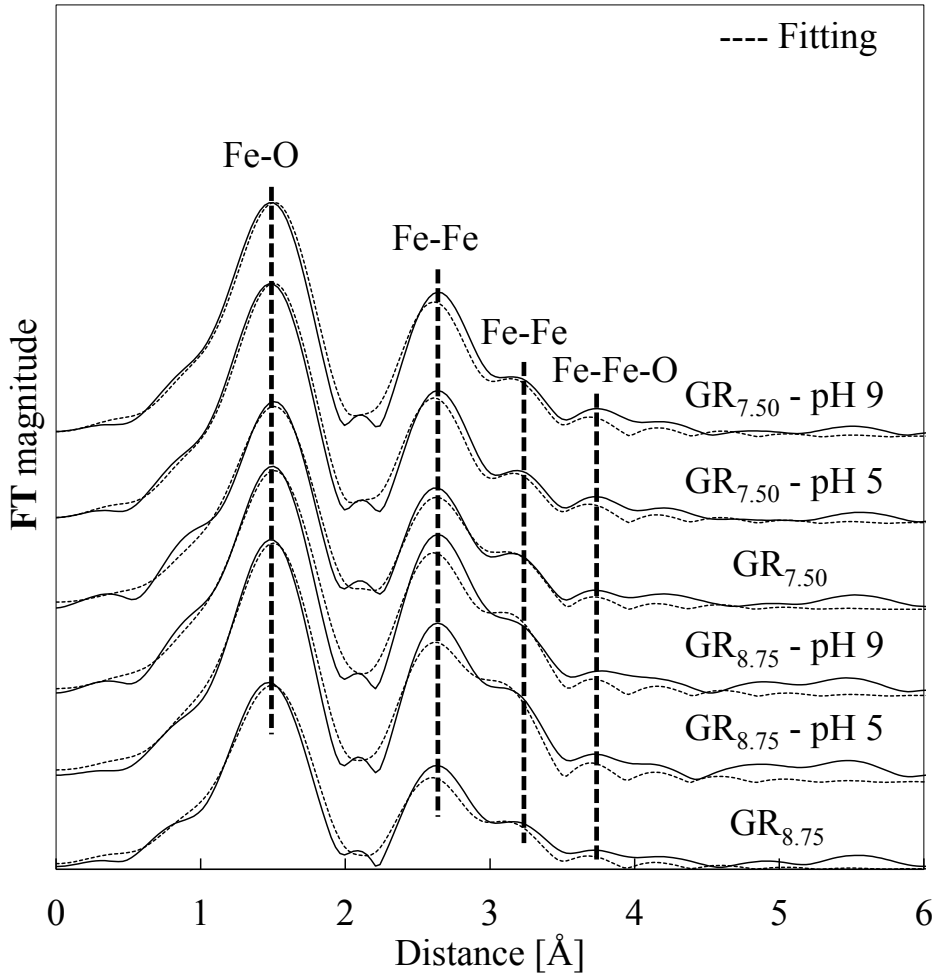


**Fig. 4.28 Fourier-transformed unfiltered spectra and fitting results of Fe K-edge before and after removal experiments**

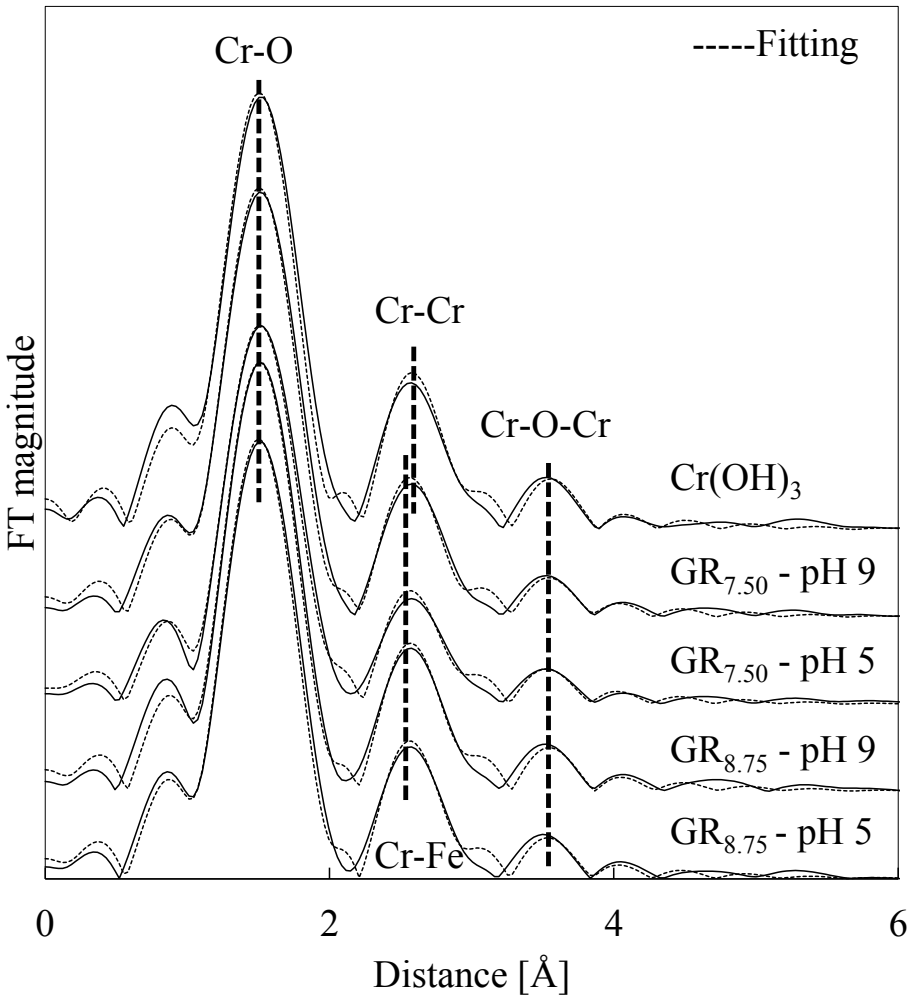


**Fig. 4. 29 Fourier-transformed unfiltered spectra and fitting results of Cr K-edge upon chromate removal**

All of the Cr K-edge fourier-transformed spectra were fitted with chromium oxides ($Cr_2O_3$) [50] and iron chromite ($FeCr_2O_4$)[51]. Moreover, pure $Cr(OH)_3$ was analysed to compare coordination numbers and interatomic distances (Fig. 4.29 and Table 4.7). Under all investigated conditions, the Cr-Cr $Cr(OH)_3$-like bonding upon chromate reduction seemed to change to Cr-Fe bonding with shorter interatomic distances and increased coordination number. This result suggests the formation of chromite. Moreover, the Cr-Fe bonding exhibited bidentate mononuclear geometry (~2.91Å). However, the corner sharing bonding Cr-O-Cr (3.94Å) increased significantly especially for $GR_{7.50}$, thus supporting the previous speculation about the lateral inclusion of chromium into GR.

## 4.4 Summary

GR represents an interesting alternative to ferrihydrite as removing agent for chromate. However, before real processes could be implemented a full understanding of the immobilization mechanism is required. In particular, the effect of pH during the preparation of GR and chromate removal must be elucidated as it could lead to different removal performances and end-products.

The increase of pH from 7.50 to 8.75 in the preparation of GR, determined a larger inclusion of sulfate and sodium ions within the GR interlayer and an increase of surface area. The higher pH also determined the enlargement of the crystal lattice and the increase of single corner Fe-Fe coordination *via* oxygen. $GR_{8.75}$ was found to be 1.7 times more efficient than $GR_{7.50}$ and 6.7 times more efficient than ferrihydrite in terms of required moles of Fe for removed Cr. Both $GR_{8.75}$ and $GR_{7.50}$ exhibited the highest removal efficiency at pH 5. At this pH, $GR_{8.75}$ oxidized mostly to goethite whereas magnetite was the predominant product at pH 9. These are important results aiming to implement real processes. Moreover, a lower amount of Fe and the formation of crystalline iron oxides such as goethite is expected to result in the production of smaller amount of sludge with a better solid-liquid separability.

XPS and XAFS results confirmed that $GR_{8.75}$ removes chromate mostly *via* surface reduction and oxidizes to goethite. In contrast, $GR_{7.50}$ reduces chromate mostly *via* replacement of interlayer sulfate, thereby transforming to Cr-inserted ferrihydrite.

**References**


[1] D.L. Bond, S. Fendorf, Environ. Sci. Technol. 37 (2003) 2750–2757.

[2] A. Al Mamun, M. Morita, M. Matsuoka, C. Tokoro, J. Hazard. Mater. 334 (2017) 142–149.

[3] K.B. Ayala-Luis, C.B. Koch, H.C.B. Hansen, Appl. Clay Sci. 48 (2010) 334–341.

[4] L.H.G. Chaves, Rev. Bras. Eng. Agrícola e Ambient. 9 (2005) 284–288.

[5] C.M. Rogers, I.T. Burke, I.A.M. Ahmed, S. Shaw, Environ. Technol. 3330 (2013) 1–6.

[6] K.B. Ayala-Luis, C.B. Koch, H.C.B. Hansen, Appl. Clay Sci. 50 (2010) 512–519.

[7] C. Ruby, M. Abdelmoula, S. Naille, A. Renard, V. Khare, G. Ona-Nguema, G. Morin, J.M.R. Genin, Geochim. Cosmochim. Acta 74 (2010) 953–966.

[8] H.C.B. Hansen, S. Guldberg, M. Erbs, C. Bender Koch, Appl. Clay Sci. 18 (2001) 81–91.

[9] M. Erbs, Formation and Redox Reactions of Green Rusts under Geochemical Conditions Found in Natural Soils and Sediments, Swiss Federal Institute of Technology, 2004.

[10] H. Hayashi, K. Kanie, K. Shinoda, A. Muramatsu, S. Suzuki, H. Sasaki, Chemosphere 76 (2009) 638–643.

[11] S. Loyaux-Lawniczak, P. Refait, J.J. Ehrhardt, P. Lecomte, J.M.R. Génin, Environ. Sci. Technol. 34 (2000) 438–443.

[12] L.L. Skovbjerg, S.L.S. Stipp, S. Utsunomiya, R.C. Ewing, Geochim. Cosmochim. Acta 70 (2006) 3582–3592.

[13] B.C. Christiansen, T. Balic-Zunic, P.O. Petit, C. Frandsen, S. Mørup, H. Geckeis, A. Katerinopoulou, S.L.S. Stipp, Geochim. Cosmochim. Acta 73 (2009) 3579–3592.

[14] I.A.M. Ahmed, L.G. Benning, G. Kakonyi, A.D. Sumoondur, N.J. Terrill, S. Shaw, Langmuir 26 (2010) 6593–6603.

[15] A.G.B. Williams, M.M. Scherer, Proc. 2000 Conf. Hazard. Waste Res. 4 (2000) 272–281.

[16] S. Loyaux-Lawniczak, P. Refait, P. Lecomte, J.-J. Ehrhardt, J.-M.R. Génin, Hydrol. Earth Syst. Sci. 3 (1999) 593–599.

[17] A.G.B. Williams, M.M. Scherer, Environ. Sci. Technol. 35 (2001) 3488–3494.

[18] M. Erbs, H.C.B. Hansen, C.E. Olsen, Environ. Sci. Technol. 33 (1999) 307–311.

[19] H.C.B. Hansen, Clay Miner. 33 (1998) 87–101.

[20] T. Kone, K. Hanna, M. Usman, Colloids Surfaces A Physicochem. Eng. Asp. 385 (2011) 152–158.

[21] E.J. O'Loughlin, S.D. Kelly, R.E. Cook, R. Csencsits, K.M. Kemner, Environ. Sci. Technol. 37 (2003) 721–727.

[22] E.J.O'Loughlin, S.D. Kelly, K.M. Kemner, R. Csencsits, R.E. Cook, Chemosphere 53 (2003) 437–446.

[23] H. Fadrus, J. Malý, Analyst 100 (1975) 549.

[24] H.C.B. Hansen, Clay Miner. 24 (1989) 663–669.

[25] J.M.R. Génin, A.A. Olowe, P. Refait, L. Simon, Corros. Sci. 38 (1996) 1751–1762.

[26] P. Refait, A. Gehin, M. Abdelmoula, J.M.R. Genin, Corros. Sci. 45 (2003) 659–676.

[27] B.C. Christiansen, Structure and Reactions of GRNa,$SO_4$ and the Occurrence of GR in Nature, University of Copenhagen, 2015.

[28] R. Guilbaud, M.L. White, S.W. Poulton, Geochim. Cosmochim. Acta 108 (2013) 141–153.

[29] L. Simon, M. François, P. Refait, G. Renaudin, M. Lelaurain, J.M.R. Génin, Solid State Sci. 5 (2003) 327–334.

[30] P. Refait, O. Benali, M. Abdelmoula, J.M.R. Genin, Corros. Sci. 45 (2003) 2435–2449.

[31] U. Schwertmann, H. Schwertmann, U., Fechter, Clay Miner. 29 (1994) 87–92.

[32] I.A. M. Ahmed, S. Shaw, L.G. Benning, Mineral. Mag. 72 (2008) 159–162.

[33] L. Mazeina, A. Navrotsky, D. Dyar, Geochim. Cosmochim. Acta 72 (2008) 1143–1153.

[34] J. Cao, W. Zhang, J. Hazard. Mater. 132 (2006) 213–219.

[35] M.C.F. Wander, M.A.A. Schoonen, J. Phys. Chem. C 114 (2010) 16408–16415.

[36] Rigaku, Rigaku J. 26 (2010) 23–27.

[37] L. Legrand, A. El Figuigui, F. Mercier, A. Chausse, Environ. Sci. Technol. 38 (2004) 4587–4595.

[38] A. Sumoondur, S. Shaw, I. Ahmed, L.G. Benning, Mineral. Mag. 72 (2008) 201–204.

[39] D. Brion, Appl. Surf. Sci. 5 (1980) 133–152.

[40] Y. V. Salyn, G. Leonhardt, R. Scheibe, J. Electron Spectros. Relat. Phenomena 10 (1977) 121–124.

[41] M. Oku, K. Hirokawa, J. Electron Spectrosc. Relared Phenom. 8 (1976) 475–481.

[42] A.I. Nemoshalenko, V.V., Didyk, V.V., Kriskii, V.P., Senekevich, Zh. Neorg. Khimii 28 (1983) 2182–2192.

[43] M.R. F.M. Capece, V. Di Castro, C. Furlani, G. Mattogno, C. Fragale, M. Gargano, Energy 27 (1982) 119–128.

[44] V.I. Nefedov, D. Gatin, B.F. Dzhurinskij, N.P. Sergushin, Y.V. Salyn', Zhurnal Neorg. Khimii 20 (1975) 2307–2314.

[45] L.E. Eary, D. Ral, Environ. Sci. Technol 22 (1988) 972–977.

[46] A.J. Berry, H.S.C. O'Neill, Am. Mineral. 89 (2004) 790–798.

[47] Y. Hexiong, L. Ren, R.T. Downs, G. Costin, Acta Crystallogr. Sect. E Struct. Reports Online 62 (2006).

[48] R.L. Blake, Hessevic.Re, T. Zoltai, L.W. Finger, Am. Mineral. 51 (1966) 123–129.

[49] G.A. Waychunas, B.A. Rea, C.C. Fuller, J.A. Davis, Geochim. Cosmochim. Acta 57 (1992) 2251–2269.

[50] H. Sawada, Mater. Res. Bull. 29 (1994) 239–245.

[51] A. Kyono, S.A. Gramsch, T. Yamanaka, D. Ikuta, M. Ahart, B.O. Mysen, H.-K. Mao, R.J. Hemley, Phys. Chem. Miner. 39 (2012) 131–141.

[52] S. Fendorf, M.J. Eick, P. Grossl, D.L. Sparks, Environ. Sci. Technol. 31 (1997) 315–320.

# [Chapter 5]
# Industrial application of green rust for Cr(VI) removal through coprecipitation

## 5.1 Introduction

The chromium in tannery process is used only as Cr(III). However, under aerobic conditions and relatively high-temperature, a partial conversion of Cr(III) to Cr(VI) is unavoidable [1,2]. Since the conversion, as well as stability, is kinetically and thermodynamically favoured in water, Cr(VI) can be found in the final wastewater, from where it is discharged to natural water bodies [3].

Although the most recent technologies in wastewater treatment allow removing chromate from water, many of them are not efficient enough at low concentrations and under the alkaline conditions of tannery effluents. In addition, the current state of the art in chromate removal lacks sustainability. This is because they might imply too high costs that developing countries like Bangladesh cannot afford for wastewater treatment.

In the recent years, researchers tried to overcome the sustainability issue by developing adsorbing materials for chromate from bio-agricultural waste, namely bio-sorbents. However, though cost-effective, the raw materials required to produce bio-sorbent are often geographically localized and seasonal.

Coprecipitated green rust (GR) might solve both efficiency and sustainability issues as it could be generated from simple precursors like Fe(II) and Fe(III) salts or even from waste streams. In chapter 4, GR was shown effective to remove low concentrations of chromate from water. However, the investigation was conducted entirely using simple Cr-bearing solutions under Ar-atmosphere; conditions that were clearly not representative of the real aerobic conditions in wastewater treatment plants. Aiming to implement treatment processes, this is an important aspect that must be considered because GR contains significant portions of Fe(II) and could oxidize easily. In this view, the main challenge related to the use of GR to remove chromate from water is performing the removal before GR oxidizes and loses reducing power. Considering this aspect means the use of GR should be tested from complex wastewater systems, under open-air atmosphere. So far, there are no records in the literature of research works addressing this issue.

This chapter addresses the practical application of GR in complex wastewater systems under open-air atmosphere. For this purpose, a new experimental campaign was performed preparing GR directly from synthetic solutions simulating the real wastewater, without using any glovebox. Since GR might lose efficiency under real complex conditions, this chapter provides also a new comparison with ferrihydrite (Fh).

## 5.2 Materials and methods

### 5.2.1 Materials and stock solutions

All chemicals used in this study were analytical grade reagents from Wako Chemical Industries (Japan). The Cr(VI) solution was prepared by dissolving $K_2CrO_4$ in deionized water. GR was produced by mixing stock solutions of $FeSO_4 \cdot 7H_2O$ and $Fe_2(SO_4)_3 \cdot nH_2O$ while Fh was prepared by dissolving $Fe(NO_3)_3 \cdot 9H_2O$ in deionized water. When investigating the use of GR and Fh from simple Cr-bearing solutions under Ar atmosphere, all experiments were carried out in a gas displacement type acrylic glove box equipped with pass box and oxygen meter (As-One, Japan). When investigating the use of GR from a complex Cr media under air atmosphere, experiments were performed without using any glove box.

The effluent generated after wastewater treatment section of BSCIC tanneries in Savar, Dhaka presents a total chromium concentration of 10-15 mg/L at pH 8.1-8.25 with 0-0.2 mg/L of dissolved oxygen (DO), 100-350 mg/L of biochemical oxygen demand (BOD) and 250-1000 mg/L of chemical oxygen demand (COD). However, based on the information provided in chapter 2, it should be clear that the wastewater produced in the tannery process is very complex and practically impossible to reproduce in lab. Therefore, in this section we prepared synthetic solutions simulating the main characteristics of the wastewater in terms of pH, DO and COD. The substances contributing to the COD were deliberately chosen based on the process inputs or inputs described in chapter 2 and listed in Table 2-9. These substances are mostly the saturated and unsaturated fatty acids contained in the natural fat of the skin and released throughout the tannery process, mostly in liming. The composition of the synthetic wastewater, hereafter referred to as "real-wastewater" is shown in Table 5.1. The DO of the solution was initially fixed to less than 0.1 mg/L like in the real effluent generated after wastewater treatment. The COD was fixed at 265 mg/L and measured by the titration method [4] (Fig. 5.1 and formula 1).

$$COD\ (mg/L) = (a-b) \times f \times (1000/V) \times 0.2 \quad (1)$$

Where, a is the volume of consumed $KMnO_4$ for sample (mL), b is the volume of consumed $KMnO_4$ for blank (mL), f is constant factor and V is the sample volume (mL).

During GR coprecipitation, pH and ORP were continuously monitored using pH meter (Thermo Scientific) and ORP meter (Horiba Scientific).

**Table 5.1 Synthetic wastewater composition**

| | |
|---|---|
| Lauric acid (mg/L) | 34.5 |
| Formic acid (mL/L) | 2.0 |
| Sodium thiosulfate (mg/L) | 20.0 |
| Formaldehyde (mL/L) | 3.0 |
| Sodium sulphide (mg/L) | 11.6 |
| Sodium chloride (mg/L) | 60.0 |
| Cr(VI) (mg/L) | 10.0 |

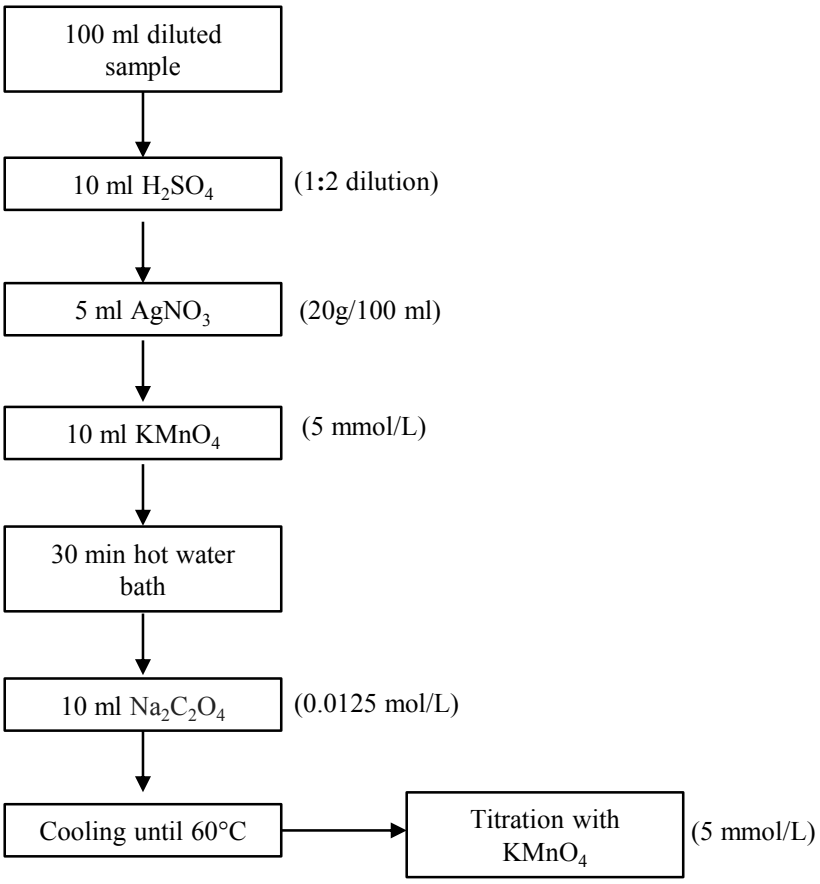


**Fig. 5.1 Process flow for COD measurement**

### 5.2.2 Stability and behaviour of GR and ferrihydrite in complex wastewater system

Batch experiments were performed to assess (i) the stability of Cr(VI) within the simulated wastewater, (ii) the formation and stability of GR within the same media, and (iii) the ability of GR to perform the removal under the same conditions.

The sustainability of two major Cr species such as Cr(VI) and Cr(III) was tested

in terms of residual Cr concentration upon dissolution of Cr(VI) or Cr(III) in the solution reproducing the synthetic wastewater at pH 8.25 (±0.25) (Table 5.2).

The coprecipitation of Fh with Cr(VI) was investigated for different Cr/Fe molar ratio. In the experiments with GR, the Fe(II)/Fe(III) ratio was set as 2 and used as total Fe input. The pH was continuously monitored during the experiments and adjusted to 5, 7, 9 (± 0.05) through the addition of 0.1 M $HNO_3$ and 0.1 M KOH. After 1 hour under stirring, the suspensions were filtered using 0.1-μm membrane filters.

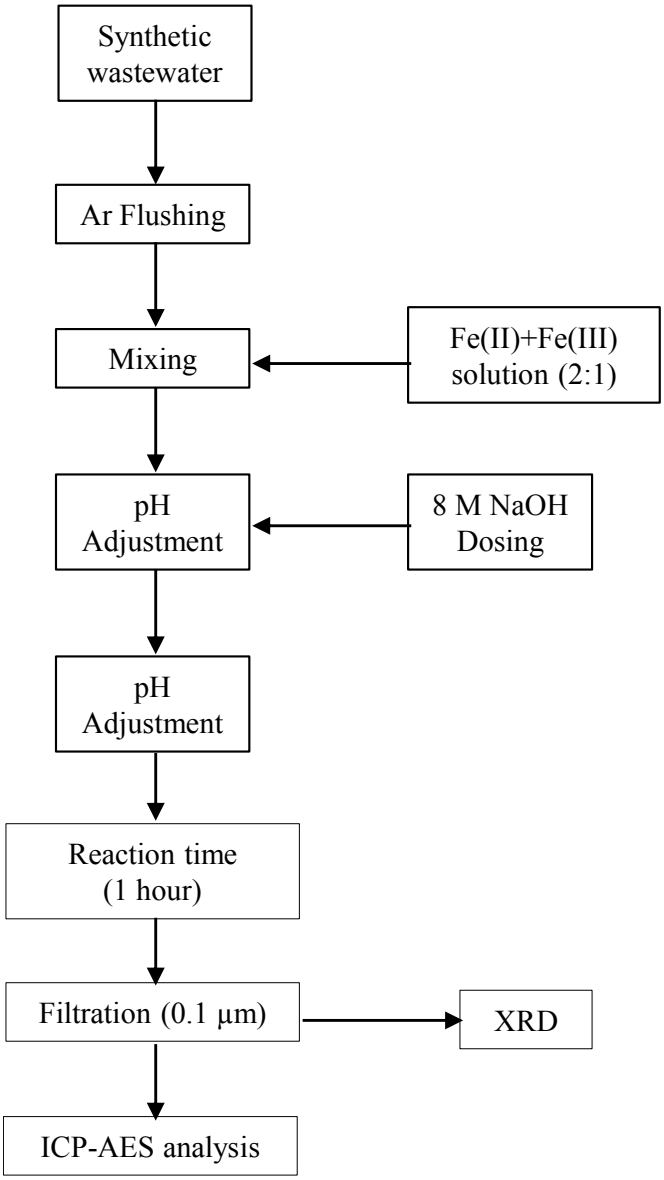


**Fig. 5.2 Flow chart of coprecipitation experiments from synthetic wastewater containing GR and chromate**

### 5.2.3 Analysis

**(i) ICP-AES analysis**

The filtrates were analyzed by inductively coupled plasma-atomic emission spectrometry (ICP-AES) using an SPS-7800 atomic emission spectrometer (Seiko Instruments Inc., Chiba, Japan). The detailed measuring conditions are the ones described in chapter 3, Table 3-1.

**(ii) XRD analysis**

The solid residues were analyzed by x-rays diffraction (XRD) to determine phase composition and crystal structure upon chromate removal. The x-ray diffractometer (Geiger flex RAD-IX, Rigaku Corp. Japan) was equipped with a copper target (Cu–Kα). The detail measuring condition is given in Table 3-2 in chapter 3. To avoid the oxidation of samples between experiments and analysis, the collected paste samples from Ar atmosphere were mixed with glycerol and transferred to the XRD chamber [9]. A crystal sample holder was used and the derived pattern was not corrected for background diffraction.

## 5.3 Results and discussion

### 5.3.1 Cr(VI) and Cr(III) sustainability test

The sustainability of two major Cr species of Cr(VI) and Cr(III) in synthetic wastewater and glucose solution clearly confirmed that only chromate can exist in solution under the alkaline conditions of the real wastewater (Table 5.2).

**Table 5.2 Sustainability of chromate in complex wastewater (pH = 8.25 ± 0.25; DO = 0-0.2 mg/L; Initial Cr concentration: 10 mg/L)**

| Chemical species | Residual Cr (mg/L) |
|---|---|
| Glucose with Cr(VI) | 10.07 |
| Glucose with Cr(III) | 0.18 |
| Synthetic wastewater with Cr(VI) | 9.30 |
| Synthetic Wastewater with Cr(III) | 1.83 |

[Initial Cr concentration: 10 mg/L]

### 5.3.2 Removal of chromate by coprecipitation with Fh and GR

The removal of chromate from water by coprecipitation with Fh and GR was preliminary assessed through experiments from simple Cr-bearing solution and at Ar atmosphere. Results in Fig. 5.3 highlighted that GR was more effective than Fh at both pH 5 and 7. For Fh, the higher chromate removal observed at pH 5 can be reasonably explained through the higher zeta potential at this pH [10]. Although Fh at pH 5 adsorbed chromate completely, 3.96 mmol/L of Fe were required to achieve the removal. In contrast, only 0.96 mmol/L Fe were required to remove the same 0.19 mmol/L Cr. The 4 times lower amount of iron required with GR is expected to determine a significantly lower production of sludge upon chromate removal.

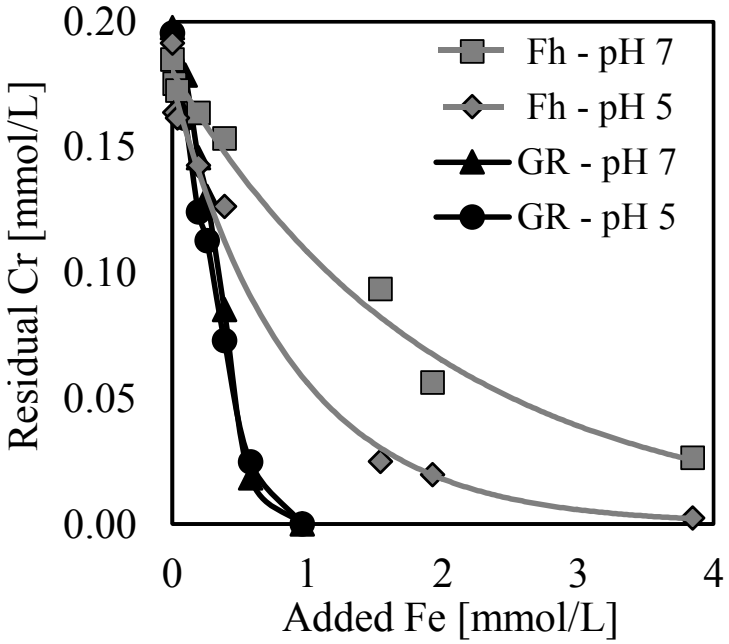


**Fig. 5.3 Chromate removal in coprecipitation with GR and Fh at pH 5 and 7 (Ar-atmosphere)**

### 5.3.3 XRD analysis

The XRD spectra of upon chromate removal with Fh at pH 5 and pH 7 exhibited the typical pattern of Fh (Fig. 5.4). This evidence highlighted that chromate was removed through a kind of adsorption that does not imply any structural change, namely outer-sphere surface complexation. The only exception was observed at Cr/Fe 0.5 (pH 5) as the XRD spectra exhibited the broadening of the peak at 34°. As described in the previous chapters, such peak broadening suggests the insertion of Cr into Fh and highlights a

change of removal mechanism from outer-sphere to inner-sphere surface complexation [10]. On the contrary, the XRD spectra of GR upon chromate removal at pH 5 and 7 exhibited a new peak at 30° (Fig. 5.5). The new peak reveals the oxidation of GR to Cr-inserted Fh and it was observed already at Cr/Fe molar ration 0.5 and 0.1. This evidence highlights as chromium can be inserted in the crystal structure already from low Cr/Fe ratio, possibly during the formation of GR.

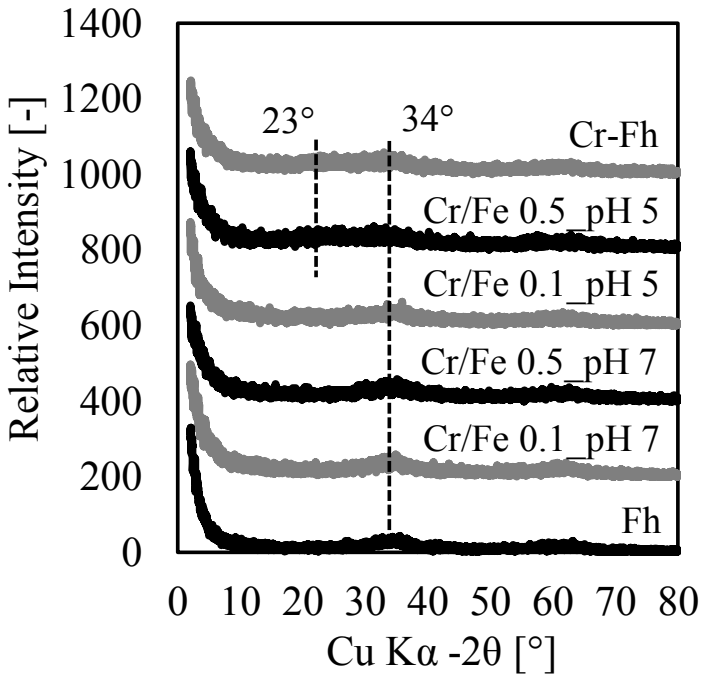


**Fig. 5.4 XRD patterns of solid residue upon coprecipitation of chromate with Fh at pH 5 and 7 (Ar-atmosphere)**

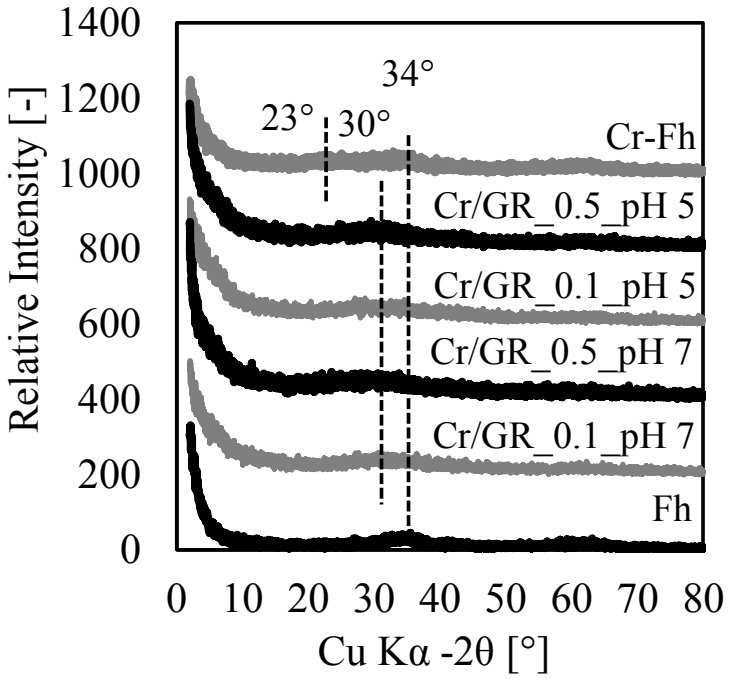


**Fig. 5.5 XRD patterns of solid residue upon coprecipitation of chromate with GR at pH 5 and 7 (Ar-atmosphere)**

### 5.3.4 Effect of Chemical Oxygen Demand (COD)

By increasing the COD in water, the residual Cr concentration significantly decreased (Fig. 5.6). To exclude the possibility that chromate was immobilized due to some species contributing to COD, a control experiment was performed without GR. The residual Cr concentration in control experiments was very close to the initial one (10 mg/L), thus confirming that the immobilization was actually performed by GR. The larger removal of chromate observed by increasing the COD can find an explanation in the increased concentration of alkaline cations like $Na^+$. As previously reported, at higher pH during GR preparation determines a change of the surface charge from positive to negative [11], and results into a larger inclusion of $Na^+$ (from NaOH) within GR structure. As a consequence, GR's structure expands, surface area increases, and more chromate can be removed. In these experiments, increasing the COD according to the wastewater composition determined also an increase of $Na^+$ concentration due to oxidable species like sodium sulphide and thiosulfate. Accordingly, a more stable and efficient GR might have generated [12] and more chromate could be removed.

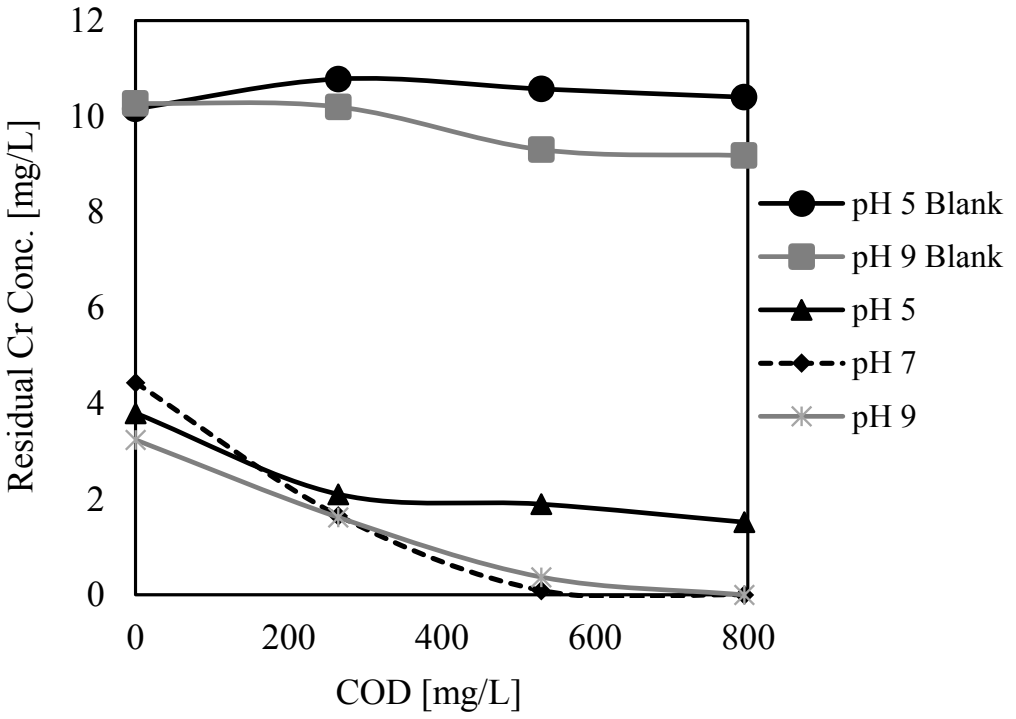


**Fig. 5.6 Effect of COD on chromate removal at pH 5, 7 and 9 with fixed Cr/GR(T-Fe) ratio 0.5 (Ar-atmosphere)**

### 5.3.5 Coprecipitation experiments with GR under open-air atmosphere

The ability of GR to resist oxidation and immobilize chromate from the complex tannery wastewater under open air atmosphere was verified at pH 8.25 (± 0.25), which is the one out of the CETP. The Eh(vs SHE) and pH trends recorded during GR formation are shown in Fig. 5.7. The points (a), (b) and (c) in Fig. 5.7 refer to the photos in Fig. 5.8, taken during the experiments. The trend shown in Fig. 5.7 is very similar to the one observed for GR under Ar atmosphere (chapter 4). Titrating at pH 8.25 determined a first potential drop from 300 to about 0 mV within 2-4 minutes and a further drop to -100 mV in the next 10 minutes. At the same time, the colour of the suspension turned first to light reddish and quickly to light-green (Fig. 5.8a) suggesting the formation of GR. The Eh drop observed within 15 minutes was clearly associated with the decrease of the Fe(III)/Fe(II) ratio for the formation of GR [13]. Finally, after 20-24 minutes the Eh gradually increased and the suspension turned reddish-green suggesting the oxidation of GR to Fh. Pre-experiments (result not shown) showed that when the pH was fixed over 9, the GR colour lasted for only around 5 minutes. After this time, GR oxidized to first to magnetite, whose formation is favoured by high pH [14], and then to Fh.

The graph in Fig. 5.7 highlighted slightly higher values of Eh and a change within a shorter period of time compared to what previously shown in chapter 4. The difference can be reasonably considered as the consequence of the partial oxidation of $Fe^{2+}$ by the oxygen dissolved in solution under open-air atmosphere.

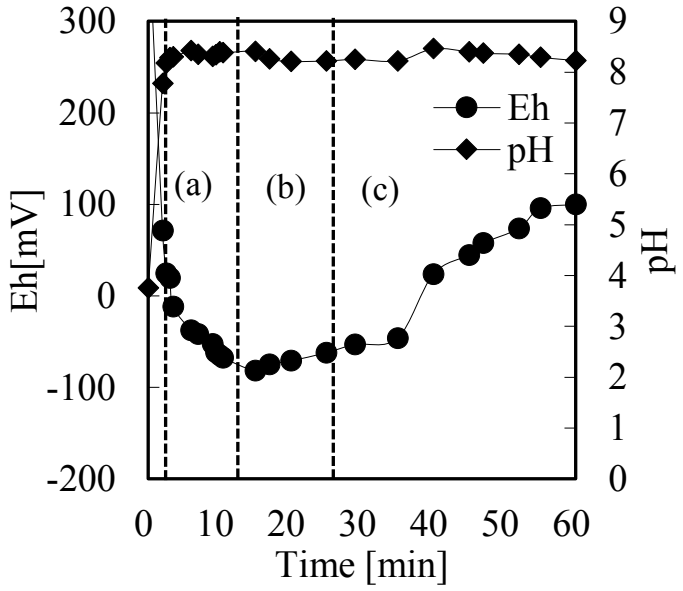


**Fig. 5.7 experimental pH and Eh during formation and coprecipitation of GR with chromate (synthetic wastewater). The different regions in the Fig. refer to (a) GR formation, (b) slight to moderate oxidation (c) Fh formation**

The experimental DO was found to be constant right after adding the Fe(II)-Fe(III) solution and then started increasing very slowly up to the formation of GR. The DO accounted for less than 1 mg/L when GR formed and then dramatically increased following the oxidation to Fh.

The final solid products after removing chromate from synthetic wastewater were analysed by XRD. The XRD spectra showed the typical pattern of Cr-inserted Fh, as suggested by the XRD peak shift from 34° to 28° (Fig. 5.9). In the previous chapters, the XAFS analysis revealed that a close and compact insertion of Cr was possible only without a significant enlargement of the Fh structure. As a consequence, the Cr-Fe bonding would be stronger and the immobilized Cr would not be easily released into the environment. The Cr-inserted Fh found under open-air atmosphere suggests a similar consideration.

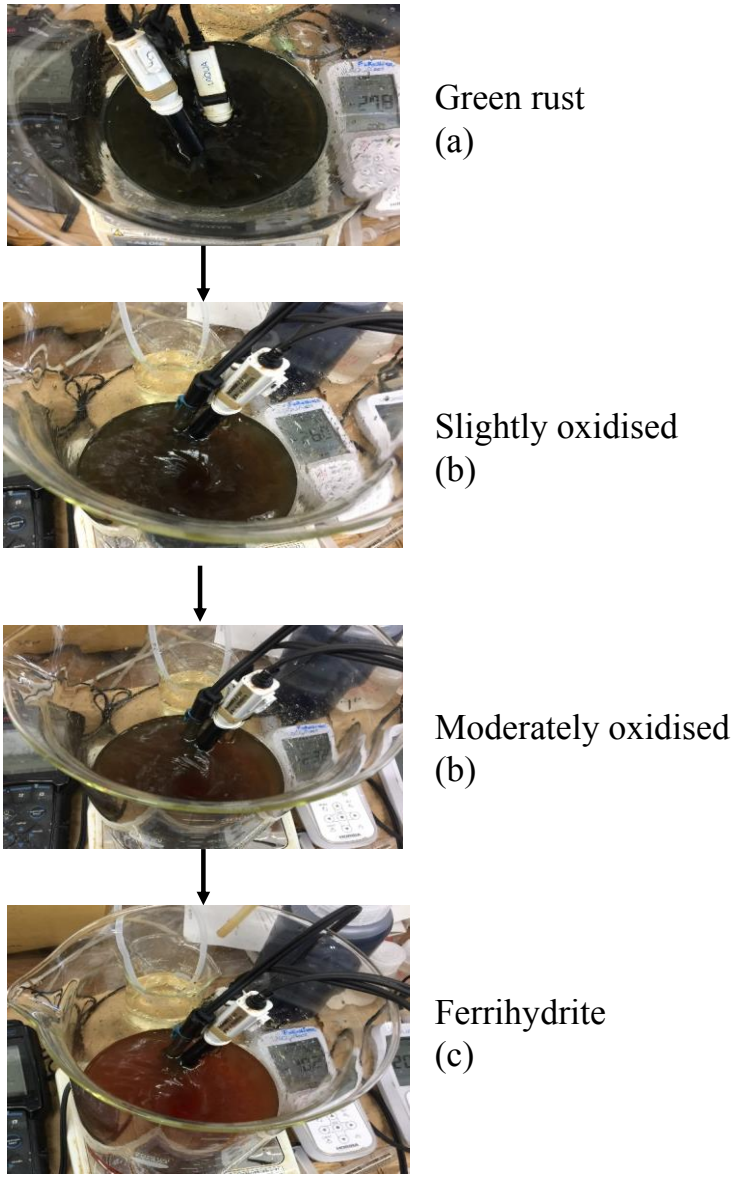


**Fig. 5.8 colour change during coprecipitation experiments. The photos (a), (b) and (c) correspond to the (a), (b), (c) regions in Fig. 5. 7**

The coprecipitation experiments with Fh (chapter 3) revealed that Cr/Fe molar ratio of 0.05 was effective to remove low concentrations of chromate. In contrast, GRs, enabled to achieve the same performance at a considerably lower Cr/T-Fe molar ratio (0.1, 0.2, 0.3) in the pH range 8.25-9.

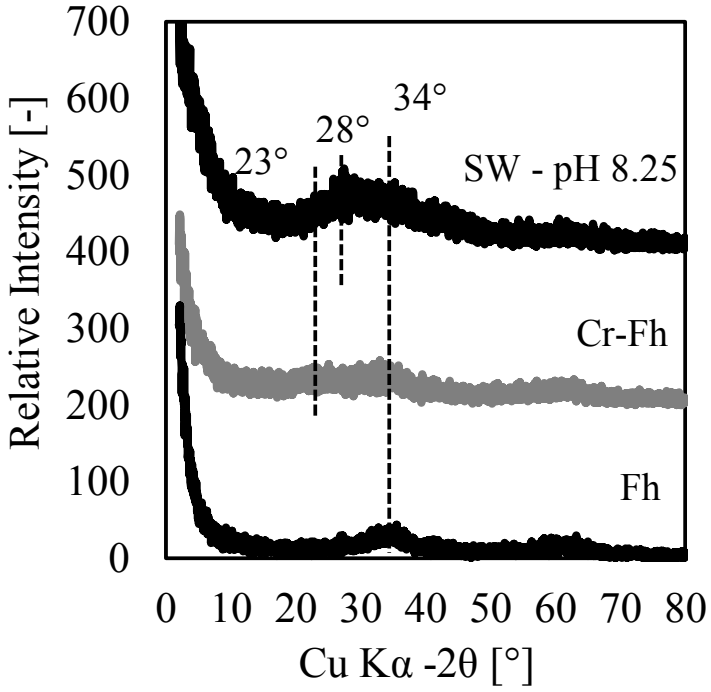


**Fig. 5.9 XRD patterns of Fh, Cr-inserted Fh and final product obtained in the coprecipitation of synthetic wastewater with GR at pH 8.25**

### 5.4 Engineering considerations on GR-Cr coprecipitation at the BSCIC

The formation of GR starts in 2 to 4 minutes, whereas a complete oxidation to Fh takes place in 20-24 minutes. For this reason, the design of the precipitation tank must be based on a minimum retention time of 24 minutes (Fig. 5.10). Given the total volume of wastewater of 20000 $m^3$/day processed at the BSCIC tannery CETP, the precipitation tank must be divided into 3 compartments comprising the total volume of 111.08 $m^3$. The division of each compartment would be realized by the hanging reinforced concrete cement (RCC) walls to promote the maximum retention time with the minimum space. The precipitation sludge could be removed mechanically and an additional clarifier might be useful to ensure the maximum sedimentation.

The formation of GR would take place within the first sub-compartment as the retention time is 4 minutes, whereas the other three sub-compartments would ensure to maximize the retention time up to 24 minutes. The cross-section view of the precipitation tank is shown in Fig. 5.10 while the specifications of the tank and the design calculation are given in Table 5.3.

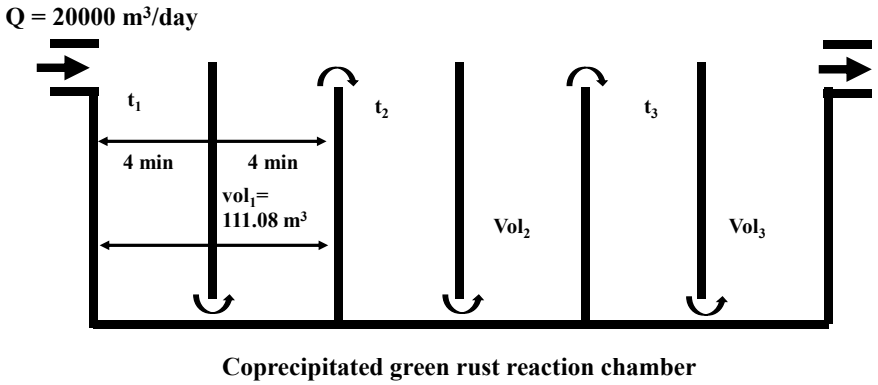


**Fig. 5.10 Simplified representation of coprecipitation tank**

**Table 5.3 Specification of GRs coprecipitation tank at the BSCIC tannery estate**

| Specification | Calculation/description |
|---|---|
| 1) Flow rate calculation | 20000 [$m^3$/d] /(24 [h/d] × 3600 [sec/h]) = 0.2314 $m^3$ of wastewater /sec |
| 2) Total retention time is 24 min | Retention time for each compartment = 24/3 = 8 min (4 min+4 min) |
| 3) Volume of the each compartment ($t_1$) | Volume = flow rate X retention time in each compartment. = 0.2314*8*60 [$m^3$]= 111.08 $m^3$ Each tank is of equal volume (V) $V_1$= $V_2$=$V_3$= 111.08 $m^3$ |
| 4) Design of each compartment (111.07 $m^3$) of the reaction chamber | Assumptions: height = 4 m, width = 3.5 m Therefore, Length = 111.08 [$m^3$]/(4 [m] × 3.5 [m])= 7.93 m |
| 5) Total RCC works | (Basement floor + intermediate wall + side wall) = (32.48 + 35.07 + 64.96) [m3] = 132.51 m3 |
| 6) Construction cost (Land value is not included as the area is dedicated for CETP by the government of Bangladesh) | Total construction costs: (132.51 [$m^3$] ×128.5 [USD/$m^3$]) = 17010.1 USD. |

### 5.5 Revised central effluent treatment plant at BSCIC tannery estate

If chromate was coprecipitated with GR based on results discussed in this chapter, the precipitation tank would be installed after the oxidation ditch B (Fig. 5.11). The tanning sludge obtained in the coprecipitation with GR should be disposed of in a landfill [15] or re-processed to recover Cr. The recovered Cr could be reused within the same tanning process after acidification, thereby lowering the costs associated with the overall manufacturing/wastewater treatment operations.

The sludge from pre-tanning and post tanning would not be treated by GR due to the very low concentration of Cr(VI). The waste stream from pre-tanning and post-tanning could be potentially used for the preparation of poultry feed [16]. However, special care and attention are required to ensure the optimal prevention of chrome contamination.

Since Cr was found able to inhibit the biomass involved in the biological wastewater treatment [17], the removal of BOD and COD would be performed after Cr recovery and coprecipitation with GR. The very low DO and high COD in the tannery effluent suggests that an anaerobic biological treatment would be ideal. The anaerobic treatment would remove more than 70% of the colour [18] and might generate useful biogas.

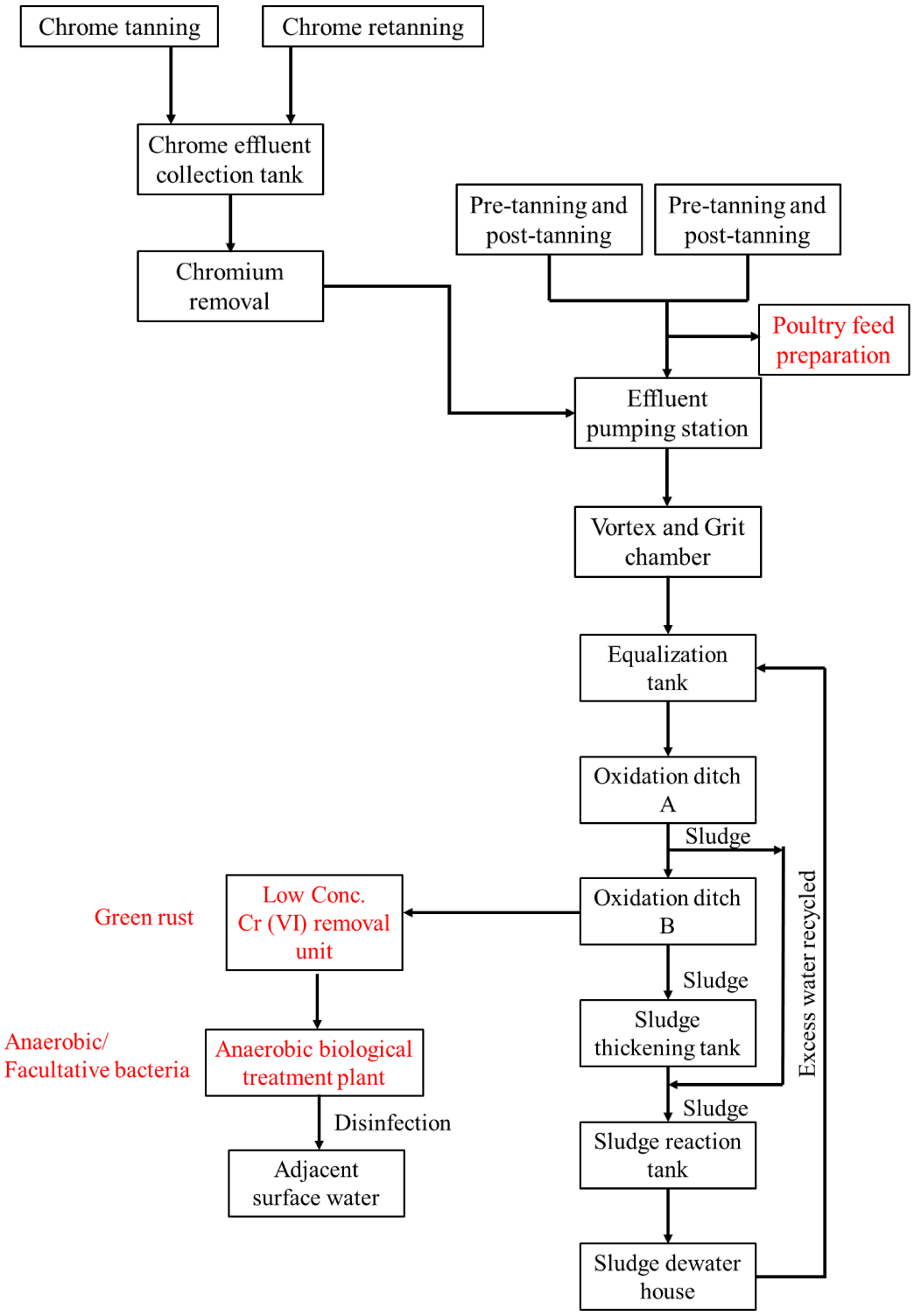


**Fig. 5.11 Revised flowchart of the CETP at the BSCIC tannery estate**

## 5.6 Summary

Conventional Cr removal system failed to remove the chromate generated at the BSCIC tannery industrial estate (Bangladesh). Low chromate concentrations and the slight alkalinity of the produced wastewater represent the main reason why commercial removing systems failed. The coprecipitation of chromate with GR represents a valid option to overcome these issues with satisfactory sustainability as iron oxide species are largely available worldwide, even from waste streams. However, GR is very prone to oxidation and it was not known whether would efficient in real wastewater systems under open-air atmosphere. This chapter provided evidence that this operation is actually possible. Even in the presence of 265 mg/L of COD and open-air atmosphere, GR could form, resist to oxidation and completely remove chromate. Previous XRD and XAFS results suggests that the generated sludge is a dense product with good solid-liquid separability from where could be also recovered.

**References**


[1] R. Rakhunde, L. Deshpande, H.D. Juneja, Crit. Rev. Environ. Sci. Technol. 42 (2012) 776–810.

[2] B. Qiu, C. Xu, D. Sun, H. Yi, J. Guo, X. Zhang, H. Qu, M. Guerrero, X. Wang, N. Noel, Z. Luo, Z. Guo, S. Wei, ACS Sustain. Chem. Eng. 2 (2014) 2070–2080.

[3] WHO, Chromium in Drinking-Water (Background Document for Development of WHO Guidelines for Drinking-Water Quality), Geneva, Switzerland, 1996.

[4] Water Environment, APHA, Standard Methods for the Examination of Water and Wastewater Part 1000 Standard Methods for the Examination of Water and Wastewater, 1999.

[5] C. Tokoro, S. Suzuki, D. Haraguchi, S. Izawa, Materials (Basel). 7 (2014) 1084–1096.

[6] C. Tokoro, T. Sakakibara, S. Suzuki, Chem. Eng. J. 279 (2015) 86–92.

[7] C. Tokoro, Y. Yatsugi, H. Sasaki, S. Owada, Resour. Process. 8 (2008) 3–8.

[8] D. Haraguchi, C. Tokoro, Y. Oda, S. Owada, J. Chem. Eng. Japan 46 (2013) 173–180.

[9] H.C.B. Hansen, Clay Miner. 24 (1989) 663–669.

[10] A. Al Mamun, M. Morita, M. Matsuoka, C. Tokoro, J. Hazard. Mater. 334 (2017) 142–149.

[11] R. Guilbaud, M.L. White, S.W. Poulton, Geochim. Cosmochim. Acta 108 (2013) 141–153.

[12] B.C. Christiansen, K. Dideriksen, A. Katz, S. Nedel, N. Bovet, H.O. Sørensen, C. Frandsen, C. Gundlach, M.P. Andersson, S.L.S. Stipp, Inorg. Chem. 53 (2014) 8887–8894.

[13] I.A.M. Ahmed, L.G. Benning, G. Kakonyi, A.D. Sumoondur, N.J. Terrill, S. Shaw, Langmuir 26 (2010) 6593–6603.

[14] A. Sumoondur, S. Shaw, I. Ahmed, L.G. Benning, Mineral. Mag. 72 (2008) 201–204.

[15] L.T. Mazumder, S. Hasan, M.L. Rahman, J. Environ. Sci. Toxicol. Food Technol. 3 (2013) 44–51.

[16] S. Parvin, L.T. Mazumder, S. Hasan, K.A. Rabbani, M.L. Rahman, J. Environ. Sci. Toxicol. Food Technol. 11 (2017) 82–89.

[17] G. Durai, M. Rajasimman, J. Environ. Sci. Technol. 4 (2011) 1–17.

[18] S.K. Biswas, L.A. Lisa, N.A. Banu, A. Islam, A.K. Roy, Plant Environ. Dev. 4 (2015) 13–20.

# [Chapter 6]
# Conclusions

The tannery is the complex industrial process to transforms the semi-soluble protein “collagen” present in animal raw hides or skin to highly durable commercial leather products. Due to low labour cost and less stringent environmental legislations, tannery processes are implemented mainly in developing countries like Bangladesh, where the leather manufacturing accounts for approximately 500 million USD per year.

In spite of obvious advantages to the country’s economy, the leather manufacturing determines a great environmental burden as tanning operations result in the production of highly polluted wastewater. The main pollution load of tannery wastewater is represented by high COD and BOD due to fat release in liming operations. However, the major environmental threat arises from the presence of Cr(VI). Chromium is used in tanning as Cr(III) sulfate (15-30 kg/ton of raw hides) to confer fine texture, flexibility and durability to the leather products. Nevertheless, due to naturally oxidizing conditions through the process, part of the residual Cr(III) from tanning is oxidized to Cr(VI) and ends-up in the final wastewater. Since Cr(VI) is a well-known mutagenic and carcinogenic agent, these wastewater represents a serious threat to the eco-system surrounding the tannery estates.

The recent scientific literature reports of innovative methods and removing agents to immobilize chromate. High-performance adsorbents such as activated carbon and ion-exchange resins were found efficient to remove chromate from the water. However, they require adequate skills for operation and maintenance and too high costs for developing countries. Bio-adsorbent derived from agricultural waste were identified as a more sustainable option to remove chromate. Low costs, ease of operation and the possibility of disposal after use are their main figures of merit. However, these bio-adsorbents exhibit a lower efficiency at low chromate concentration and in alkali conditions. In addition, the raw materials required to produce them are highly localized and sometimes seasonal.

The ideal adsorbent should be efficient at low chromate concentration and in slightly alkaline conditions, easily available and cost-effective for developing countries like Bangladesh. Given their low-cost and widespread availability, removing Cr(VI) with iron oxide species would be highly sustainable from both economic and environmental points of view. In this view, this research work investigated the use of two different iron oxide compounds as removing agents for Cr(VI). The investigated removing agents are ferrihydrite and green rust.

The main findings of this work are summarized as follows:

(1) Chromate coprecipitation with ferrihydrite ($Fe_2O_3 \cdot 0.5H_2O$) is more selective and efficient than simple adsorption method.
(2) The immobilization mechanism shifts from outer-sphere/monolayer adsorption to inner-sphere/multi-layer adsorption by increasing the Cr/Fe ratio in both adsorption and coprecipitation. In adsorption, the mechanism changes from Cr/Fe = 1 whereas in coprecipitation the shift occurs from Cr/Fe = 0.25.
(3) XRD results highlighted that such change of mechanism corresponds to the formation of a chromium-inserted ferrihydrite compound.
(4) EXAFS fittings supported discussion of mechanism shift. Higher molar ratios favour immobilization through inner sphere complexation with the formation of bidentate binuclear Cr–Fe bonds and expansion of ferrihydrite structure. This result has a clear impact on chromate immobilization and manipulation of end products. Whereas the chromate immobilized via outer-sphere complexation could be easily released and/or recovered, the one immobilized via inner-sphere complexation would be bound stronger to ferrihydrite for a safer disposal.
(5) Green rust (GR) properties depend on pH during preparation. Increasing the preparation pH from 7.50 to 8.75 produces a larger inclusion of $SO_4^{2-}$ and $Na^+$ within the GR interlayer, thereby resulting into: (i) increase of surface area, (ii) enlargement the crystal lattice, and (iii) increase of single corner Fe-Fe coordination via oxygen.
(6) The GR prepared at pH 8.75 ($GR_{8.75}$) was found to be 1.7 times more efficient than the one prepared at pH 7.50 ($GR_{7.50}$) and 6.7 times more efficient than ferrihydrite in terms of moles of Fe required to remove a fixed amount of Cr from the water. Both GRs exhibited the highest removal efficiency at pH 5.
(7) $GR_{8.75}$ oxidizes mostly to goethite at pH 5 and to magnetite at pH 9. $GR_{7.50}$ oxidizes to Cr inserted ferrihydrite.
(8) For $GR_{8.75}$, the increase of Fe-Fe edge sharing and double corner sharing coordination numbers suggests that chromate was removed *via* surface reduction. In contrast, the increase of significant single corner sharing Fe-Fe coordination via oxygen suggests that $GR_{7.50}$ removes chromate *via* sulfate replacement in the interlayer. This results

presented scientifically significant information about Cr-Fe and Fe-Fe binding geometries. The new information would have a clear impact when a real process was implemented. The high efficiency of GR and the predominant bidentate mononuclear Cr-Fe coordination would result in an efficient chromate removal with the smaller generation of a dense sludge with good solid-liquid separability.

(9) GR can remove chromate below 0.05 mg/L also under open-air atmosphere and from complex wastewater systems. This was a completely new approach for GR since all previous works described results obtained under non-oxidizing controlled atmosphere and from simple Cr bearing solutions. The final sludge after removal will be a Cr-inserted ferrihydrite product that should grant an easy solid-liquid separation.

The goal of this thesis was to study the removal of chromate from tannery wastewater by sustainable removing agents suitable for developing countries. All results presented in chapters 3, 4 and 5 are proof that this goal was successfully achieved and will enrich the scientific literature on Cr(VI) removal. Based on these results, an operation of chromate coprecipitation with GR could be integrated within the already existing CETP at the BSCIC tannery estate. In this view, this thesis lays the foundations for a more sustainable future of leather manufacturing and will help to preserve both environment and human health in the tannery estate area.

# Appendices
# [Doctoral thesis synopsis
# and
# List of research achievements]

## Doctoral Thesis Synopsis

The tannery is a complex industrial process to transform animal raw hides or skin to leather goods. The process requires a variety of chemical inputs including Cr(III) sulfate (15-30 kg/ton of raw hides) which is used to confer fine texture, flexibility and durability to the leather products. However, due to naturally oxidizing conditions in different sections of the process, relatively large amounts of Cr(VI) are generated and discharged into the process effluents. Since Cr(VI) is a well-known mutagenic and carcinogenic agent, the nearby environment and human health are exposed to a serious threat.

Aiming to solve the problem, the government of Bangladesh has recently shut down the most polluted Hazaribagh tannery area and ordered to move the operations to the Bangladesh Small and Cottage Industries Corporation (BSCIC) tannery estate in Savar, which is equipped with a central effluent treatment plant (CETP). Nevertheless, the final effluent still exhibits high BOD (100-350 mg/L) and COD (250-1000 mg/L), low DO (0-0.2 mg/L) and a total concentration of chromium of about 10 ~ 15 mg/L in alkali conditions (pH 8.1-8.25) even after the treatment. As a matter of fact, whereas Cr(III) can be efficiently removed via neutralization-precipitation as oxide/hydroxide in the wide range of pH, Cr(VI) and its most stable species chromate, is more difficult to remove from the water due to high mobility.

The recent scientific literature reports of innovative removing agents to immobilize the chromate via adsorption. High-performance adsorbents such as activated carbon and ion-exchange resins require high costs and adequate skills for operation and maintenance. Bio-adsorbent like as agricultural waste exhibit low cost and ease of operation in spite of a lower efficiency towards the removal of low concentrations of Cr(VI). In addition, they are highly localized and sometimes seasonal. The ideal adsorbent should be efficient, easily available and cost-effective for developing countries like Bangladesh. In this context, the development of an innovative and sustainable method to remove chromate from water is highly anticipated.

This thesis is organized in six chapters. The general information about the threat from Cr(VI) pollution is presented in the first chapter along with a literature survey on conventional technologies and recent innovation in Cr(VI) removal. The second chapter

narrows down on the Cr(VI) pollution at the BSCIC tannery estate in Savar (Bangladesh) by describing the leather manufacturing and by providing a mass balance of Cr and a description of the wastewater generated in the process. The third and fourth chapter addresses the use of iron oxide compounds such as ferrihydrite and green rust respectively as efficient and sustainable adsorbing agent for chromate. Given the natural availability of natural iron oxide species, the removal of Cr(VI) would be highly sustainable from economic and environmental points of view. However, the removal mechanism must be fully understood and removing condition must be optimized before a real process could be implemented.

The first iron oxide studied in this thesis is ferrihydrite ($Fe_2O_3 \cdot 0.5H_2O$), a hydrous ferric oxyhydroxide mineral with a nanoporous structure that can operate the removal of Cr(VI) via adsorption or coprecipitation. The use of ferrihydrite is described in the third chapter through a comparison of chromate removal by coprecipitation and adsorption at pH 5 and pH 7. The obtained results highlight that coprecipitation at pH 5 determines the largest removal of chromate, with an almost double sorption density than adsorption. The Brunauer–Emmett–Teller (BET) type adsorption isotherms, zeta potential trends, XRD and EXAFS fitting results highlight that the sorption mechanism shifts from outer sphere to inner sphere complexation by increasing the Cr/Fe molar ratio. The same shift can be achieved by conducting coprecipitation over adsorption. This evidence can be thoroughly explained considering the enhancement of bidentate binuclear Cr–Fe bonds and resulting in the expansion of the ferrihydrite structure for a larger amount of chromate. This result represents a totally new finding and has a clear impact on chromate immobilization and manipulation of end products. The chromate immobilized via outer-sphere complexation could be easily released and/or recovered whilst the one immobilized via inner-sphere complexation would bound stronger for a safer disposal.

Although the immobilization of chromate by ferrihydrite was proven effective and the mechanism was clearly elucidated, the slow removal kinetics and the generation of a large amount of sludge represent major drawbacks for the implementation of real processes. Therefore, the fourth chapter of this thesis addresses the study of an alternative adsorbing agent, possibly more efficient than ferrihydrite. The targeted alternative adsorbent was identified in green rust (GR), a layer double hydroxide (LDH) of Fe(II) and Fe(III) intercalated with sulfate ions (sulfate-GR) and water molecules. Whereas GR

has already been proven efficient to immobilize chromate with a faster kinetics than ferrihydrite, the removal mechanism and its dependence on the pH are still unknown. Based on a previous study showing the expansion of GR's crystal lattice beyond pH 8.50, the role of pH in GR preparation and chromate removal was extensively investigated. The obtained results present completely novel aspects. The increase of pH from 7.50 to 8.75 in the preparation of GR, determines a larger inclusion of $SO_4^{2-}$ and $Na^+$ within the GR interlayer, an increase of surface area, enlargement of the crystal lattice and increase of single corner Fe-Fe coordination via oxygen. The different pH during the preparation determines also a different removal mechanism. The GR prepared at pH 8.75 immobilizes chromate mainly via surface redox reaction, whilst the one prepared at pH 7.50 performs the reduction from the LDH interlayer upon ion exchange between chromate-sulfate. By means of an extensive discussion of XRD, XPS and XAFS results, the fourth chapter presents novel information about the Cr-Fe and Fe-Fe binding geometries. The high efficiency of GR in chromate removal and the lower production of denser sludge are proven to be the consequence of bidentate mononuclear Cr-Fe coordination.

All research works in literature were performed by producing and using GR under non-oxidizing control atmosphere and from simple Cr bearing solutions. However, unwanted oxidations might take place under air-atmosphere because GR contains significant portions of Fe(II). Therefore, the industrial applicability of GR still presents challenging aspects. The fifth chapter demonstrates the applicability of coprecipitated GR to remove chromate under open-air atmosphere and from complex water media resembling the wastewater of BSCIC tannery estate, Savar, Bangladesh. The obtained results confirm that GR can be successfully produced under naturally oxidizing condition even in the presence of organic contaminants such as fatty acids and protein-like compounds. The chapter highlight that GR resists oxidation for over 10 minutes and remove Cr(VI) from 10 mg/L to <0.05 mg/L in less than 10 minutes. This kind of finding also represents a novel aspect of this research as it is being reported for the first time.

Overall, this research work solved the problem of the removal of low concentrations of Cr(VI) from water by using efficient, low cost and easily accessible iron oxide compounds. The work lays the foundation for sustainable management of Cr(VI) pollution, which is expected to improve environmental compliance of developing countries like Bangladesh. As for the scientific significance of this research, the new

findings will enrich the scientific literature on Cr(VI) removal and will provide useful information to implement real processes. Although all original findings of this research are summarized in the concluding six and last chapter, I would like to highlight them also in this synopsis.

The removal mechanism of chromate by ferrihydrite can be shifted from outer-sphere to inner-sphere surface complexation by increasing the Cr/Fe molar ratio and by preferring coprecipitation over adsorption. This finding could potentially affect the management of the end-product as an inner sphere bound chromate will be more strongly bound and more suitable for disposal. In contrast, an outer-sphere bound chromate could be potentially recovered.

The removal mechanism of chromate by GR is strongly influenced by the pH during preparation and use. The reasons behind the higher efficiency of GR for chromate removal and the generation of a lower amount of a denser precipitation sludge are identified by the bidentate-mononuclear Cr-Fe coordination.

GR can be efficiently prepared and used to remove low concentration of chromate under an open-air atmosphere from a complex water media resembling the targeted wastewater produced at the BSCIC tannery estate in Bangladesh.

**List of research achievements**

**Abdullah al MAMUN（As of July, 2018）**

| By Type | Particulars |
|---|---|
| Journal Article | 1. **A. A. Mamun**, M. Morita, M. Matsuoka, C. Tokoro, Sorption mechanisms of chromate with coprecipitated ferrihydrite in aqueous solution, *Journal of Hazardous Materials*, 2017, Vol. 334, pp. 142-149.<br>2. **A. A. Mamun**, M. M. Khin, G. Granata, C. Tokoro, Removal of chromate from tannery wastewater: the applicability of sulfate-green rust in real coprecipitation processes, *Resources processing*, 2018, Vol. 65, pp. 1–7.<br>3. **A. A. Mamun**, A. Onoguchi, G. Granata, C. Tokoro, Role of pH in green rust preparation and chromate removal from water, *Applied Clay Science*, 2018, Vol. 165, pp. 205-213. |
| Academic conference | 4. **A. A. Mamun**, M. Morita, C. Tokoro, Sorption mechanisms of chromate with ferrihydrite through coprecipitation in aqueous solution, Goldschmidt (Yokohama, Japan), 26 June-1 July, 2016, p. 355<br>5. Y. Mitani, K. S. Oo, **A. A. Mamun**, M. Matsuoka, C. Tokoro, Comparison of arsenic removal mechanism in various ferric additions in co-precipitation and adsorption process, The 14th Korea /Japan international symposium on resources recycling and materials science (Incheon, South Korea), 7-8 July, 2016, p. 291.<br>6. **A. A. Mamun**, Y. Mitani, M. Morita, C. Tokoro, Ferrihydrite adsorptive performance evaluation in heavy metal removal in coprecipitated aqueous solution, 5th International doctoral symposium (Sapporo, Japan), 9-11 November, 2016, p. 28.<br>7. C. Tokoro, Y. Mitani, T. Kato, **A. A. Mamun**, Mineralogical control of the form of ferric/ferrous precipitates for effective treatment of acid mine drainage, International mineral processing congress 2016 (Québec, Canada), 11-15 September, 2016, p. 11.<br>8. **A. A. Mamun**, A. Onoguchi, M. Morita, M. Matsuoka, C. Tokoro, Removal mechanism of Cr(VI) with green rust sulfate based on pH in |

| | |
|---|---|
| | aqueous solution, spring conference, MMIJ (Chiba, Japan), 27-29 March, 2017, p. 91.<br>9. A. Onoguchi, T. Uchida, **A. A. Mamun**, G. Granata, C. Tokoro, Fundamental study on elimination of selenium using the high purity green rust, International conference of chemical engineers (Tokyo, Japan), 9-10 August, 2017, p. 86.<br>10. **A. A. Mamun**, A. Onoguchi, G. Granata, C. Tokoro, Elucidation of pH dependent sorption mechanism of chromate with green rust sulfate through XAFS analysis, spring conference, MMIJ (Tokyo, Japan), 29 March, 2018, p. 76.<br>11. A. Onoguchi, T. Yo, **A. A. Mamun**, G. Granata, C. Tokoro, Comparison of removal mechanism between selenite and selenite by green rust, spring conference, MMIJ (Tokyo, Japan), 27 March, 2018, p. 42.<br>12. **A. A. Mamun**, A. Onoguchi, G. Granata, C. Tokoro, Sorption mechanism of chromate by ferrihydrite and sulfate green rust: comparison by XAFS analysis. 5th International arsenic symposium (Miyazaki, Japan), 22-25 June, 2018, pp. 86-89. |
| Poster presentation | 13. **A. A. Mamun**, A. Onoguchi, G. Granata, C. Tokoro, Study on sorption mechanism of chromate with GR Sulfate by XAFS analysis. The 14th resources, materials and environment technology and research exchange meeting (Tokyo, Japan), 4 August, 2017, p. 15.<br>14. **A. A. Mamun**, M. Morita, M. Matsuoka, C. Tokoro, Investigation on Chromate sorption mechanism with coprecipitated ferrihydrite through XAFS analysis, The 13th resources, materials and environment technology and research exchange meeting (Ibaraki, Japan), 4 August, 2016, p. 46.<br>15. A. Onoguchi, T. Uchida, **A. A. Mamun**, M. Matsuoka, C. Tokoro. Fundamental study on green rust coprecipitation by aeration method, the 13th resources, materials and environment technology and research exchange meeting (Ibaraki, Japan), 4 August, 2016, p. 09. |

**Acknowledgements**

I thank my advisor Professor Dr. Chiharu Tokoro for her constant support, guidance and for creating a comfortable atmosphere in which I could grow in my scientific approach.

I also express my profound gratitude to Assistant Professor Dr. Giuseppe Granata for his guidance and mentorship throughout the doctoral journey.

I am grateful to both the referee; Professor Dr. Shuji Owada and Professor Dr. Katsunori Yamaguchi, for reviewing my thesis as well as for valuable suggestions.

I also acknowledge the moral support given by Professor Dr. Mohammad Mosharraf Hossain and Dr. Mohammad Sujauddin.

I thank my parents, Md. Abu Yusuf and Shamsun Nahar, for their unconditional love and their years of dedication and sacrifice for my education.

I thank my wife Afroza Sultana Simu for her unfailing support, unending patience and selfless heart. In addition, Nazmun Nahar, Abdullah Al Nubaid, Nabiha Nashid have also been an encouragement to me.

Abir, Hasan, Raju, Ahmed, Deny, Rashed vi, Mizan vi, Rajib vi are also deserving my thanks; their friendship is a blessing.

I would like to thank all the Tokoro lab members, friend and colleague at home, who have made the years at Waseda possible, enjoyable, and whose support is reflected in the completion of this degree.